**INSTITUTE OF PHYSICS**
**GEORG -AUGUST-UNIVERSITY-GOETTINGEN**

# Magnetic and Electrical Properties of $Nd_{0.66}(Sr_{1-y}Li_y)_{0.34}MnO_3$ manganites

Doctoral Dissertation
Submitted for the degree of Doctor of Science in Physics
of the Faculty of Science

By
Nagat El- Sebaey Farag Hamad

M.Sc. Menoufia University,
El- Menoufia - Egypt

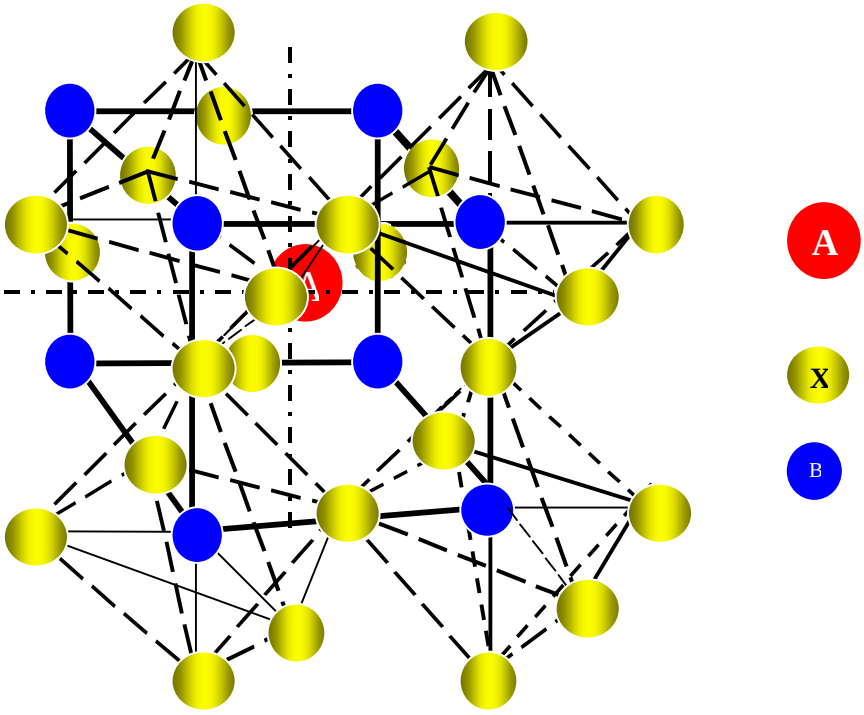


Dezember. 2003
Goettingen, Germany

## CONTENTES

Subject Page

Acknowledgement..... 3

**CHAPTER I : INTRODUCTION**

1.1. Motivation ..... 4

1.2. Perovskite Structure ..... 4

1.3. Single site electronic states of d-electrons and d – band formation ..... 6
1.4. Representation of Crystal field states ..... 7
1.5. Jahn-Teller Effect ..... 8
1.6. Double-exchange mechanism – pair site electronic states ..... 8
1.6.1. Zener bond qualification ..... 9
1.7. Superexchange model ..... 9
1.8. Magnetic and Crystal Structures of $Nd_{1-x}Sr_xMnO_3$ ..... 10
1.9. $Sr^{+2} \leftrightarrow Li^{+}$ Monovalent cation substitution ..... 11

**CHAPTER II : EXPERIMENTAL TECHNIQUES**

2.1. Sample Preparation ..... 12
2.1.1. Lattice site substitution ..... 12
2.1.2. Charge substitution ..... 12
2.1.3. Determination of the composition ..... 13
2.2. Sample characterization ..... 15
2.2.1. Scanning Electron Microscopy (SEM) ..... 15
2.2.2. X-ray powder diffraction ..... 15
2.3. Measurement of the Specific Heat Capacity ..... 24
2.4. Magnetization Measurements ..... 25
2.5. Resistivity Measurement ..... 27
2.5.1. Magnetoresistance measurement ..... 28
2.6.Thermoelectric Power Measurement ..... 29
2.7.Transient Thermoelectric Effects (TTE) measurement ..... 30
2.7.1. TTE - transient (III) – data reduction and corrections ..... 30
2.8. Heat diffusivity and heat conductivity ..... 31

**CHAPTER III : RESULTS**

3.1. Magnetization ..... 33
3.1.1. Magnetic Susceptibility ..... 33
3.2. Resistivity ..... 39
3.2.1. Magnetoresistance ..... 45
3.3. Specific Heat Capacity $C_P(T)$ ..... 48
3.4. Thermoelectric Power (TEP) ..... 51
3.5. Heat diffusivity and heat conductivity ..... 55

## CHAPTER IV : DISCUSSION

4.1. Calculation of the tolerance factor.....60
4.2. Zener bond blocking.....26
4.3. Magnetic Coupling.....62
4.4. Resistivity.....64
4.4.1 Resistivity for $y \geq 0.4$.....65
4.4.2 Resistivity for $y < 0.4$.....65
4.4.3. Magnetoresistance.....66.
4.5. Thermoelectric Power (TEP).....66
4.5.1 .TEP of the compounds with $y \geq 0.4$.....67
4.5.2.TEP of the compounds with $y < 0.4$.....67
4.6. Heat conductivity.....69

CONCLUSION.....70

REFERENCES.....71-73

## ACKNOWLEDGEMENTS

I am deeply grateful to Prof. Dr. K. Baerner for his constant and inexhaustible help, and I truly thank him for the big scientific freedom he always provided, without which most of this work would not exist.
I'm also in debt to Prof. Dr. I.V. Medvedeva; Institute of Metal Physics, Russia; for his continuous interest and support to this topic.
I address my thanks to the members of the group, Dr. J. Liebe, Dr. A. Kattwinkel, M. Boshta, I. Elkassab,V. Morchshakov and W. Hahn for their valuable help in the experimental work and for the nice atmosphere they created inside the group.

I am grateful to the Herrn Frenzel, head of the mechanics workshop, Herrn Langohr, head of the electronic workshop, and all their coworkers for the enceinte, competent and prompt job.

I am in debt to Prof. Dr. U. Sondermann from Institut für Mineralogie, Petrologie und Kristallographie der Phillipps-Universität Marburg for the Scanning Electron Microscopy, X-ray diffraction and X-ray flurosceince measurements and Prof. Dr. E. Gmelin for the specific heat measurement.

Frau E. Rohrmoser, and Frau H. Afshar, are kindly acknowledged for their continuous help with all the small and big administrative problems that a foreigner always has in a foreign country.

My sincere thanks to all the members of the IV. Physikalisches Institut in Goettingen, who always make the working atmosphere enjoyable and relaxed.

Finally, my thoughts inevitably go to my parents, my family ( Maher, Ahmed, Hagar, Sara and Soheila) and to all those persons who always, critically, constructively supported my choices and my work. To them I address my deepest gratitude and the best wishes for a brilliant continuation. I would like to thank and highly appreciate the Egyptian Government for financing my study program.

Goettingen, Dezember 2003

# CHAPTER I

# INTRODUCTION

## 1.1.Motivation

Recently renewed interest in the unusual transport and magnetic properties of the manganates and their role in potential application were occurred. etails of the transport and magnetic properties can also be explained by the blocking (rehabilitation) model where a Zener resonant state $Mn^{+4}$- e- $Mn^{+4}$ is converted into a pair of crystal field states $Mn^{+3}/Mn^{+4}$. While no spectular behaviour of the MR was found. Because of the Li- pair formation prospects to use the manganates surface for electrolysis reaction are good. Conformations of the predicted formation Li-pair might come from (future) photoemission or isotope effect measurements.

In this work, Sr was substituted by Li in the perovskite-type $Nd_{0.66}Sr_{0.34}MnO_3$ by the ceramic route.The reasons for that were manifold .

(1) In ceramics , aside from an intrinsic MR which is large only around the Curie temperature $T_C$ , a large MR which is related to grain (or phase) boundaries is generally observed for all $T < T_C$ . $Li^+$, on the other hand, is considered to be a rather small ion which could decorate the grain boundaries and thus eventually improve their magnetoresistive properties[1,2].

(2) Another application aspect is the use of the monovalent doped manganites as oxidation catalysts or as cathodes in solid oxide fuel cells and eventually as electrodes in other (low temperature) electrochemical reactions. Specifically, $Li^+$ and $Li_2^+$ could serve as a model ion for potential : $2H \rightarrow H_2$ catalytic action at the manganite interface.

(3) A more fundemental question concernes the role of Li in manganites; when $Sr^{2+}$ is substituted by $Li^{1+}$ ,one would expect to change the $Mn^{3+}/ Mn^{4+}$ disproportion towards $Mn^{4+}$ [3,4]. However , as $Li^{1+}$ is considered to be a rather small ion , its comprehensive role is still undecided ,i.e. whether it is positioned as an interstitial or occupies a Sr site. If $Sr^{2+}$ is substituted by $Li_2^+$, the Li – pair could occupy adjoining substitutional and interstitial sites or locally form $Li_2O$ .

## 1.2.Perovskite Structure

The general perovskite formula is $ABX_3$, where "A" and "B" are cations and "X" is an anion. The "A" and "B" cations can have a variety of charges and in the original mineral perovskite ($CaTiO_3$) the A-cation is divalent and the B-cation is tetravalent. However, for the purpose of this introduction , only trivalent rare-earth cations are considered, whilst the anion is always oxygen. The A-cation is larger than the B-cation: the A-site in the structure is 12 co-ordinated by oxygen anions whilst the B-site is octahedrally coordinated by oxygen .The structure of a cubic perovskite is shown in Fig(1.1). However , perovskites can exist in a number of different crystal structures; which are usually created by a non – symmetric distortion of the cubic structure.

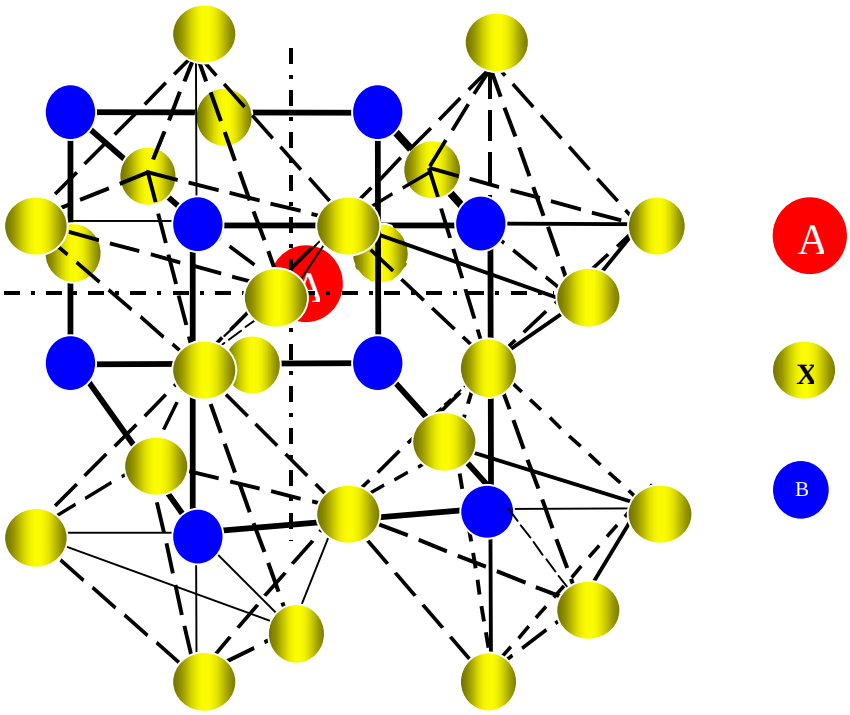


Fig.1.1: Cubic perovskite unit cell.

The rare-earth perovskites have been widely studied in the past using X-ray diffraction techniques. The first study was carried out in 1927 by Goldschmidt [5] and concentrated on $YAlO_3$ and $LaFeO_3$ [6]. Many early studies reported that the perovskites showed mainly cubic or monoclinic structures, and as time went on there were many other structures proposed such as tetragonal or orthorhombic. The lack of conclusive structural determinations amongst these early studies were due to the relative inaccuracies of the X-ray photographic techniques and were compounded by the small magnitude of the structural distortions [7]. Recent studies have been able to more accurately determine the structure and thus can be used as a starting point for modelling. Another way to look at the perfect cubic perovskite structure is to consider corner linked $BO_6$ octahedra with interstitial A cations, see Fig(1.1) . In an idealised cubic perovskite $ABX_3$ constructed of rigid spheres, each cation is large enough to be in contact with an oxygen anion, whereupon the radii of the ions can be related via:

$$R_A + R_O = \sqrt{2}\,(R_B + R_O) \qquad (1\text{-}1)$$

Here, $R_A$, $R_B$, and $R_O$ are the ionic radii of the A-site and B-site cations and the oxygen ion respectively. However, in a real structure, the ions are not rigid spheres and as the A cation decreases in size, there will come a point where it will be too small to remain in contact with the anions of the cubic structure. Therefore the B-O-B links bend slightly, tilting the $BO_6$ octahedra to bring some anions into contact with the A cations. To allow for this distortion, a constant, t, is introduced into the above equation,
and we have :

$$R_A + R_O = t\sqrt{2}\,(R_B + R_O) \qquad (1\text{-}2)$$

The factor t is known as the tolerance factor and can be used as a measure of the degree of distortion of a perovskite from ideal cubic. Therefore, the closer to cubic, the closer the value of the tolerance factor is to 1. This distortion from cubic to orthorhombic is depicted in Fig(1.2), where shaded oxygen octahedra are used .

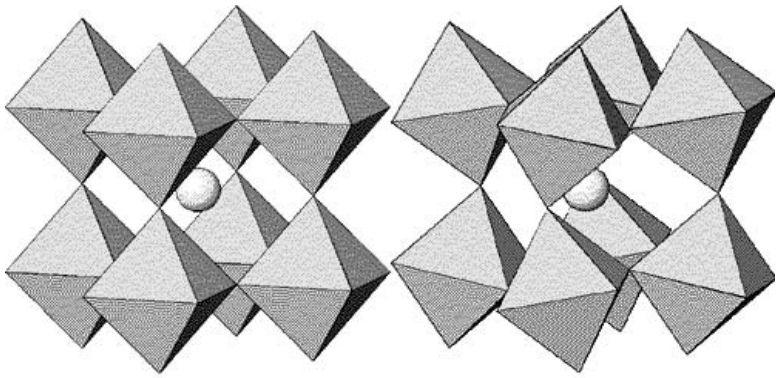

Fig.1.2: Perovskite distortion from cubic (on the left) to orthorhombic (on the right) [8].

Limiting values for the tolerance factor have been determined through experiment and thus it can be said that the perovskite will be cubic if $0.912 < t < 1.0$, and will be orthorhombic if $0.50 < t < 0.912$. For all our substances $Nd_{0.66}(Sr_{1-y}(Li_Z)_y)_{0.34}MnO_3$ the second relation is fulfilled : see table 1 in chapter 4 for $\langle r_A \rangle$ , $\langle t \rangle$ versus y .

## 1.3. Single site electronic states of d-electrons and d – band formation

The atomic orbitals of transition-metal elements are constructed as eigenstates under the spherical potential generated by the free transition-metal ion. When a solid is formed, the atomic orbitals form bands due to the periodic potential of the atoms. The bandwidth is basically determined from the overlap of two d - orbitals on two adjacent transition metal ions each. Because of the relatively small radius of the wave functions as compared to the lattice constant of crystals, d-electron systems have in general a smaller overlap and hence smaller bandwidths than alkaline metals. In transition-metal compounds, the overlap is often determined by indirect transfer between d orbitals through ligand p orbitals. This means that the bandwidth is determined by the overlap or better, hybridization of the d wave function at a transition metal atom and the p wave function at the adjacent ligand atom if the ligand atoms make bridges between two transition-metal atoms. Because of this indirect transfer through ligand atomic orbitals, the d bandwidth becomes in general even narrower. Another origin of the relatively narrow bandwidth in transition-metal compounds is that 4s and 4p bands are pushed well above the d band , whereupon screening effects by the 4s and 4p electrons do not work well. In any case, because of the narrow bandwidth, the tight-binding models constructed from atomic Wannier orbitals provide a good starting point. For further discussions on this point, readers are referred, to the textbook edited by Rado and Suhl [9], and in particularl to the articles by Herring [10] and Anderson [11,12].

The bands that are formed are under the strong influence of anisotropic crystal fields. Because the free atom 3d orbital has the total angular momentum L = 2, it has a fivefold degeneracy ($L_Z$ = 2 , 1 , 0 , -1 , -2) for each spin and hence a total tenfold degeneracy including the spin . This degeneracy is lifted by the anisotropic crystal field.

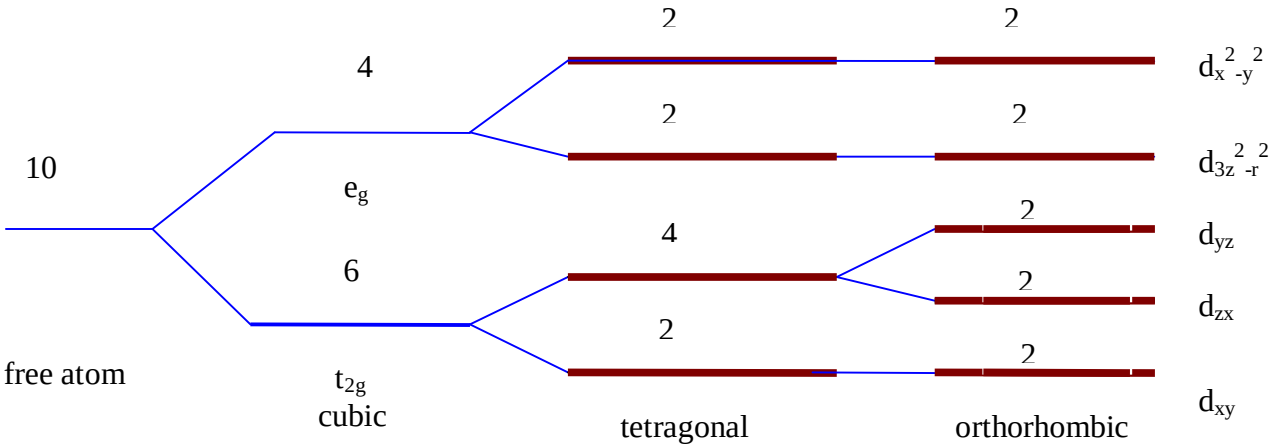


Fig.1.3. Crystal-field splitting of 3d orbitals under cubic, tetragonal, and orthorhombic symmetries. The numbers cited near the levels are the degeneracy including the spin.

Fig(1.3) shows an example of the crystal field splitting, where the cubic lattice symmetry leads to a higher energy level of a fourfold degenerate $e_g$ orbital as compared to the sixfold degenerate orbital, $t_{2g}$ . When a transition-metal atom is surrounded by ligand atoms with an octahedral configuration, the $e_g$ orbital has an anisotropy field with a larger amplitude in the direction of the principle axes, namely, toward the neighboring ligand atoms. The basis of these orbitals may be expanded by $d_{x^2-y^2}$ and $d_{3z^2-r^2}$ orbitals. On the other hand, when the $t_{2g}$ orbital has an anisotropy with larger amplitude of the wave function toward other directions it may be represented by $d_{xy}$ , $d_{yz}$ , and $d_{zx}$ orbitals.

## 1.4. Representation of Crystal field states

The quantum mechanical wave function of an electron takes various shapes when bound to an atomic nucleus by the Coulomb force. Consider a transition-metal atom in a crystal with perovskite structure. It is surrounded by six oxygen ions, $O^{2-}$, which give rise to the crystal field potential, hinder the free rotation of the electrons and quenches the orbital angular momentum by introducing the crystal field splitting to the d orbitals. Wave functions pointing toward the $O^{2-}$ ions have a higher energy as those pointing between them. The former wave functions, $d_{x^2-y^2}$ and $d_{3z^2-r^2}$, are called $e_g$ orbitals, where as the latter , $d_{xy}$, $d_{yz}$ , and $d_{zx}$ , are called $t_{2g}$ orbitals, see Fig (1.3) and Fig (1.4) .

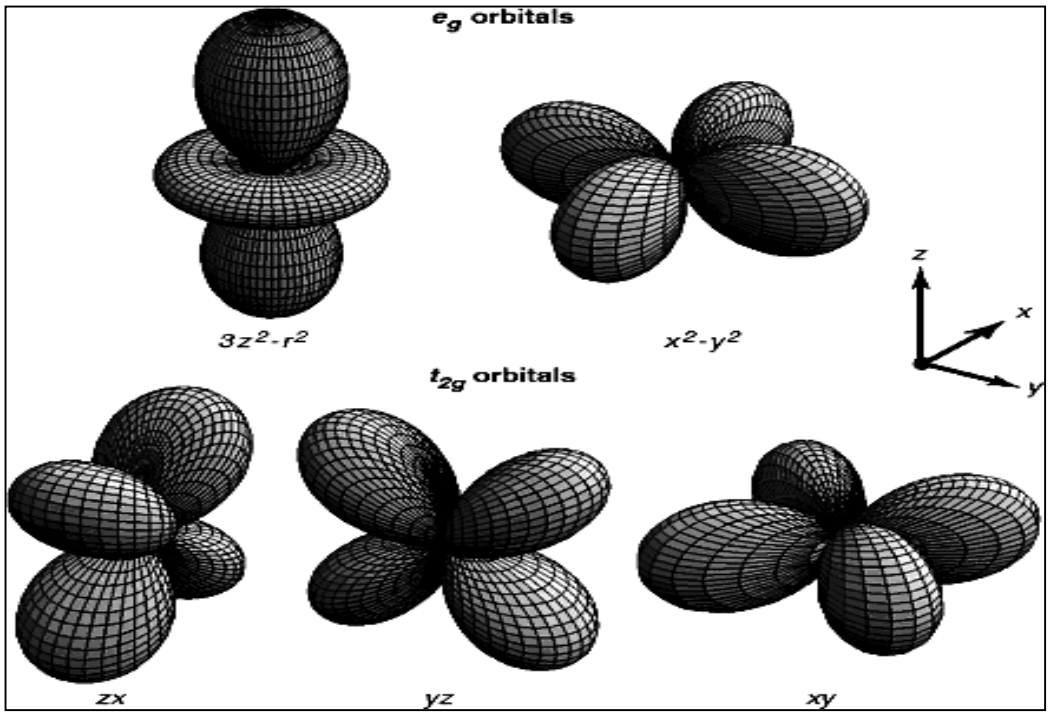


**Fig. 1.4:** Five d orbitals. In the cubic crystal field, this fivefold degeneracy is lifted to two $e_g$ orbitals [($x^2 - y^2$) and ($3z^2 - r^2$)] and three $t_{2g}$ orbitals [(xy), (yz), and (zx)]

## 1.5. Jahn-Teller Effect

Because the Fermi level crosses bands mainly formed by $t_{2g}$ orbitals, the $t_{2g}$ band is the relevant band for low-energy excitations in the case of the above mentioned octahedron structure. By contrast, in transition-metal compounds with heavy transition-metal elements such as Cu and Ni, the $t_{2g}$ band is fully occupied and far below the Fermi level, whereupon the low-energy excitations are expressed within the $e_g$ band, which is formed from $e_g$ atomic orbitals. If degenerate $t_{2g}$ or $e_g$ orbitals are partially filled, this generally leads again to degeneracy of the ground state, which frequently induces the Jahn-Teller distortions to lift the degeneracy.

The static Jahn-Teller effect is a spontaneous structural distortion which results in a splitting of degenerate electronic states so that the energy of the overall system is reduced. For octahedral coordination, susceptible species are $d^4$, $d^9$ , and low spin $d^7$ in which 1 or 3 electrons occupy $e_g$ . The effect is small when the degeneracy is in the $t_{2g}$ group.

## 1.6. Double-exchange mechanism – pair site electronic states

The simultaneous observation of itinerant electron behavior and ferromagnetism in the manganites is explained by Zener's double- exchange mechanism [3]. The basic process of this mechanism is the hopping of a d-hole from $Mn^{4+}$ ($d^3$, $t_{2g}^3$ , S = 3/2 ) to $Mn^{3+}$ ($d^4$, $t_{2g}^3 e_g^1$ , S = 2) via the oxygen , so that the $Mn^{4+}$ and $Mn^{3+}$ ions change places :

$$Mn^{3+}O^{2-}Mn^{4+} \leftrightarrow Mn^{4+}O^{2-}Mn^{3+} \qquad (1\text{-}3)$$

This involves the transfer of an electron from the $Mn^{3+}$ site to the central oxide ion and simultaneously the transfer of an electron from the oxide ion to the $Mn^{4+}$ site . Such a transfer is referred to as double-exchange (DE), and the around state of the pair is characterised not only by the electron hopping but also by a parallel alignment of the residual ion spins S =3/2 and the free

electron spin S =1/2 see Fig(1.5) . The double-exchange is strongly affected by structure parameters such as the Mn-O-Mn bond angle or the Mn-O-Mn transfer integral .

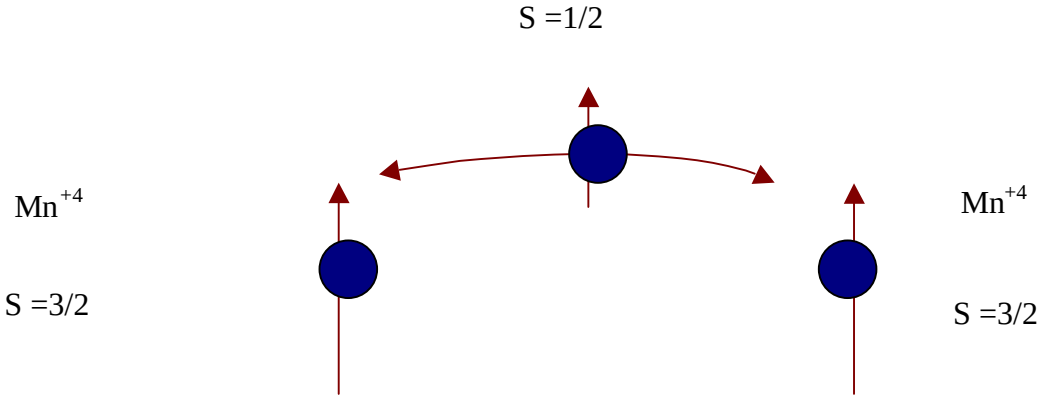


Fig.1.5 : Zener resonant state

## 1.6.1. Zener bond qualification

Goodenough [13] has put forward the suggestion that for a Zener resonant state (like described in paragraph 1.5) to form one needs an additional qualification , i.e the $Mn^{3+}$ - $Mn^{4+}$ octahedral pair has to be completely surrounded by octahedra which contain $Mn^{3+}$ as central ion , i.e. we have to combine pairs of $Mn^{3+}[\ OMn^{3+}]_6$ and $Mn^{4+}[\ OMn^{3+}]_6$ .Rao [14] has refined this idea by noting that the left part of this pair exactly corresponds to the local molecular situation in $RMnO_3$ and the right part to the local situation in $R_{1/2}A_{1/2}MnO_3$. These two compounds limit the existence region of the hole doped manganites $R_{1-x}A_xMnO_3$ . Thus, taking the two sides of the pair as a molecular phase separation , the probability of the existence of a $RMnO_3$ region is 2x and that of a $R_{1/2}A_{1/2}MnO_3$ phase region is (1-2x) , according to the lever rule for phase separations and normalizing the concentration range $0 < x < ½$ to $0 < 2x < 1$ . The probability of finding a pair $Mn^{+3}$- $Mn^{+4}$ without consideration of its environment , however, is x (1-x) according to the formula $R_{1-x}\,A_x\,Mn^{+3}{}_{1-x}\,Mn^{+4}{}_x\,O_3$ . Thus, in summary, the number of active Zener bonds and with it both the Zener carrier concentration and the Curietemperature $T_C$ are proportional to x (1-x) (2x) (1-2x) .This gives a maximum $T_C$ at $x = 0.305$ as is observed . If the bond qualification is not met , say by a second neighbouring valence $Mn^{+4}$ or by a substitute ion for Mn in a neighbouring octahedral site , say $Fe^{+3}$ , the Zener electron gets localized , but is rather weakly bonded (trap site) . These trap or blocking sites also constitute scattering sites for the remaining free Zener carriers.

## 1.7. Superexchange model

The magnetism is governed not only by double exchange, but also by the nature of the superexchange interactions. While delineating the nature of the double exchange and superexchange interactions , de Gennes suggested that a non –collinear magnetic structure forms at intermediate concentrations between the antiferromagnetic and ferromagnetic states. It may also be recalled from the Goodenough Kanamori rules that the $Mn^{3+}$- O - $Mn^{4+}$ superexchange interaction is mostly ferromagnetic while the $Mn^{3+}$- O - $Mn^{3+}$ and $Mn^{4+}$- O - $Mn^{4+}$ interactions are both antiferromagnetic. Thus, with double exchange increasingly blocked , because of the increasing importance of the negative superexchange interactions we expect canted or spincompensated magnetic states with increasing Li –doping ,if Li substitution introduces blocking sites .

## 1.8. Magnetic and Crystal Structures of $Nd_{1-x}Sr_xMnO_3$

We begin with the description of our base compound by examining the x-T phase diagram of the $Nd_{1-x}Sr_xMnO_3$ system for $0.3 < x < 0.8$ , as shown in Fig(1.6). In the distorted perovskite crystal structure, the Mn ions are surrounded by six O ions, and the $MnO_6$ octahedra form a pseudo-cubic lattice with Nd or Sr ions occupying its body-centered positions . Due to the buckling of the octahedra, however, the unit cell becomes orthorhombic with dimensions $\sqrt{2}x\sqrt{2}x2$ of the O´ cubic cell . Fig(1.7) shows the orthorhombic unit cell of the manganite $Nd_{0.45}Sr_{0.55}MnO_3$ .

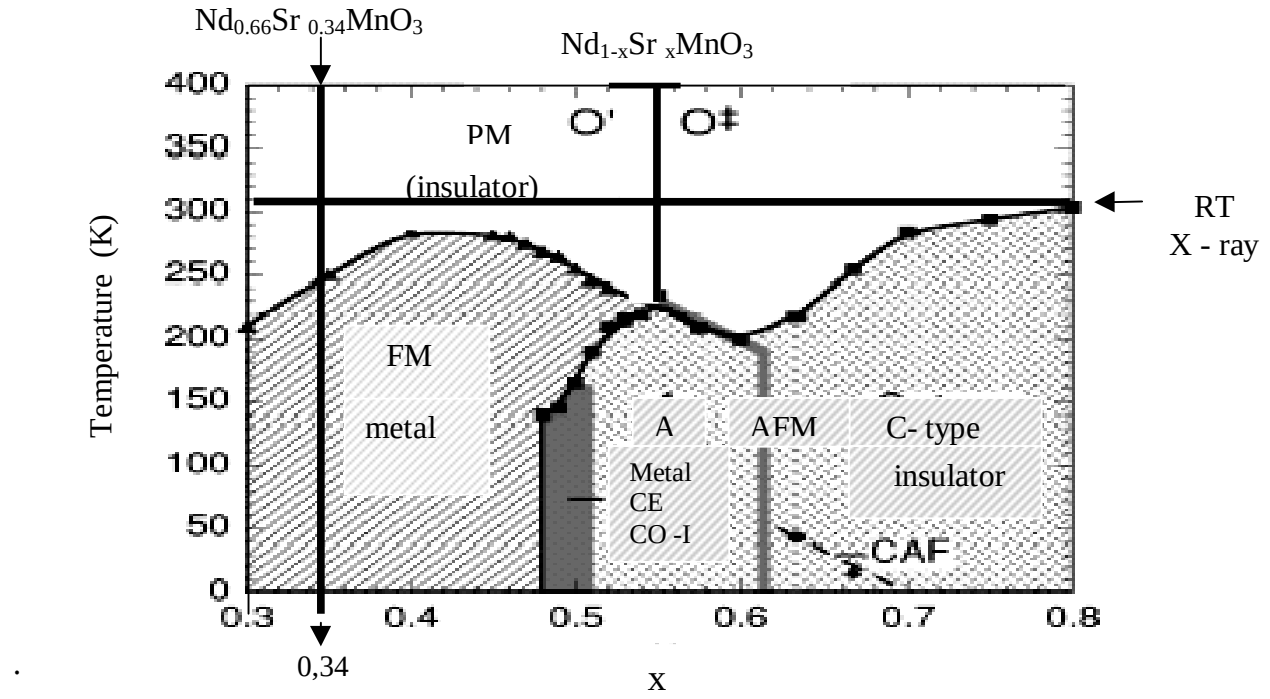


Fig .1.6: Phase diagram of $Nd_{1-x}Sr_xMnO_3$ [15] Each phase is denoted by capitalized labels; PM: paramagnetic insulating, FM: ferromagnetic, AFM: antiferromagnetic, CO-I: charge ordered insulator, CE: CE-type charge/spin order, A: A-type antiferromagnetic order, C: C-type antiferromagnetic order, CAF: possible canted antiferromagnetic order.

There are two orthorhombic phases displayed. One is the O´ phase with $c/\sqrt{2} < b < a$ [16] , which appears in the lower Sr concentration region specifically for $x \leq 0.55$ at room temperature. The other is a pseudo-tetragonal $O^{\ddagger}$ phase with $a \approx b < c/\sqrt{2}$ for $x \geq 0.55$. At low temperatures, on the other hand, the region of the O´ phase expands, and the phase boundary shifts towards $x \approx 0.60$. In addition, a monoclinic structure was detected near the low-temperature structural phase boundary. For $0.55 \leq x \leq 0.60$, a structural transition from the O´ phase to the $O^{\ddagger}$ phase coincides with the AFM transition temperature $T_N$ . For $x < 0.48$ , i.e also for our base compound $Nd_{0.66}Sr_{0.34}MnO_3$ the ground state is a ferromagnetic metal.

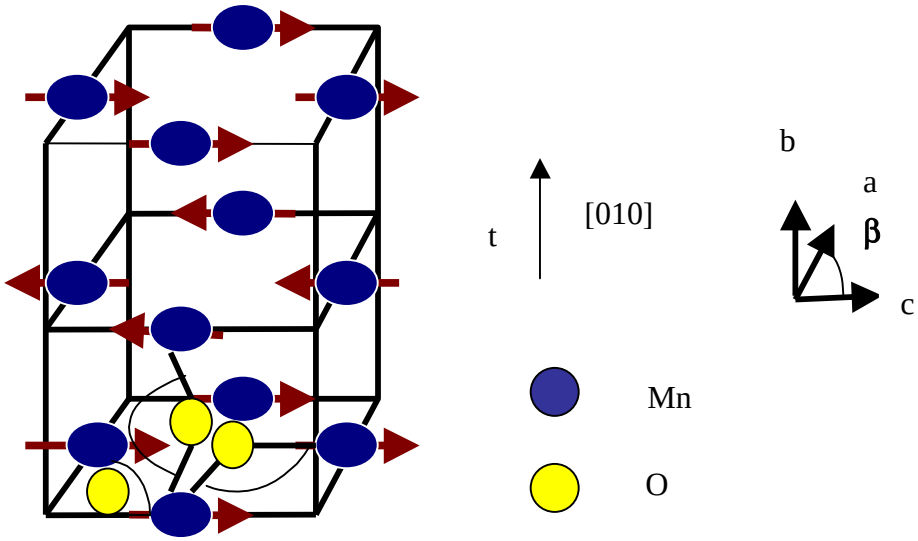


Fig.1.7: The orthorhombic unit cell of the manganite $Nd_{0.45}Sr_{0.55}MnO_3$ [17] .

## 1.9. $Sr^{+2} \leftrightarrow Li^{+}$ Monovalent cation substitution

The electric and magnetic properties of oxides of the perovskite type structure have been an important subject in recent solid state physics and chemistry. However there are only few reports on perovskite manganites doped with monovalent (alkali-) metal ions. Some compounds substituted by monovalent alkali metals such as $K^+$, $Rb^+$, $Na^+$ were synthesized and tested as oxidation catalysts for exhaust gases within internal combustion engines [18]. Recently, these compounds have also been investigatied as potential giant magnetoresistance MR candidates [19–21] and as cathodes for solid oxide fuel cells .

# CHAPTER II

# EXPERIMENTAL TECHNIQUES

## Preparation of the Samples and Characterization

### 2.1. Sample Preparation

If one wants to substitute the divalent $Sr^{2+}$ in $Nd_{0.66}\ Sr_{0.34}MnO_3$ by the monovalent $Li^{1+}$ one can attempt either a site substitution : $Sr^{2+} \leftrightarrow Li^{1+}$ , hoping that the charge disproportion $Mn^{+4}/\ Mn^{+3}$ will shift to ensure the charge balance ,or one can try for a charge replacement substitution : $Sr^{2+} \leftrightarrow Li_2^{1+}$,hoping that the Li – pair will occupy adjoining substitutional and interstitial sites.

### 2.1.1. Lattice site substitution

The target formula for substitutional site replacement would be :

$$Nd_{0.66}\ (Sr_{1-y}\ Li_y\ )_{0.34}MnO_3 \qquad (I)$$

and accordingly a fraction $0 < \alpha < 1$ of the molecular weight sum :

$$0.66[Nd_2O_3] + 0.34\ y\ [Li_2CO_3] + 2*\ 0.34\ (1-y)\ [SrCO_3]\ + [Mn_2O_3]$$

has to be weighed in .The brackets indicate the molecular weight , i . e $[Nd_2O_3] = 336.48$ g , $[Li_2CO_3] = 73.89$ g , $[Mn_2O_3] = 157.87$ g , $[SrCO_3] = 147.63$ g .
For the stoichiometry , only the relative amounts of the the cations Nd , Sr , Li , Mn have to be considered , as gaseous $CO_2$ is supposed to leave the sample , while $O_2$ is supposed to enter the sample until the oxygen content $O_3$ is selfadjusted , at least when we heat in air .

### 2.1.2. Charge substitution

If one wants to replace one Sr by a Li – pair ,the target formula would be :

$$Nd_{0.66}\ (Sr_{1-y}\ (Li_2\ )_y\ )_{0.34}MnO_3 \qquad (II)$$

Here the following mole fractions have to be added:

$$\frac{1}{2}\ .\ 0.66\ [Nd_2O_3] + 0.34\ .\ \{\ y.\ [Li_2CO_3] + (1-y)\ [SrCO_3]\ \} + \frac{1}{2}\ [Mn_2O_3]$$

Making this Li-series, we change only the composition inside the bracket . Using the weight % $Li_2CO_3$ [$a$] and $SrCO_3$ [1-$a$] under conservation of the total molar ratio ( 0.34) , for the conversion of $a$ into y and vice versa we have to use :

$$a = \frac{y[73.89]}{y[73.89] + (1-y)[147.63]} \quad ; \quad y = \frac{\xi\ [147\ .63\ ]}{[73\ .89\ ] + \xi\ [147\ .63\ ]} \quad ; \quad \xi = \frac{a}{1-a} \qquad (2\text{-}1)$$

Table 1 . The values of $a$ and the calculated values of $y$ and $\xi$ according to eq. (2 - 1)

| $a$ | $1-a$ | $y$ | 1-$y$ | $\xi = \frac{a}{1-a}$ | $\frac{a}{y}$ |
|---|---|---|---|---|---|
| 0 | 1 | 0 | 1 | 1 | -- |
| 0.02 | 0.975 | 0.0486 | 0.951 | 0.0256 | 0.514 |
| 0.05 | 0.95 | 0.0951 | 0.905 | 0.0529 | 0.526 |
| 0.075 | 0.925 | 0.1394 | 0.861 | 0.811 | 0.538 |
| 0.1 | 0.9 | 0.1817 | 0.818 | 0.1111 | 0.550 |
| 0.15 | 0.85 | 0.2607 | 0.739 | 0.1765 | 0.575 |
| 0.2 | 0.8 | 0.3331 | 0.667 | 0.2500 | 0.6 |
| 0.25 | 0.75 | 0.3997 | 0.600 | 0.3333 | 0.625 |
| 0.3 | 0.7 | 0.4613 | 0.539 | 0.4286 | 0.650 |

Since Li is a very volatile element , firing the mixtures at high temperatures will probably result in a loss of Li . Therefore it might be better to start with an excess of Li . That is why we choose to weigh in the charge substitution scenario (II) . One can speculate , however , that through selfadjustment of the volatile Li ,the final composition will be closer to the lattice site substitutional case (I) . For the resulting composition can combine both approaches using the formula :

$$Nd_{0.66}(Sr_{1-y}(Li_z)_y)_{0.34}MnO_3 \quad ; \quad 1 < z < 2 \qquad (III)$$

Which, however, leaves the actual Li - content and its distribution on substitutional and interstitial sites somewhat open .

**2.1.3. Determination of the composition**

The polycrystalline samples were prepared using standard ceramic techniques :

I . for series (1) :

stoichiometric amounts of $Nd_2O_3$ , $Li_2CO_3$ , $Mn_2O_3$ , and $SrCO_3$ powders were thoroughly mixed , pressed into tablets to avoid Li losses and heated in air at 1173 K for one day. The powder thus obtained was ground ,pelletized and sintered at 1373 K for 2 days without intermediate regrinding ; then the furnace was cooled to room temperature with a rate of 60 $^0$C /h.

II . for series (2) :

stoichiometric amounts of $Nd_2O_3$ , $Li_2CO_3$ , $Mn_2O_3$ , and $SrCO_3$ powders were thoroughly mixed , pelletized and heated in air at 1273 K for 48 h with an intermediate regrinding. The powder thus obtained was ground ,pelletized and sintered at 1473 K for 48 h with intermediate regrinding ; then the furnace was cooled to room temperature with a rate of 60 $^0$C /h.

The determination of the Li- content cannot be done by X-ray fluorescence (EDX), as the Li – nuclear scattering cross section is too low . Chemical methods are left which , however ,consume the sample. Here we have used flame spectroscopy (Fa.Eretec , Flammen – AAS (Atomic Absorption Spectroscopy)) for determining the overall Li – content of two specific samples .The error given by Eretec is $\leq 5\%$ . The results are compiled in Table 2.

Table 2.The content of Sr and Li from the Atomic Absorbtion Spectroscopy data for y = 0.18 series(1) and y = 0.46 series(2) .

| $Nd_{0.66}(Sr_{1-y}(Li_z)_y)_{0.34}MnO_3$ | Sr (exp.) [weight %] | Sr (calc.) [weight %] | Li (exp.) [weight %] | Li (calc.) [weight %] | |
|---|---|---|---|---|---|
| | | | | z =1 | z =2 |
| $Nd_{0.66}(Sr/Li)_{0.34}MnO_3$ Series(1) , y = 0.18 | 11.6 | 11.5 | 0.34 | 0.2 | 0.4 |
| $Nd_{0.66}(Sr/Li)_{0.34}MnO_3$ Series(2) , y = 0.46 | 8,61 | 7.44 | 1.01 | 0.51 | 1.02 |

Specifically, the samples with y =0.18 of series (1) and y =0.46 of series (2) were analysed .The Sr- content is recovered rather accurately i.e with an error of about 5% as given by the company , while the reported Li- content varied strongly. The average Li –content is given in table 2 with an error of ≥ 20% .This large error cannot be due to the differences in the preparation conditions alone ,as these were kept constant .Also, the physical properties change rather continuously with the nominal Li – content , see for example the almost linear drop in the metal – insulator transition temperature $T_m$ with y as shown in Fig(2.1) .Therefore we have to conclude

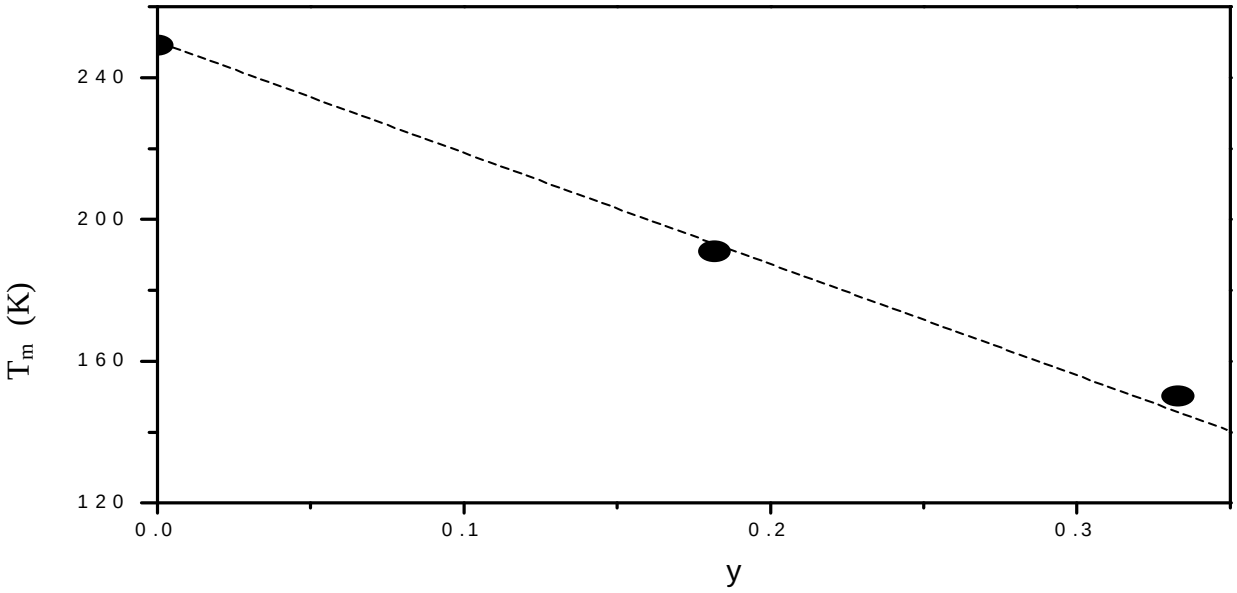


that the Spectroscopic

Fig. 2.1: The metal – insulator transition temperature $T_m$ versus Li- content y for series(1)

determination of the Li also can have a large error. Thus , while we cannot accurately determine the Li –content , we know that Li is actually distributed inside the perovskite lattice in proportional amounts . Note , that in Fig(2.1) the compound with the highest Li –content has about ½ of the Sr replaced , which suggests that the Li-doped compounds are stable only up to this composition. We can indirectly determine the Li – content of the other samples from their physical properties, here from $T_m(y)$ as depicted in Fig(2.1) , but only if z is known and constant for a given series. For the series 1,2 compounds we estimate $z_1 \approx 1.5$ (series 1) , and $z_2 \approx 2$ (series 2) from Table2 .

## 2.2. Sample characterization

### 2.2.1 Scanning Electron Microscopy (SEM)

Scanning Electron Microscopy (SEM) [Cam scan -4 with tungsten cathode from Cambridge Ltd, GB] has been used to investigate the identity and composition of single crystallites .Specifically; we have used a x-ray fluorescence extension of the SEM [energy dispersive x-ray micro analysis system "Voyager" with Si (Li) –detector and an ultra thin window from Thermo NORAN , USA ] .

Fig(2.2) suggests that the sample with y = 0 exhibits a single phase, as the habitus of all crystallites is the same. Indeed Fig.2.3a shows that every crystallite has the same x-ray fluorescence counts from Mn , O , Sr , Nd . X-ray diffraction also shows a single phase. The sample with y = 0.33 Fig(2.2) exhibits also a single phase , although the crystallites have different sizes . Again every crystallite has the same counts from Mn , O , Sr , Nd – atoms , see Fig(2.3b). In contrast, the sample with y = 1 exhibits three phases : Fig (2.2) shows three different habitus A , B ,and C . This is confirmed by the x – ray fluorescence , as all three crystallites have different counts from Mn ,O , and Nd see Fig (2.3c ) , and also by x- ray diffraction (see Chap. 2.2).
Although the relative amounts of the elements Nd , Sr , Mn and O cannot be derived from Fig(3a-c) , without a calibration, the energy dispersive x-ray detection proves their existence and equal distribution inside each crystallite .If 100 % $Li_2CO_3$ is weighed in , the perovskite structure is not stable anymore .The weighed in mixture decomposes into three phases ,as is demonstrated by Fig.2.3c .Consistently , we found the stability limit of the perovskite structure to be a $\geq 30\%$ or y $\geq$ 0.46 at % for series (1) and series (2) , respectively see Fig(2.1).

### 2.2.2 .X-ray powder diffraction

X-ray powder diffraction at room temperature was carried out using a Rigaku. X-ray diffraction spectrometer with a rotating anode and Cu Kα radiation of wavelength 1.54 Å.The analysis resolved an orthorhombically distorted perovskite structure and the Appleman-Refinement gave the lattice parameters as displayed in Table 3 . Small amounts of $Mn_2O_3$ (< 5%) were resolved for the base compound . Further secondary phases were found for the compounds containing Li : $LiMnO_3$ and $Li_2O_2$ ( < 5% ; y = 0.18).
The x –ray diffraction diagrams of $Nd_{0.66}$ $(Sr_{1-y}(Li_{Z1})_y)_{0.34}$ $MnO_3$ ; at y = 0 , 0.18 , 0.33 , 1 (series 1) are shown in Fig(2.4) The analysis of the X-ray data show that there are small extra peaks aside from the orthorhombic perovskite phase in all three the samples ; in particular , some new peaks appear at $2\theta = 32.7°$ , $2\theta = 18.7°$ , $2\theta = 44.7°$ which are indexed as $SrMnO_3$ , NdC , $LiMnO_3$ . These impurity phases appear with y > 0 and increase somewhat with increasing Li –content. The compound with y =1 definitly is a multiphase system and shows three different phases in comparable amounts. The change in the lattice parameters with increasing y up to 0.46 was less than 0.5%.

X-ray powder diffraction (XRD) was also performed on the compounds $Nd_{0.66}$ $(Sr_{1-y}(Li_{Z2})_y)_{0.34}$ $MnO_3$ ; series (2) at y = 0 , 0.05 , 0.1 , 0.14 , 0.18 , 0.26 , 0.33 , 0.40 , 0.46 , the results are shown in Fig(2.5) . The diagram show that at room temperature the synthesized samples are polycrystalline and have an orthorhombically distorted perovskite structure (Pbnm) with : a =5.464 Å , b = 7.699 Å , c = 5.451 Å at y = 0 ( see Table 3); literature values for similar compounds are shown in Table 4.The values are close , supporting the analysis used here.

The dependence of the lattice constants on the Li content of series 2 [$Nd_{0.66}(Sr_{1-y}(Li_{Z2})_y)_{0.34}MnO_3$] are also shown in Table 3 .The change in the lattice parameters with increasing y up to 0.33 is again less than 0.5%.

For both series the substitution of Li for Sr produces only very small changes of the lattice constants , probably because of the small size of $Li^+$ . The only significant changes are small and occur at large and small y . A slight decrease in a , c is observed initially ; specifically , From y = 0.1 to y = 0.33 , the lattice parameters a and c change, but not the volume . For y > 0.33 the volume of the unit cell decreases with increasing Li – content Fig(2.6) . This is similar to what is found in $La_{1-x}\,Li_x\,MnO_3$ at x = 0.2 , 0.3 where a , b decrease with increasing Li – content , while c and the volume increase [22].

Table 3 .The lattice parameters at different Li contents for $Nd_{0.66}\,(Sr_{1-y}\,(Li_{Z2})_y\,)_{0.34}Mn\,O_3$; series (2)

| Mol % $Li_2CO_3$ | a (Å) | b (Å) | c (Å) | Unit cell Volume ($Å^3$) |
|---|---|---|---|---|
| 0 | 5.464 ± 0.005 | 7.699 ± 0.005 | 5.451 ± 0.003 | 229.369 ± 0.006 |
| 0,05 | 5.444 ± 0.007 | 7.699 ± 0.003 | 5.464 ± 0.002 | 229.033 ± 0.009 |
| 0,10 | 5.447 ± 0.001 | 7.699 ± 0.001 | 5.463 ± 0.002 | 229.152 ± 0.001 |
| 0,18 | 5.449 ± 0.001 | 7.701 ± 0.005 | 5.461 ± 0.005 | 229.174 ± 0.001 |
| 0,26 | 5.451 ± 0.003 | 7.700 ± 0.006 | 5.459 ± 0.002 | 229.171± 0.001 |
| 0,33 | 5.452 ± 0.002 | 7.699 ± 0.007 | 5.459 ± 0.002 | 229.191± 0.001 |
| 0,40 | 5.447 ± 0.008 | 7.694 ± 0.009 | 5.455 ± 0.009 | 228.680 ± 0.009 |
| 0,46 | 5.443 ± 0.002 | 7.688 ± 0.006 | 5.453 ± 0.003 | 228.254 ± 0.002 |
| $La_{0.8}Li_{0.2}MnO_3$ [22] | 5.527 | 5.494 | 7.780 | 352.600 |
| $Nd_{0.7}Sr_{0.3}MnO_{3-\delta}$ [23] | 5.463 | 7.698 | 5.453 | 229.321 |

Table 4 . Lattice constants for similar compounds.

| Compound | a (Å) | b (Å) | c (Å) |
|---|---|---|---|
| $Nd_{0.5}Sr_{0.5}MnO_3$ [24] | 5.430 | 7.630 | 5.470 |
| $Nd_{0.5}Sr_{0.5}MnO_3$ [25] | 5.445 | 7.532 | 5.515 |
| $Nd_{0.45}Sr_{0.55}MnO_3$ [25] | 5.440 | 7.512 | 5.494 |
| $Nd_{0.9}Sr_{0.1}MnO_3$ [26] | 5.450 | 5.812 | 7.697 |
| $Nd_{0.5}Sr_{0.5}MnO_3$ [26] | 5.466 | 5.697 | 7.829 |

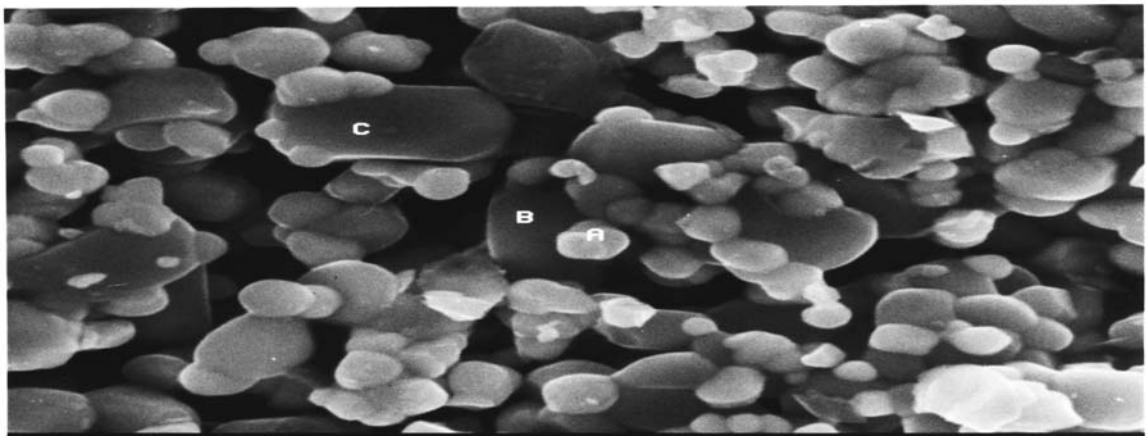


c) $Nd_{0.66}(Sr_{1-y}(Li_{Z1})_y)_{0.34}MnO_3$ with y = 1

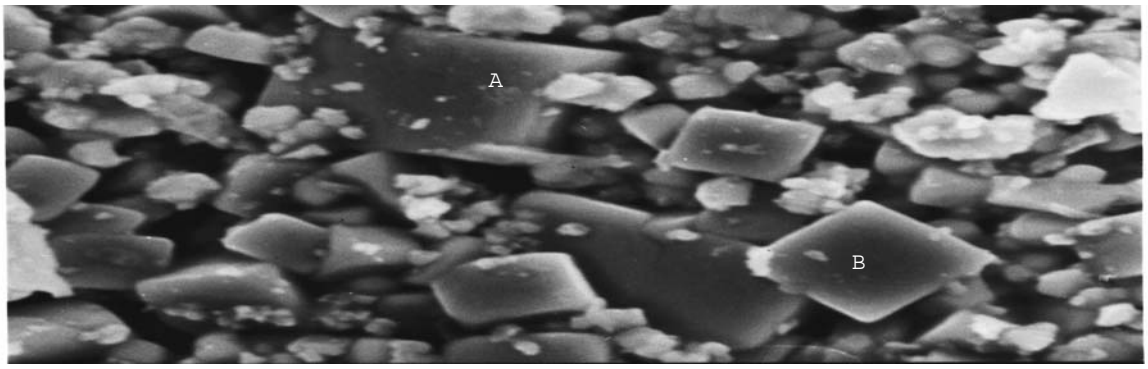


b) $Nd_{0.66}(Sr_{1-y}(Li_{Z1})_y)_{0.34}MnO_3$ with y = 0.33

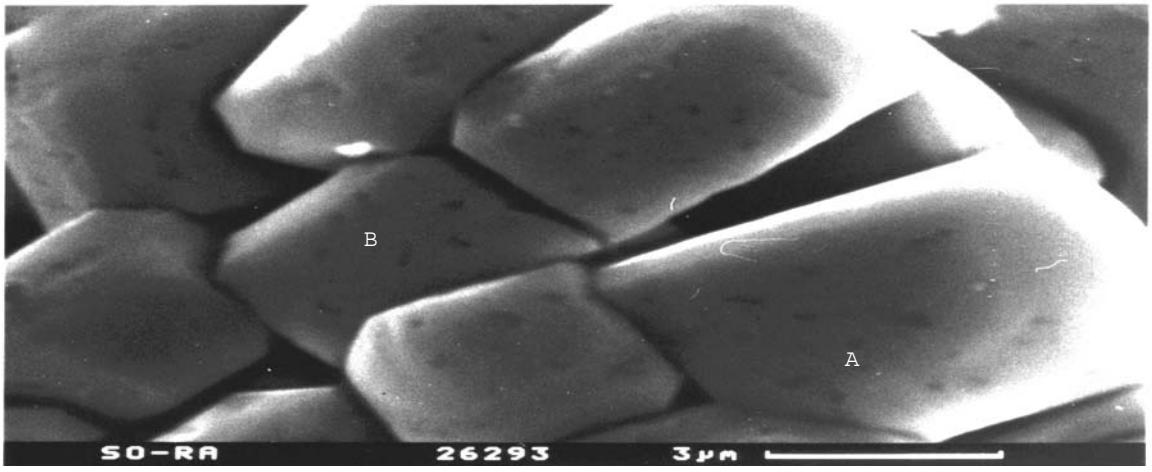


a) $Nd_{0.66}(Sr_{1-y}(Li_{Z1})_y)_{0.34}MnO_3$ with y = 0

Fig.2.2: Scanning electron images of $Nd_{0.66}(Sr_{1-y}(Li_{Z1})_y)_{0.34}MnO_3$ with y = 0 (a), y = 0.33 (b) and y =1 (c) ( series 1).

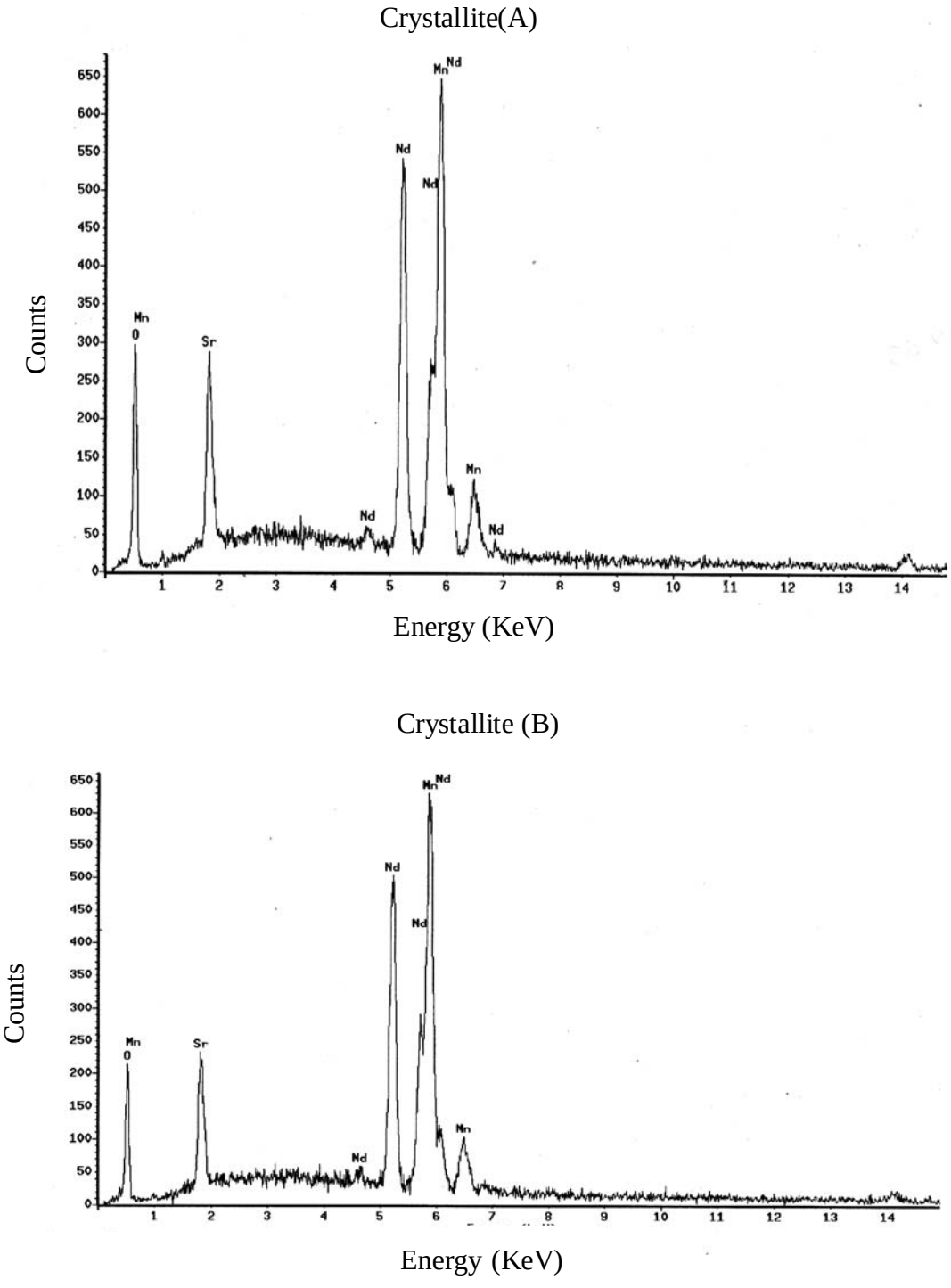


Fig.2.3a: Mn , O , Sr , Nd X – ray fluorescence counts in two different crystallites of $Nd_{0.66}(Sr_{1-y}(Li_{Z1})_y)_{0.34}MnO_3$ with y = 0; (series 1)

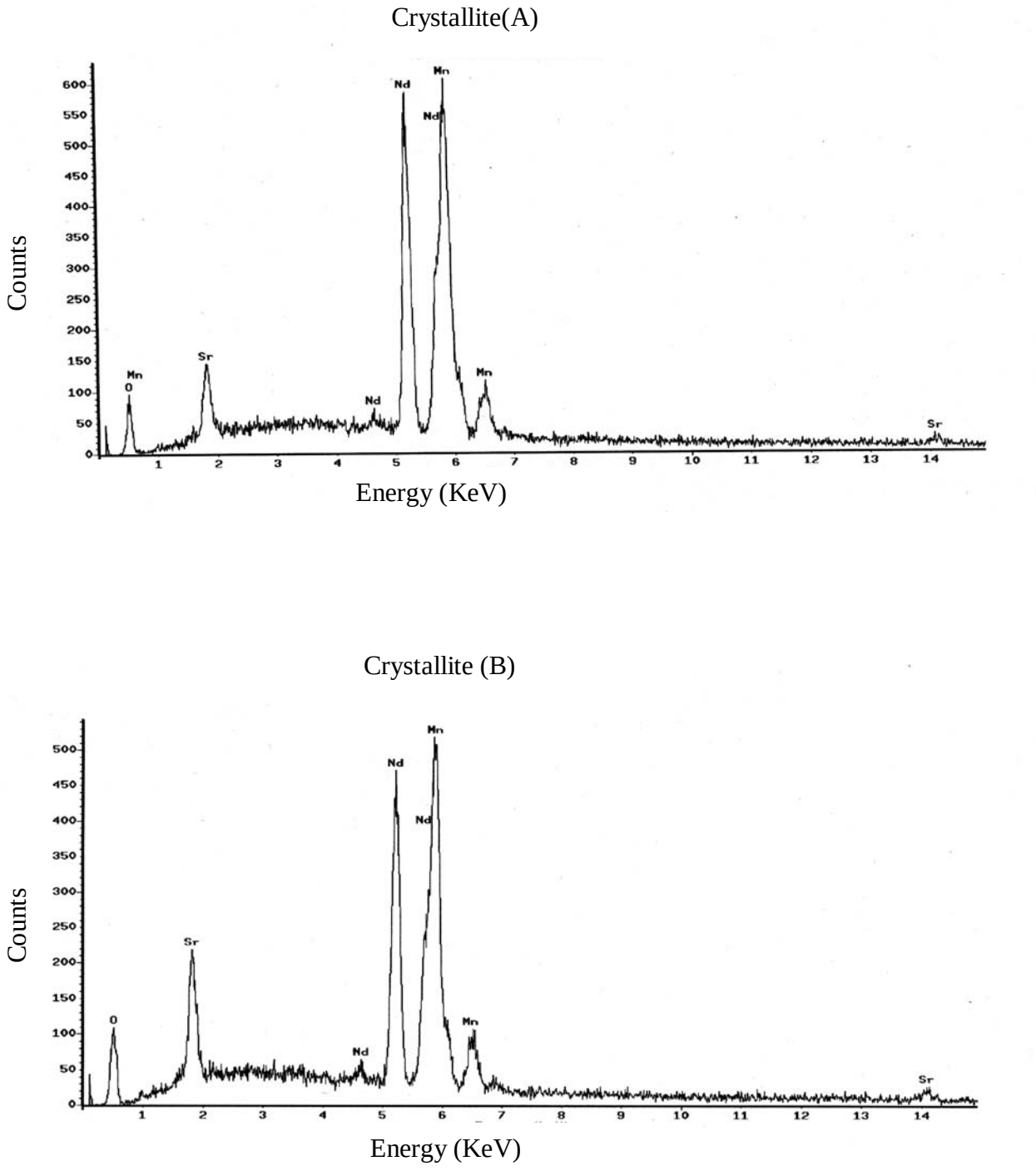


Fig.2.3b: Mn, O , Sr , Nd X – ray fluorescence counts in two different crystallites of $Nd_{0.66}(Sr_{1-y}(Li_{Z1})_y)_{0.34}MnO_3$ with y = 0.33 (series 1) .

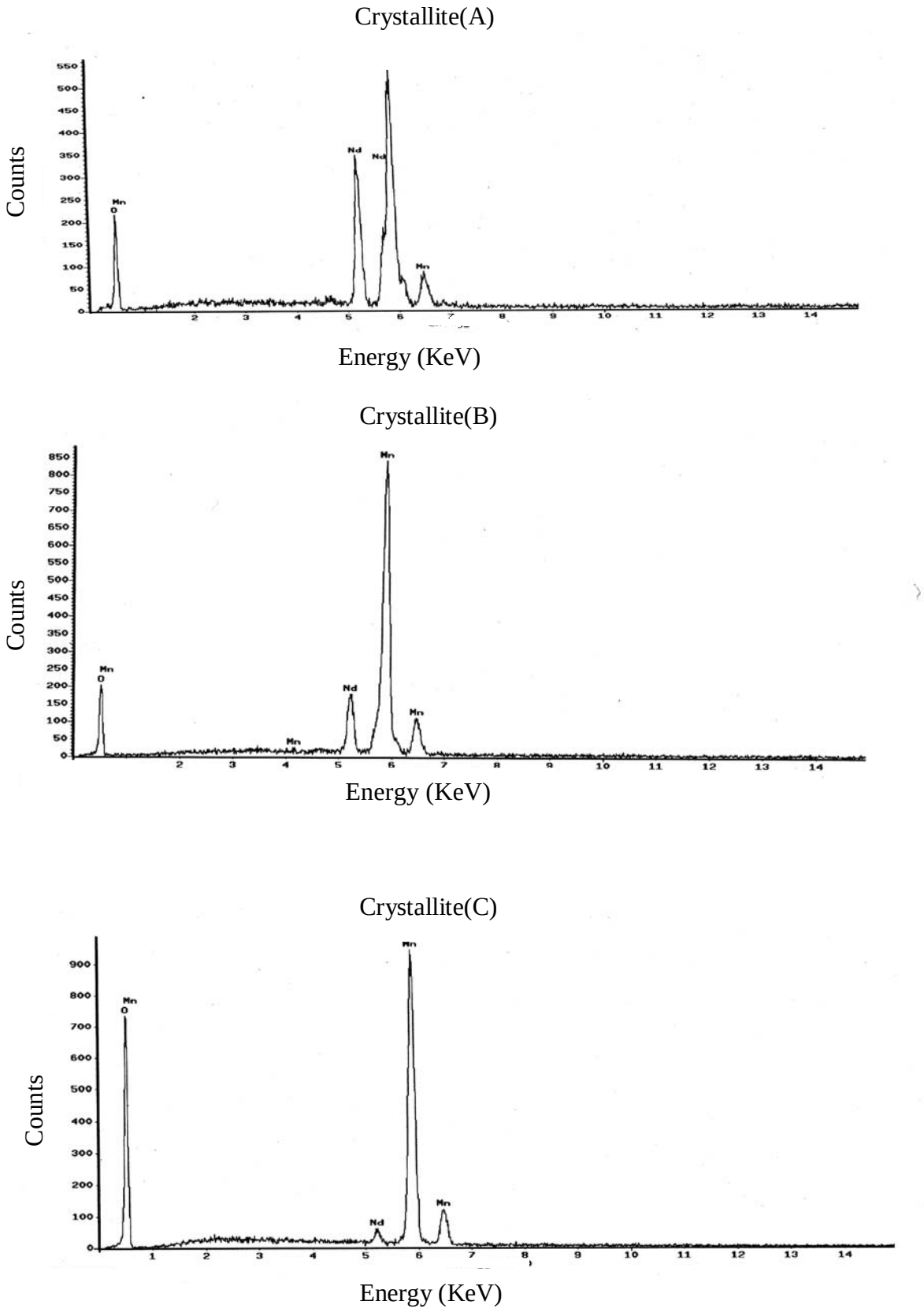


Fig.2.3c: Mn , O , Nd X – ray fluorescence counts in three different crystallites A , B ,C of $Nd_{0.66}(Sr_{1-y}(Li_{Z1})_y)_{0.34}MnO_3$ with y = 1 showing three different phases (series 1) .

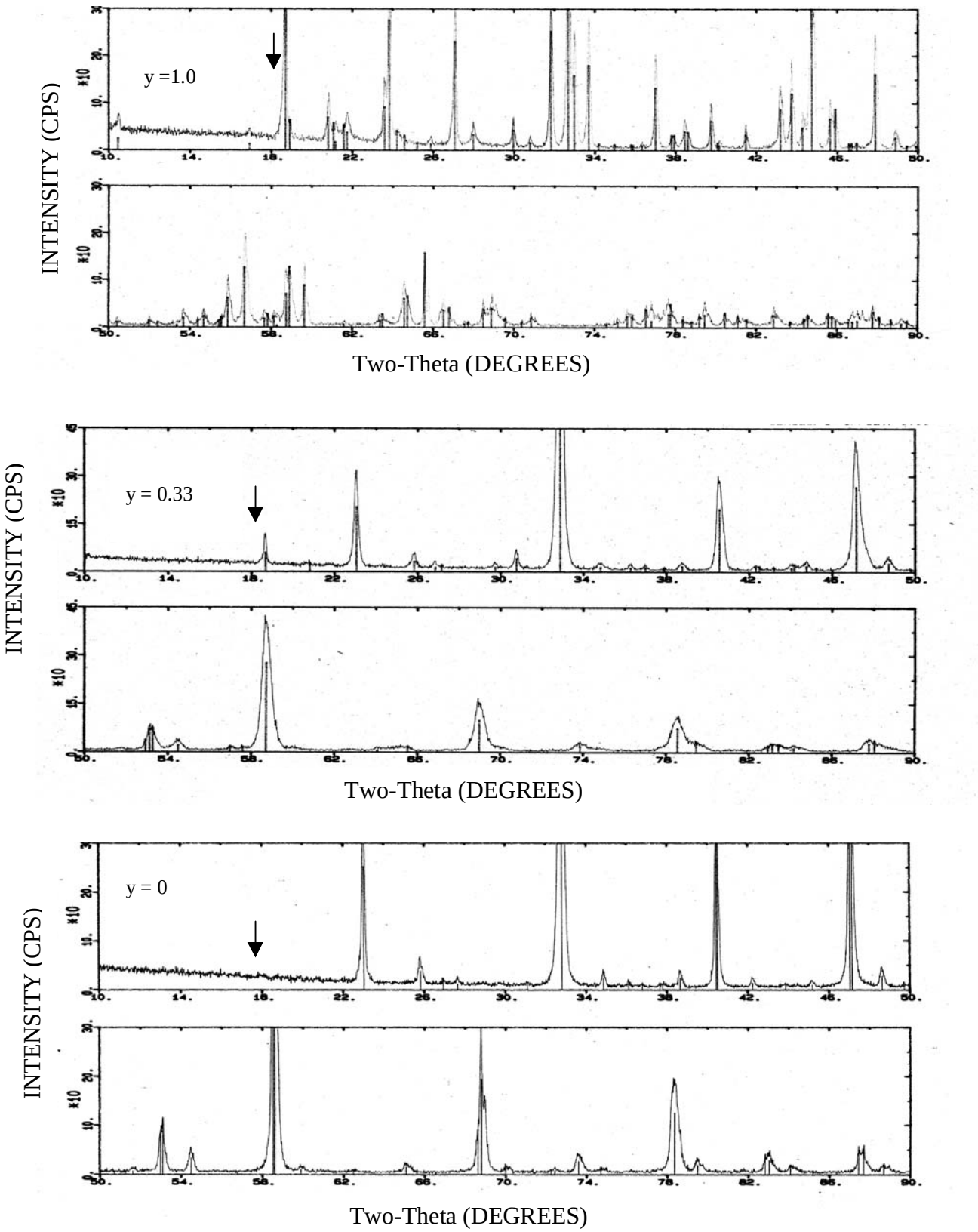


Fig.2.4: X-ray diffraction diagram for $Nd_{0.66}\ (Sr_{1-y}(Li_{Z1})_y)_{0.34}\ MnO_3$
with y = 0 , 0.33 , 1 ; series (1)
arrows : small peaks related to impurity phases

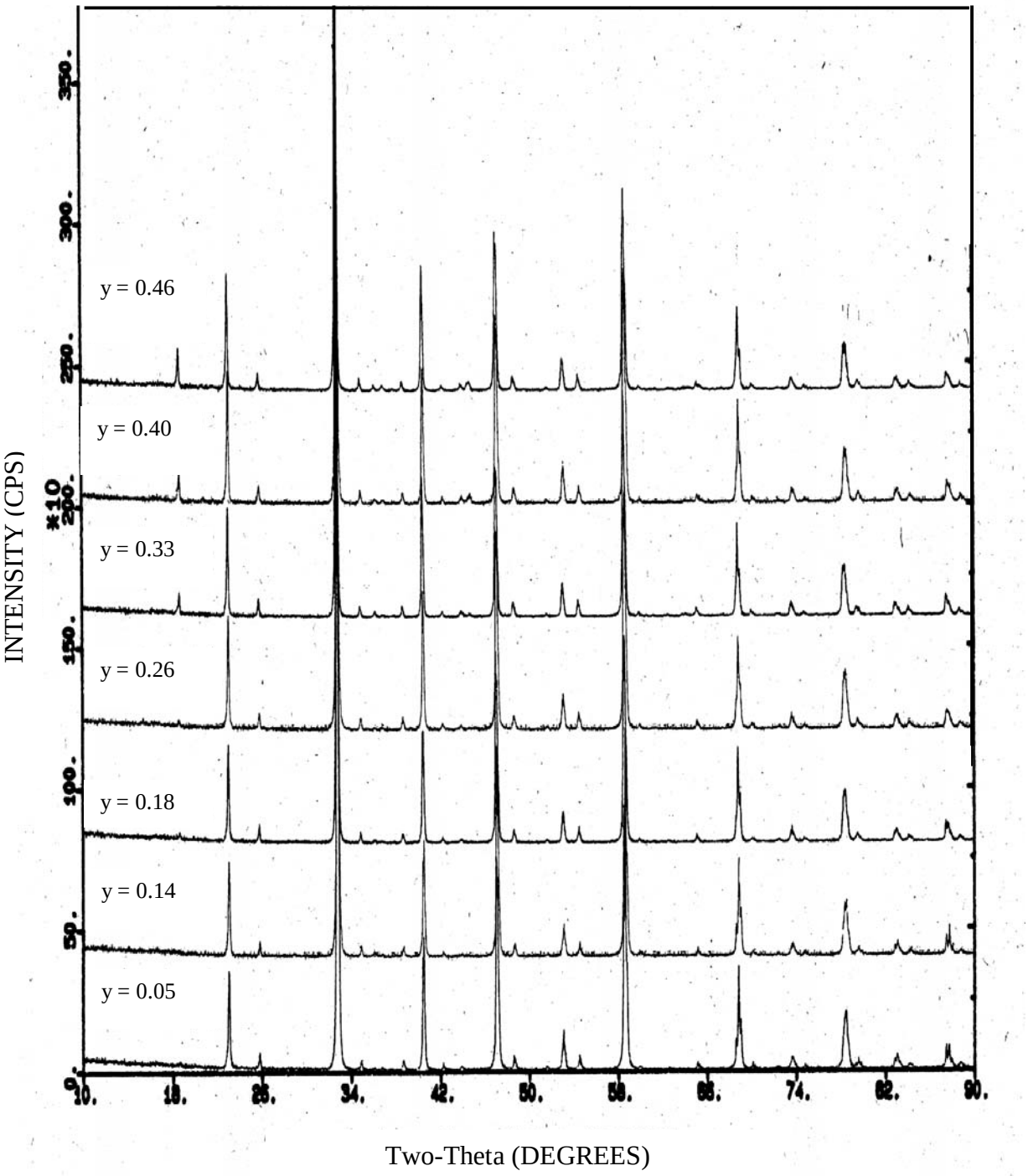


Fig.2.5: X-ray diffraction diagram for $Nd_{0.66}$ $(Sr_{1-y}(Li_{Z2})_y)_{0.34}MnO_3$ with y = 0.05 , 0.14 , 0.18 ,0.26 , 0.33 , 0.40 , 0.46 ; series (2)

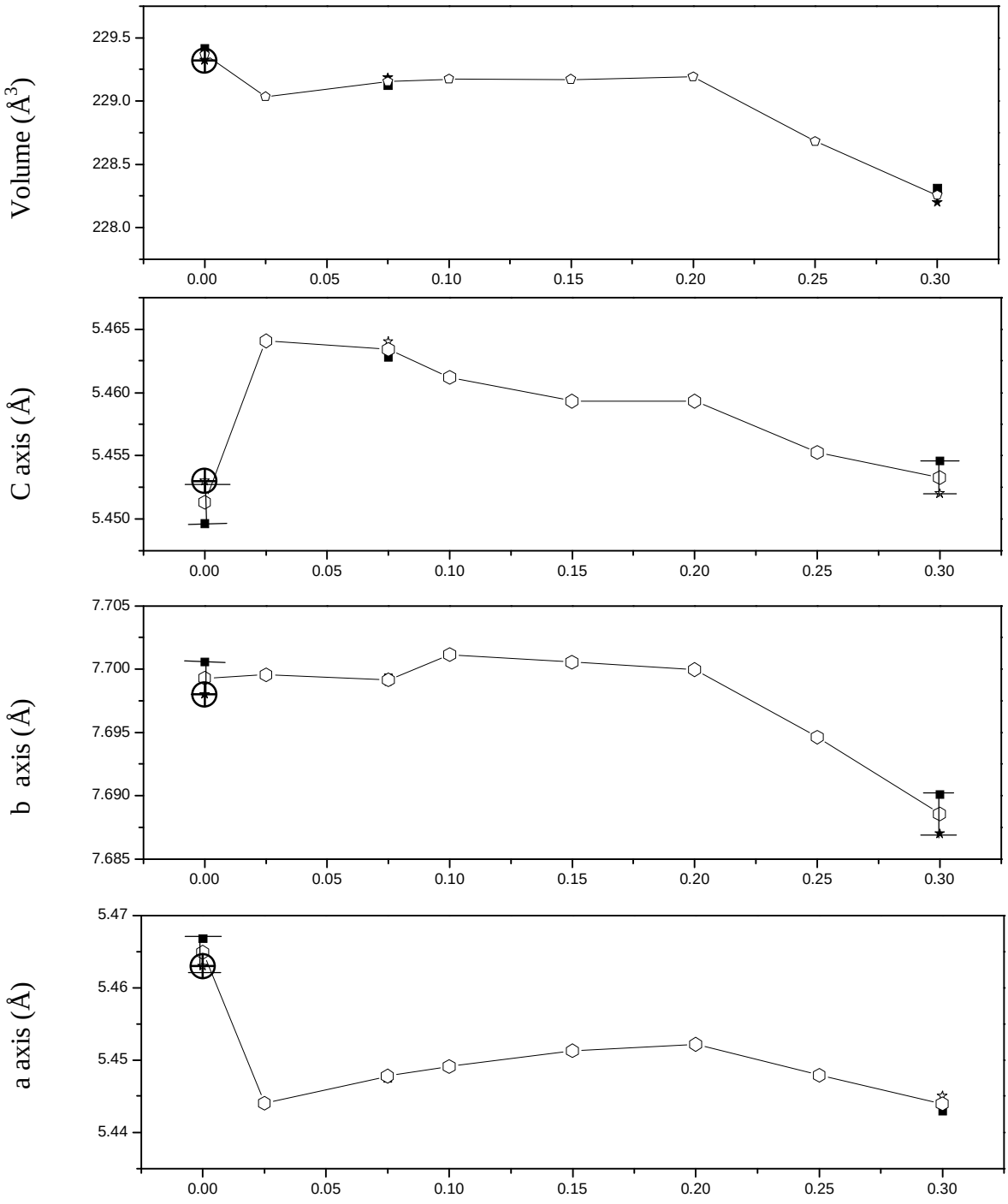


Fig.2.6: The dependence of the lattice constants on the Li content y for $Nd_{0.66}(Sr_{1y}(Li_{Z2})_y)_{0.34}MnO_3$ with y = 0 , 0.05 , 0.1 , 0.14 , 0.18 , 0.26 , 0.33 , 0.40 , 0.46 series (2) ( $\oplus$ for $Nd_{0.7}Sr_{0.3}MnO_{3-\delta}$ [23]) , preparational error shown for y = 0)

## 2.3.Measurement of the Specific Heat Capacity

The specific heat capacity measurements were carried out using a differential scanning calorimeter (Perkin Elmer DSC-2), calibrated for the temperature and caloric scales according to the GSFTA (German Society For Thermal Analysis) recommendations using sapphirs as the reference material in conjuction with pure argon gas [27] The heat capacity of a substance is defined as the amount of heat required to raise the temperature of the substance by 1 K The heat capacity of a monoatomic substance varies from zero at low temperatures to a constant value of 6R/2 at very high temperatures (the Dulong-Petit Law). In a solid, the heat is stored in the vibrations of atoms, and the lattice heat capacity can be described by Debye's theory.

Phase transitions can also be identified in heat capacity measurements. In particular, second order phase transitions give rise to discontinuities in those thermodynamic properties which are defined as second derivatives of the Gibb's free energy with respect to temperature; the heat capacity is just such a thermodynamic property. An example of a second-order transition is the paramagnetic to ferromagnetic phase transition . Fig(2.7) shows $C_P(T)$ of the compound $Nd_{0.66}Sr_{0.34}MnO_3$ . The magnetic phase transition is at $T_C$ = 248 K .

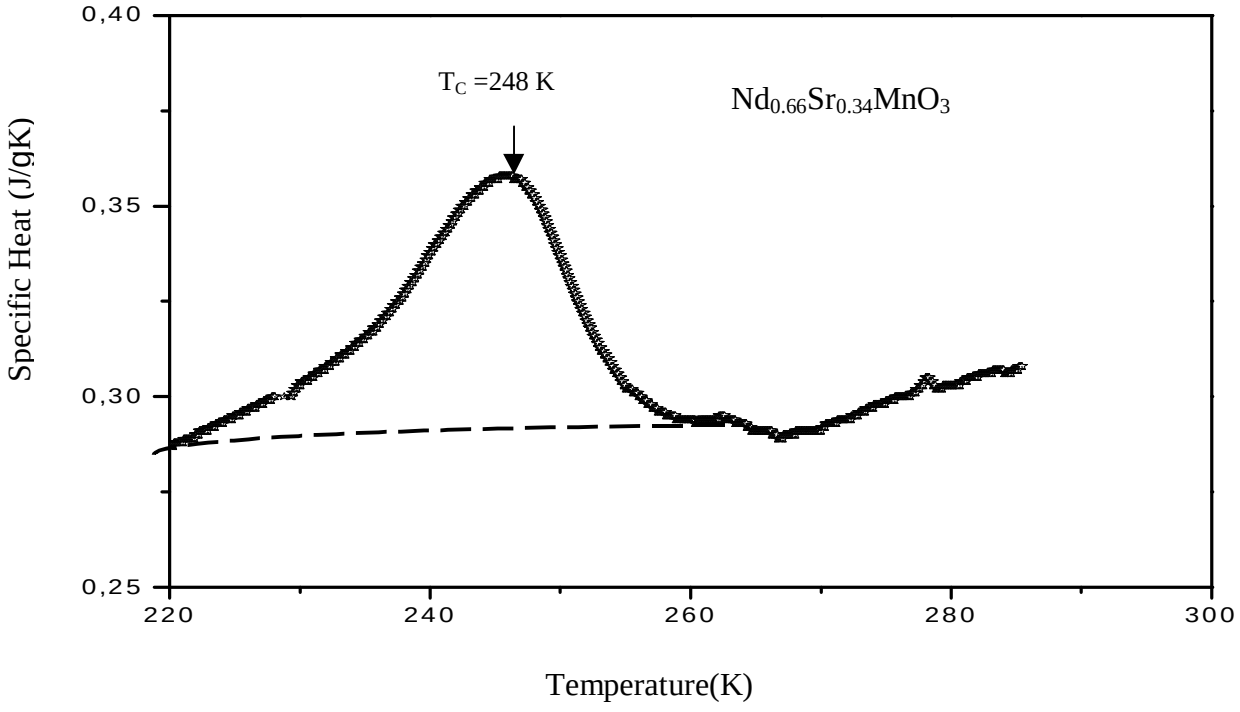


Fig.2.7 :Temperature dependence of the specific heat capacity $C_P(T)$ near the magnetic phase transition of $Nd_{0.66}Sr_{034}MnO_3$ as measured by the DSC method , dashed line : Debye Law.

## 2.4. Magnetization Measurements

The temperature dependence of the magnetization of our samples was measured between 77 K and 325 K using a Faraday balance Fig(2.8) and a magnetic field of 0.5T .The magnetization was measured during heating after cooling the sample down to 77 K in a magnetic field of 0.5T ( field cooled - F C).

The Faraday balance is a standard tool for precision studies of weakly magnetic materials. When a sample with a magnetic moment $\mu$ is placed in a magnetic field gradient dH/dx , it will experience a force $F$ of magnitude

$$F = \mu \frac{dH}{dx} \qquad (2\text{-}1)$$

When the magnetisation $M$ , defined by the vector sum of an ensemble of magnetic moments $\overline{\mu}_i$ in a volume V, $M = \frac{\sum_i \overline{\mu}_i}{V}$ is introduced , one writes :

$$M = \chi \ H \qquad (2\text{-}2)$$

In the Faraday method the primary magnetizing field, H, is usually produced by a horizontal electromagnet. The field gradient is made to be along the vertical direction, so that the magnetic force will add to (or subtract from) the sample's weight, and this can be detected with a sensitive microbalance. In our experiments we use two different Faraday systems ; they differ only in the manner in which the field gradient is produced.

To create the magnetic field gradient dH/dx , specially shaped pole caps on the electromagnet were used. The design of these caps produces a region in space over which the "force function," H * dH/dx, is constant, so that the force on a sample in this region is directly proportional to $\chi$ . With this method, the main field and the field gradient are not independent, but increase together as the current in the electromagnet is increased. This means that the susceptibility sensitivity of the instrument varies as the square of the applied field, and that the moment sensitivity is linear with the applied field .The susceptibility can be defined per gram or per $cm^3$ of the material .With $\overline{\mu} = \sum_i \mu_i$ :

$$\text{a)} \quad \mu = \chi_V * H * V$$
$$\text{b)} \quad \mu = \chi_m * H * m \qquad (2\text{-}3)$$

Following eq. (2-2) to eq. (2-4) we can write :

$$F = m \ \chi_m \ H \frac{dH}{dx} \qquad (2\text{-}4)$$

Where m is the mass of the sample , $\chi_m$ is the mass susceptibility and $\chi_v$ is the volume magnetic susceptibility . If one wants to measure the magnetization $M$ , from eq. (2-1) , it follows

$$M = \frac{F_x}{V \cdot \frac{\partial H}{\partial x}} \qquad (2\text{-}5)$$

where $V$ is the unit volume .The magnetic moment per magnetic ion : $n = \mu/\mu_B$ , can be also determined using the formula :

$$n = \frac{m_{mol} F_x}{m N_A \mu_B \frac{\partial H}{\partial x}} \qquad (2\text{-}6)$$

where $\mu_B = 0.9273.10^{-23}$ [Am²]

$N_A = 6.023.10^{23}$ [ $mol^{-1}$]

$m_{mol}$ : the molecular mass in [ kg/mol ] m : the mass of the sample

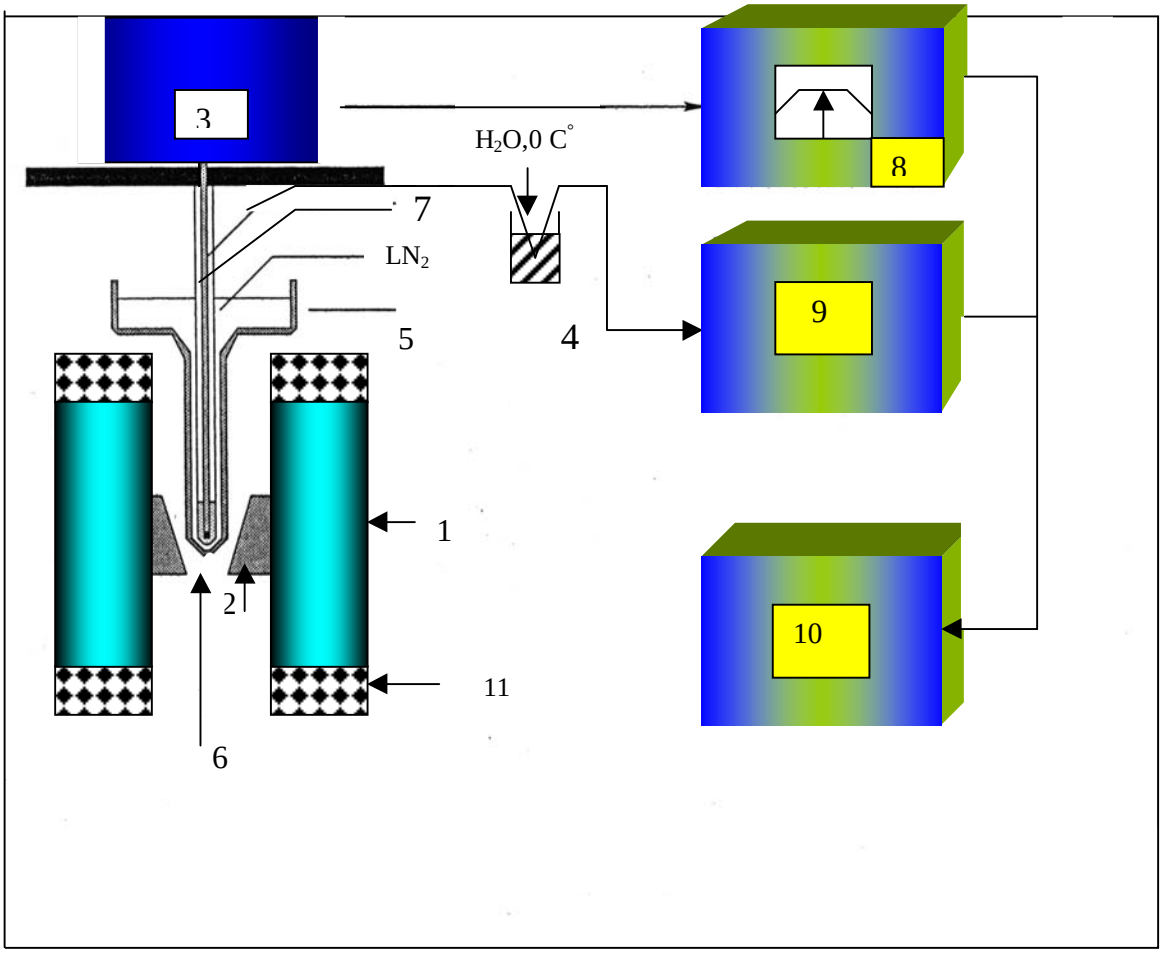


1 . Magnet core
2 . Pole caps
3. Balance (mg)
4 . Thermocouple
5. Dewar-vessel
6 . Sample
7 . The sample holder
8 . Electronic balance
9 . Digital multimeter
10 . PC
11 . Magnet coils

Fig.2.8: Block diagram used for measuring the magnetization .

## 2.5. Resistivity Measurement

The temperature dependence of the resistiviy of the Li – doped $Nd_{0.66}Sr_{0.34}MnO_3$ samples was measured between 77 and 320 K using the standard four-probe method as shown in Fig (2.9) . The 4 wire method eliminates the contact resistances and thus gives more accurate resistance measurements and is in particular needed if the value of the resistance is low .

The resistivity ρ then is obtained from R and the geometry of the sample using :

$$\rho = R \cdot \frac{S}{L} \qquad (2\text{-}7)$$

Here R is the resistance of the sample, $S$ is the cross sectional area and $L$ is the length between the voltage electrodes . $S$ and $L$ are constant for any sample with fixed contacts .The cross sectional area of the samples is between 2.5 and 5 $mm^2$ and $L$ *is* around 10 – 12 mm . In the four point resistance measurement, we supply the sample with some known current I from a current source and measure the voltage V generated across the sample voltage contacts using a separate set of wires.

### 2.5.1.Magnetoresistance measurement

The magnetoresistance is the relative change in the electrical resistance or resistivity of the sample produced by the application of a magnetic field . It is generally defined by ,

$$MR = [\Delta\rho/\rho(0)] = [(\rho(0)-\rho(H)) / \rho(0)] \qquad (2\text{-}8)$$

where ρ(H) and ρ(0) are the resistances or resistivities of the sample at a given temperature in the presence and absence of a magnetic field H respectively ( here H = 0.5T) .

The magnetoresistance (MR) can be negative or positive. The magnetoresistance of the samples was sometimes measured using a slow field pulse. In order to produce the field pulse the magnet was moved mechanically on and off the cryostat or slowly shut off and on , while the resistivity versus temperature curve ρ(T) was slowly recorded at temperatures between 77 K and 325 K. The direction of the magnetic field was perpendicular to the direction of the current across the sample. If the MR was large enough , ρ(T) curves at H = 0 and H = 0.5T were measured consecutively and the magnetoresistance ratio was calculated for each temperature .

## 2.6.Thermoelectric Power Measurement

The thermoelectric power was obtained using a conventional set-up and a pulsed power technique for stabilizing the temperature . Fig(2.10) shows the specifics of the set-up for measuring in the temperature range 77-320K. The sample should be not too high-ohmic , i.e. < 100 kΩ over the covered temperature range. The sample has also to fit into the brackets of the sample holder; that limits it's dimentions to :thickness about 1-1.5 mm, diameter about 3 mm. The sample faces should be completely covered by the lead brackets , otherwise one gets an inhomogenous temperature gradient.The surface should be clean and flat . When the temperature gradient ΔT builds up across the sample , a thermovoltage $V_{th} = S\Delta T$ can be detected at the sample contacts which consists of two contributions ,

1. one coming from the lead contacts with a small thermopower $S_{pb}$
2. the other coming from the actual sample thermopower $S_s$ .

The resulting thermopower is

$$S = S_{pb} + S_s \qquad (2\text{-}9)$$

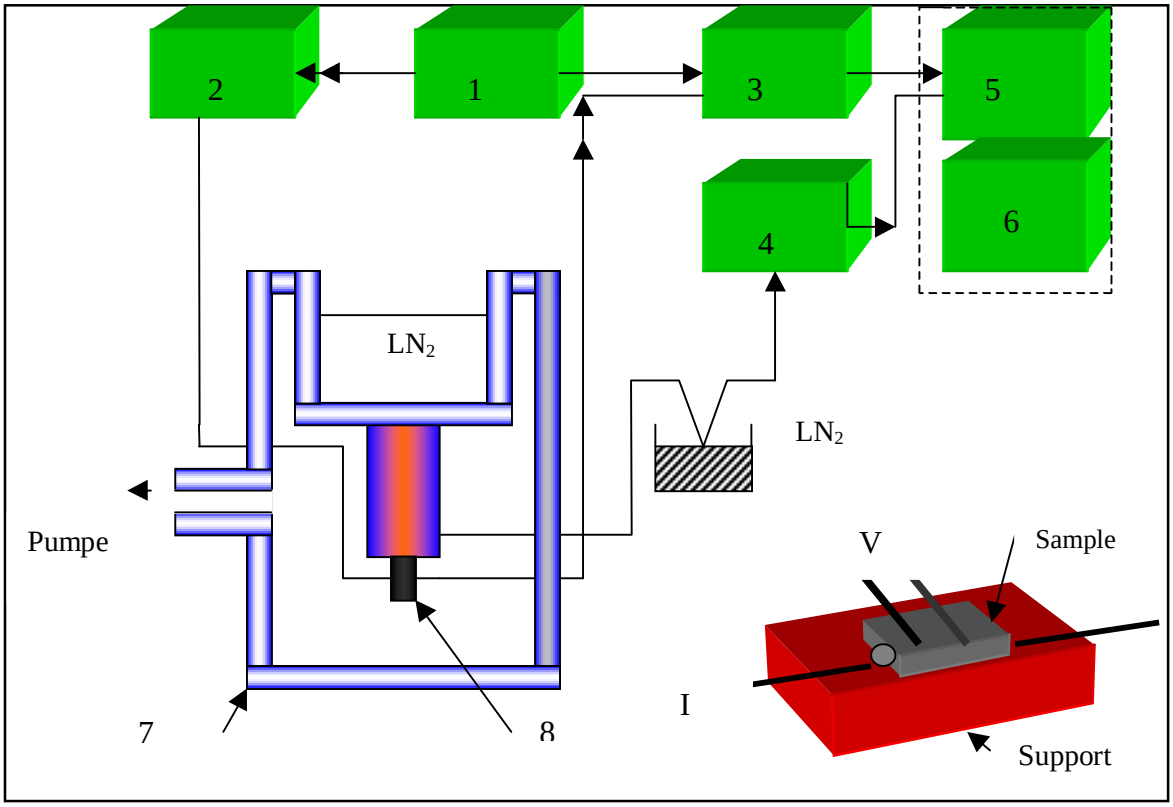


1. Current source (1 mA-10 mA )
2. Transformer
3. Lock-In Amplifier
4. Digital multimeter
5. AD–Converter
6. Computer
7. Cryostate
8. Sample

Fig. 2.9: block diagram for the circuit used in measuring the resistivity

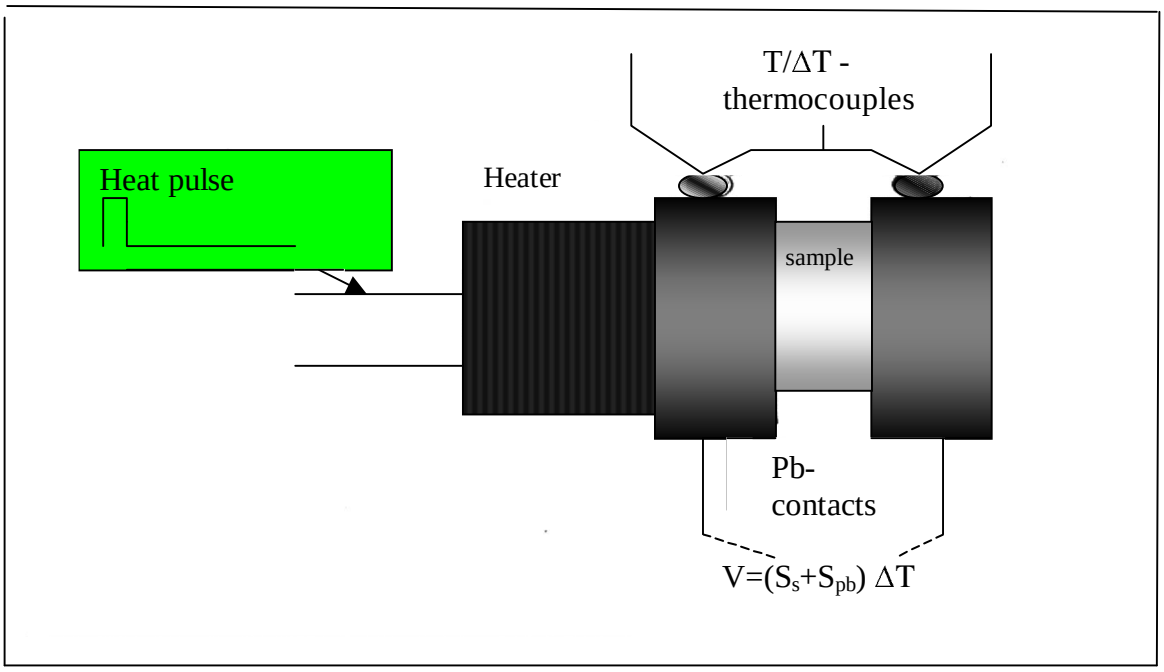


Fig.2.10: Thermoelectric power measurement ; Sample holder .

## 2.7. Transient Thermoelectric Effects (TTE) measurement

The time resolved thermoelectric power (TTE) has been proposed as a transient method for determining carrier life times, carrier diffusivity , carrier mobilities and trap levels in crystalline and amorphous semiconductors, but it also allows to determine the Seebeck voltage S(T) and the heat diffusivity D(T) of metals and semiconductors .
A light pulse which is limited in space and time falls on the one end of a rectangular sample . Standard dimensions are : thickness = 1 mm, length = 5-7 mm .The temperature range was 50-325K . Voltages appear at the end faces which decay with time . These voltage transients sometimes overlap and are empirically described using a superposition of exponentials:

$$V(t)=V\infty+\sum a_i \exp(-t/\tau_1) \qquad (2\text{-}10)$$

Where $a_i = V(0)_i - V(\infty)_i$ ; is the relaxtion amplitude of i-th relaxtion process or the i-th carrier type in case of a multicarrier system.
Specifically, the observed TTE decay curves consist of three stages , each with a characteristic relaxation time $\tau_i$

1- StageI: photodiffusion decay (Dember effect); it is related to the recombination of electron hole pairs generated by the light and diffusing into the dark zone of the sample .
2- StageII: (Transient Seebeck effect); it is due to the diffusion of thermally generated majority carriers from higher to lower temperature regions of the material.
3- Stage III: (quasistatic Seebeck effect); it is the phonon diffusion from the hot point (illuminated section) to the cold point of the material.

### StageI:Photodiffusion (Dember effect)

After the TTE voltage of $V_1(t)$ stageI attains its maximum, the decrease is exponential with a characteristic relaxation time $\tau_1$ . According to the conventional theory of carrier recombination processes ,the minority carrier lifetime $\tau$ determines the relaxation time $\tau_1$ . The initial amplitude of the stage I transient is called the Dember voltage $V_D$ :

$$V_D = G_o k_B T/e(\mu_n-\mu_p)/(n\mu_n-p\mu_p)\ (1/(D/\tau+s)) \qquad (2\text{-}11)$$

$$D = (n+p)\, D_n\, D_p/\ (nD_n+pD_p) \qquad (2\text{-}12)$$

Where D is the ambipolar diffusion coefficient, n,p majority carrier concentrations ,$G_o$ is the photon flux ,$\mu_n$ and $\mu_p$ are the drift mobilities , s is the surface recombination coefficient , $D_n$ and $D_p$ are the diffusion coefficients of the electrons and holes , respectively
For n-type

$$G_o = \delta n/\tau_n\, d \quad , \quad n = n+\delta n,\ p=\delta p \qquad (2\text{-}13)$$

For p-type

$$G_o = \delta n/\tau_p\, d \quad , \quad p = p+\delta p,\ n=\delta n \qquad (2\text{-}14)$$

Where $\delta p$ , $\delta n$ are the excess electron and hole concentrations, $\tau_n$ and $\tau_p$ are the lifetimes of electrons and holes (the relaxation time $\tau_1$) , and d is the width of the light beam, respectively .

**StageII. (Transient Seebeck effect)**

As the recombination of the light- generated electron-hole pairs is nearly completed (stageI) , thermally generated minority carriers still diffuse from the higher- to the lower- temperature region of the sample; this is just the transient Seebeck effect (stageII). At the beginning of stageII, the TTE voltage is not zero but has a finite value, implying the existence of an internal electric field .This field arises because a small amount of the electrons and holes stay apart in trap sites thus avoding the fast recombination. According to Sasaki et al [28] , the TTE voltage $V_2(t)$ can be described as:

$$V_2(t) = V_s + (V_o - V_s)\,(1-\exp(-t / \tau_2)) \qquad (2\text{-}15)$$

where in case of mobile electrons :

$$\tau_2 = eL_n^2 / 2k_B T \mu_n \qquad (2\text{-}16)$$

$\tau_2$ is the relaxation time of stage II , $L_n$ the diffusion lenth , according to [29]

**StageIII . (Quasistatic Seebeck Effect)**

The final stage(III) voltage of the decay curves $V_3(t) = S.\,\Delta T(t)$ is considered to be associated with the heat flow along the sample .In general, if a temperature gradient $\partial T/\partial x$ in a sample is set up there will be a heat flow of density $\omega = - k\partial T/\partial x$ , where k is the thermal conductivity . In the one dimensional case , the equation of continuity for $\omega$ along the x axis is given by

$$\partial\omega / \partial x = - \partial(\rho C_v T)/ \partial t \qquad (2\text{-}17)$$

Where $C_v$ is the specific heat per mass unit and $\rho$ the mass density .

From that we obtain the well –known heat diffusion equation

$$\partial T/ \partial t - D_T\, \partial^2 T/\partial^2 x = 0 \qquad (2\text{-}18)$$

Where $D_T = k / \rho C_v$ is the thermal diffusion coefficient

This heat diffusion equation has been solved for the (thin +long) TTE sample geometry which yields also the end face temperatures $T_1$ , $T_2$ as functions of time; from those we obtain the temperature increment $\Delta T = T_1 - T_2$ as a function of time . A computer program was set up to fit the observed transient $V_3$ (t) to this particular solution of the diffusion equation . Tests of the fitting procedure using standard materials and perpendicular heat flow corrections have been performed [30-31] .The parameters obtained from the fit are (1) the thermal diffusion coefficient D and (2) the initial amplitude $V_3(0)$ which is proportional to *S* and the maximum temperature increment $\Delta T(0)$ . With the $Nd_{0.66}(LiSr)_{0.34}Mn_3$ samples , only the StageIII transient is observed.

**2.7.1. TTE-transient (III) –data reduction and corrections.**

The light pulse is created by a halogen lamp in combination with a shutter , a lens and a slit close to the end of the sample . Contacts (usually silver paint) are applied to both sample ends and a (decaying) voltage is measured between them Fig(2.11); . In the current experiments the data aquisition is performed using Labview 5.2. In the case of thermal diffusion , the initial amplitude $V_3$ of a TTE –transient is proportional to the thermopower S ,while the decay time is related to the heat

diffusivity D. The absolute thermopower cannot be obtained, as after applying the contacts one has build a thermochain , usually Cu-silver glue- sample –silver glue –Cu . Fig(2.12) shows the sample holder. Empirically i.e. by comparing $V_3$ with conventionally measured thermovoltages , the silver glue gives a small positive linear contribution $S_{contact}$ which has to be subtracted , i.e

$$S_{exp} = S_{sample} + S_{contact} \qquad (2\text{-}19)$$

In addition, we do not measure with a constant temperature increment $\Delta T$ like it is done conventionally, but with a constant applied heat $\Delta Q$ .Thus, before one can subtract the contact contribution , one has to correct $V_3$ for a constant temperature increment. Using a constant light pulse , it is suggested to use $\Delta Q = C_p \Delta T$ for the correction, i.e. as we measure $V_3(T) = S \Delta T$,only the product $V_3 C_p / C_p(300K) = V^*_3$ is proportional to $S_{exp}$. If $V_3$ is not too small ,our corrected signal $V^*_3$ follows the conventionally measured TEP already , so that arguments concerning structure in S(T) can be made without the contact correction .However, the better procedure is to calibrate the corrected TTE- data using scattered conventional data from other sources. All this has been done . The specific heat capacity is measured at constant volume $C_V$ and at constant pressure $C_P$. However , with solids both quantities are almost the same , $C_P \approx C_V$ . While we use $C_P(T)$ for the $V_3 \rightarrow S$ conversion , it is also needed to calculate the heat conductivity k from the heat diffusivity D since (see Ch.3.8).

As the TTE-method works best with thin layer samples and as near the surfaces the oxygen content might differ from that in the bulk, with thicker samples the TTE-method has to be considered surface sensitive as compared to conventional (bulk) methods. The penetration depth of the light and with it the pertinent layer depth , is here likely given by the halogen lamp quartz glass IR-cutoff, i.e. $\leq 4$ µm. Moreover, because of the small temperature gradients we use, generally both S(T) and k(T) show sharper structure as compared to conventional measurements, in particular if there one uses larger sample volumes, which usually adds compositional imhomogeneity.
Since we can apply an impedance transformer, S can be measured also with higher impedance samples where conventional TEP- setups suffer from stray induction voltages.

## 2.8. Heat diffusivity and heat conductivity

The heat diffusivity D describes the rate at which heat diffuses through the sample. It is a function of the sample's thermal conductivity k and its specific heat capacity at constant volume $C_v$ . A high thermal conductivity will increase the sample's thermal diffusivity, as heat will be able to conduct across the sample quickly. Conversely, a high specific heat capacity will lower the sample's thermal diffusivity, since heat is preferentially stored as internal energy within the sample instead of being conducted through it.The unit of D is $m^2/s$ . D(T) is explicitely related to the thermal conductivity k according to ;

$$D = \frac{k}{c_v \rho_0} \quad \text{or} \quad k = D\, C_v \rho_0 \qquad (2\text{-}20)$$

The heat conductivity k is the rate at which heat flows within a body for a given temperature difference . Its unit is W/mK . $\rho_0$ is the density in $kg/m^3$ , $C_v$ is t he specific heat at constant volume ,i.e the amount of energy the sample stores for each degree increase in temperature, on a per unit mass basis . Its unit is J / kgK .

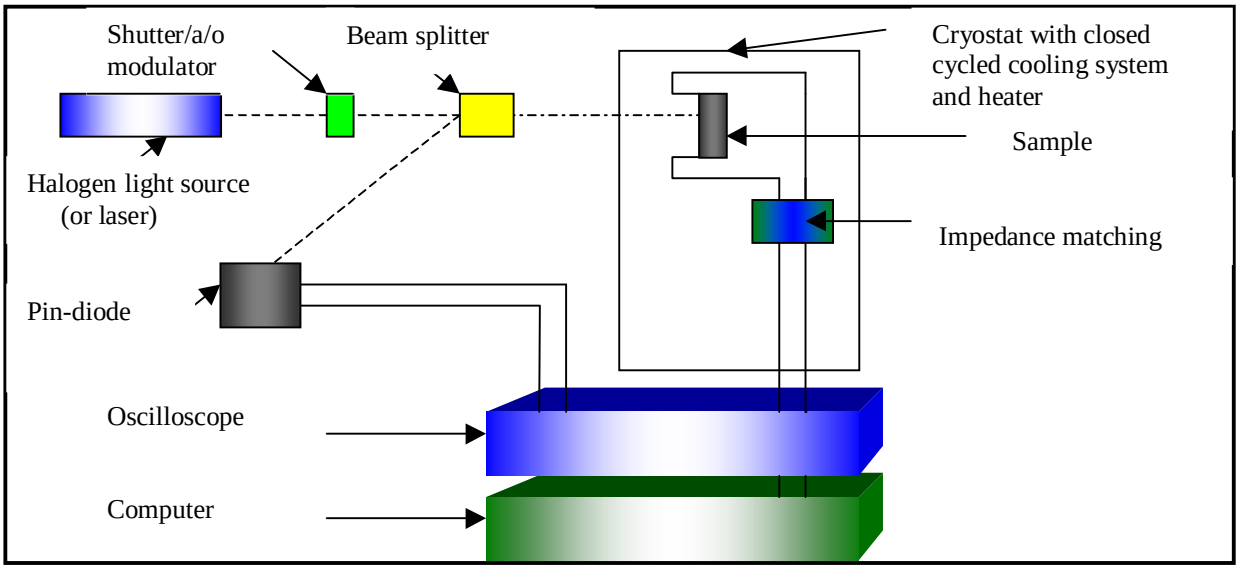


Fig.2.11: Block diagram for the circuits used in measuring the TTE-signals.

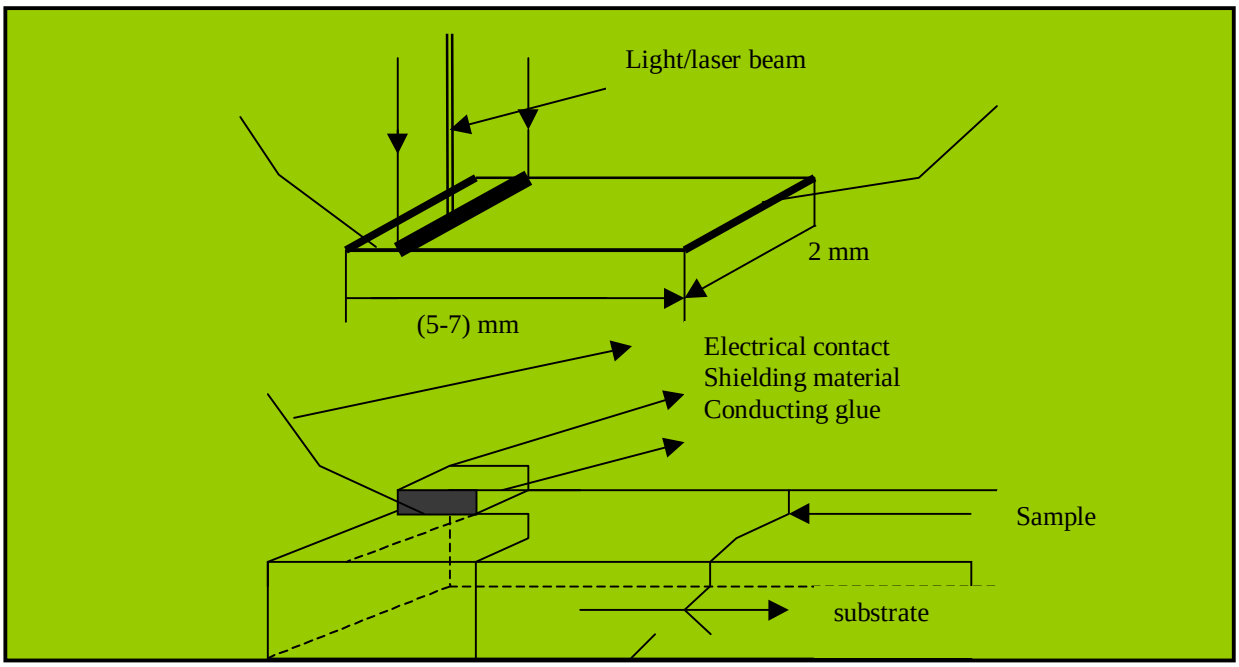


Fig.2.12: Block diagram for the sample holder used in the TTE measurement.

# CHAPTER III

## Results

### 3.1.Magnetization

The field-warmed magnetization shows that all samples undergo a ferromagnetic–paramagnetic transition.The temperature dependence of the magnetization of series (1) at y = 0 , 0.18 , 0.33 is shown in Fig(3.2) . Fig(3.3 ) and Fig (3.4) show *M*(T) of series (2) with $0 \leq y \leq 0.18$ and $0.26 \leq y \leq 0.46$ . The parent compound $Nd_{0.66}Sr_{0.34}MnO_3$ exhibits a rather sharp ferromagnetic- paramagnetic transition . $T_C$ which is here defined as the crossing of $M = 0$ and the tangent at inflection point of the *M*(T) curve; as shown in Fig(3.1) . With Li substitution ,the magnetization decreases and the magnetic transition becomes increasingly broader . However, $T_C$ of series 2 shows a recurrent behaviour i.e. it first decreases, then increases ( y = 0.1 ,0.13) and finally drops again with increasing y . Table1 shows , $T_C$ , $\theta_C$ , $M_{S0}(T = 0)$ of both series .

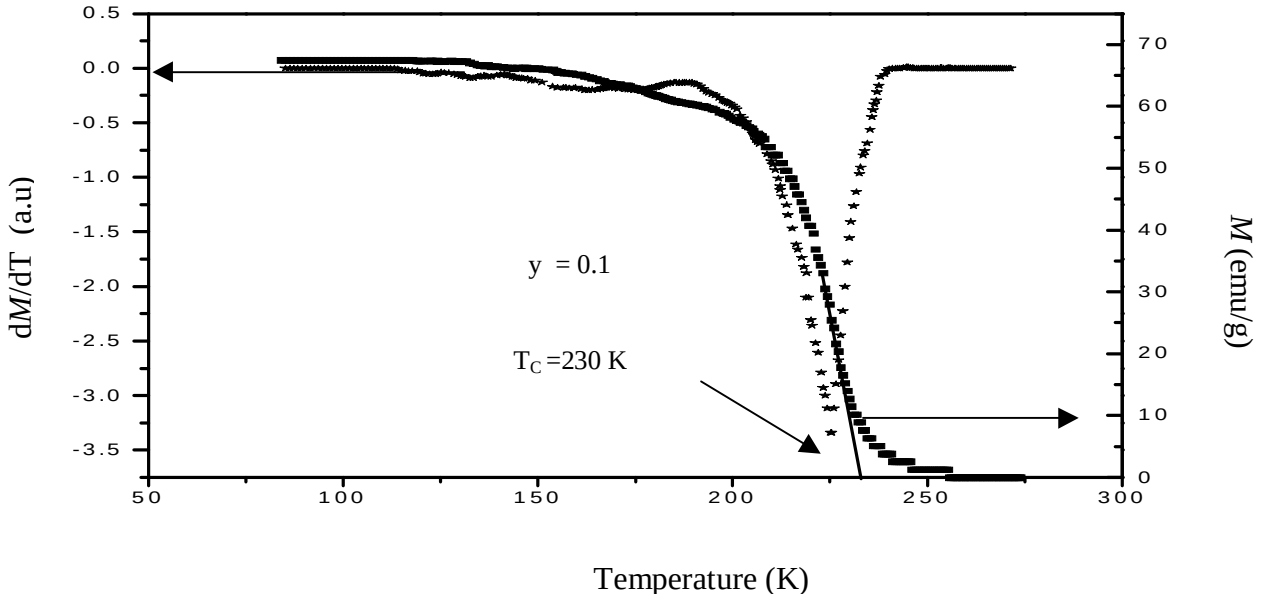


Fig .3.1: The temperature dependence of the d*M*/dT and the magnetization for $Nd_{0.66}(Sr_{1-y}(Li_{Z2})_y)_{0.34}MnO_3$ with y = 0.1 of series (2) measured in a magnetic field of 0.5T . d*M*/dT serves to determine $T_C$ = 230 K :

### 3.1.1. Magnetic Susceptibility

In Fig(3.2) the inverse Susceptibility - versus temperature $\chi^{-1}$ (T) is shown for series (1) . Fig(3.3) and Fig(3.4) show $\chi^{-1}$ (T) for series (2). Note, that the $\chi^{-1}$ (T) dependence is not linear in the whole temperature interval as predicted by the Curie Weiss law. Evidently this is related to clustering of magnetic moments. Because of the possible compositional variations in our samples , we cannot decide whether this is due to structurally based local magnetic inhomogeneities or whether we have larger spin clusters intrinsically.

The high temperature asymptotic behaviour of the susceptibility versus temperature curve, however,is supposed to allow the determination of the single spin effective paramagnetic moments which are compiled in Table1 and Table 2 together with the paramagnetic Curie temperature.

The experimental values of the Curie temperature $\theta_C$ and the effective paramagnetic moments $\mu_{eff}$ are obtained from the Curie Weiss law :

$$\chi = \frac{C}{T-\theta_C} \qquad (3\text{-}1)$$

where $\theta_C$ is the Curie temperature, C is the Curie constant . Standard molecular field theory yields :

$$C = \frac{n_0 \mu_B^2 \mu_{eff}^2 \mu_0}{3 k_B} \qquad \text{with} \qquad n_0 = \frac{N_A}{m_{mol}} \qquad (3\text{-}2)$$

| | | | |
|---|---|---|---|
| Bohr's magneton | $\mu_B$ | = $0.9273.10^{-23}$ | [Am²] |
| Avogadro's number | $N_A$ | = $6.023.10^{23}$ | [ $mol^{-1}$] |
| $m_{mol}$ : molecular weight of the sample | | | |
| Boltzmann's constant | $k_B$ | = $1.3806 .10^{-23}$ | [J/K] |
| $\mu_{eff}$ the effective paramagnetic moment | | | |
| $\mu_0$ the magnetic field constant | $_0$ | = $\mu$ 4 $\pi$ $10^{-7}$ | [ Vs / Am] |

Table 3 shows that the experimental values of the effective paramagnetic moments $\mu_{eff}$ per molecule decrease somewhat with increasing Li content.
The theoretical values of the effective paramagnetic moments $\mu_{eff}$ are obtained from .

$$\mu_{eff} = g \sqrt{\overline{S}(\overline{S}+1)} \qquad (3\text{-}4)$$

where g is the Lande-factor ($\approx$2) , $S$ =2 for $Mn^{3+}$and $S$ =3/2 for $Mn^{4+}$ . This gives $\mu_{eff}$ = 4.9 $\mu_B$ for $Mn^{3+}$ , 3.9 $\mu_B$ for $Mn^{4+}$ and 3.5 $\mu_B$ for $Nd^{3+}$. The effective paramagnetic moment per formula unit of $Nd_{0.66}(Sr_{1-y}(Li_Z)_y)_{0.34}MnO_3$ should thus be equal 7.47 $\mu_B$ for all samples . The slight drop of $\mu_{eff}$ with y suggesting a change of the crystal field and with it of the Landi factor g with increasing y .

Table 1. $T_C$ , $\theta_C$ , , $M_{S0}(T=0)$ of both series.

| Li-contentes y mol % | series(1) $T_C$ (K) | series(2) $T_C$(K) | series(1) $\theta_{C1}$ (K) | series(2) $\theta_{C1}$ (K) | Series 1 $\theta_{C2}$ (K) | Series 2 $\theta_{C2}$ (K) | $M_{0S}$ (T=0) series(1) (emu/g) | $M_{0S}$ (T=0) series(2) (emu/g) |
|---|---|---|---|---|---|---|---|---|
| 0 (2Ch2 ) | 259 | 248 | 225 | 228 | 266 | 245 | 86 | 73 |
| 0.05 | | 223 | | 202 | | 223 | | 61 |
| 0.10 | | 230 | | 225 | | 237 | | 68 |
| 0.14 | | 240 | | 227 | | 244 | | 69 |
| 0.18 | 275 | 204 | 227 | 180 | 252 | 194 | 54 | 66 |
| 0.26 | | 184 | | 155 | | 182 | | 63 |
| 0.33 | 150 | 179 | 120 | 152 | 217 | 179 | 36 | 60 |
| 0.40 | | 84 | | 70 | | 106 | | 16 |
| 0.46 | | 140 | | 123 | | 172 | | 9 |

Table 2. The effective paramagnetic moments $\mu_{eff}$ (exp. ) and (calc. ) of both series

| y | series(1) $\mu_{eff}$ (T> $T_C$) (exp. ) | series (2) $\mu_{eff}$ (T> $T_C$) (exp. ) | series (1) (calc. ) | series(2) (calc. ) |
|---|---|---|---|---|
| 0 | 8 | 7,9 | 7.47 | 7.47 |
| 0.05 | --- | 7,6 | --- | 7.47 |
| 0.10 | --- | 7,5 | --- | 7.47 |
| 0.14 | --- | 7,4 | --- | 7.47 |
| 0.18 | 7,5 | 7,3 | 7.47 | 7.47 |
| 0.26 | --- | 7,2 | --- | 7.47 |
| 0.33 | 7,3 | 7,1 | 7.47 | 7.47 |
| 0.40 | --- | 7.0 | --- | 7.47 |
| 0.46 | --- | 6,9 | --- | 7.47 |

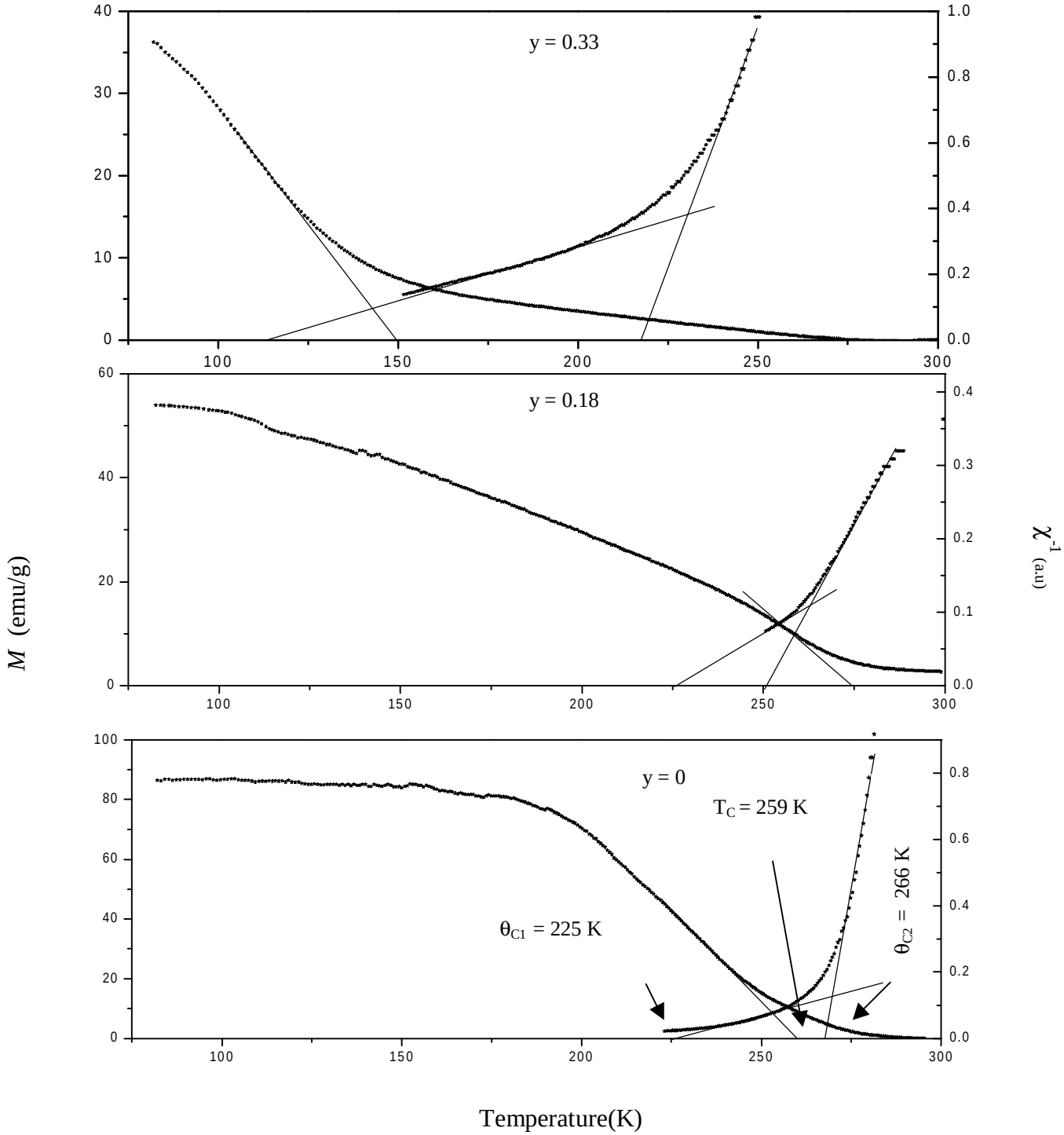


Fig.3.2: The temperature dependence of the magnetization $M$ and the reciprocal susceptibility $\chi^{-1}$ for samples $Nd_{0.66}(Sr_{1-y}(Li_{Z1})_y)_{0.34}MnO_3$ ( y = 0 , 0.18 , 0.33: series1) measured in a magnetic field of 0.5T , $\theta_C$ see Table 2.

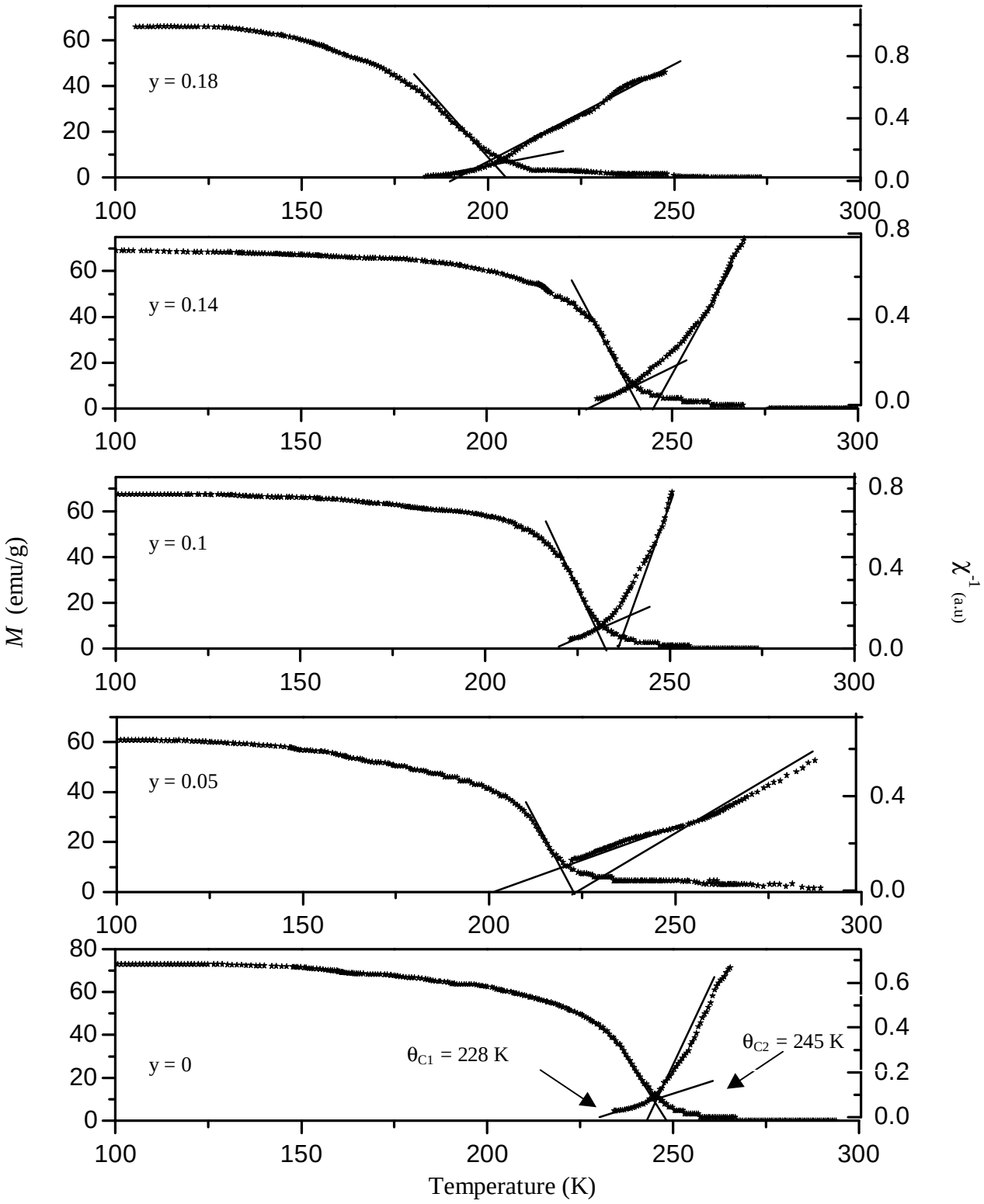


Fig.3.3: The temperature dependence of the magnetization $M$ and the reciprocal susceptibility $\chi^{-1}$ of $Nd_{0.66}(Sr_{1-y}(Li_{Z2})_y)_{0.34}MnO_3$ at ( y = 0 , 0.05 , 0.1 , 0.14 , 0.18 : series2) as measured in a magnetic field of 0.05T, $\theta_C$ see Table 2 .

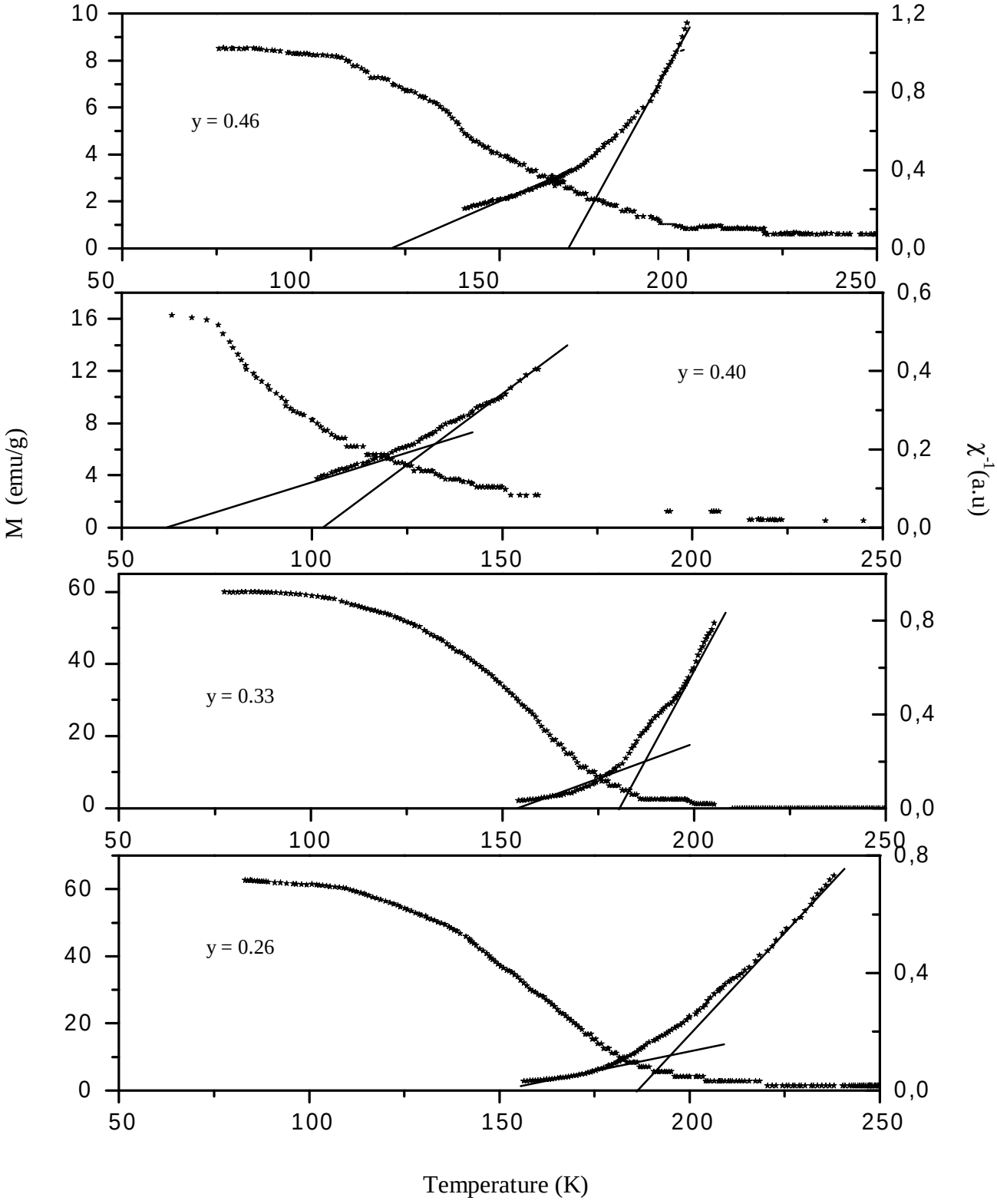


Fig.3.4: The temperature dependence of the magnetization *M* and the reciprocal susceptibility $\chi^{-1}$ of $Nd_{0.66}(Sr_{1-y}(Li_{Z2})_y)_{0.34}MnO_3$ ( y = 0.26 ,0.33 ,0.40 ,0.46 : series 2) as measured in a magnetic field of 0.5T, $\theta_C$ see Table 2.

## 3.2. Resistivity

Fig(3.5) shows the temperature dependence of the resistivity of $Nd_{0.66}(Sr_{1-y}\ (Li_{Z1})_y)_{0.34}MnO_3$ ( y = 0 ,0.18 ,0.26 ,0.46: series (1) ) samples in zero magnetic field .$T_m$ decreases rapidly with the Li content as shown in Table4 ,where $T_m$ defined as the temperature of the maximum of the ρ(T) curve. Also, the resistivity of the sample at the metal – insulator (M-I) transition temperature ($\rho_m$) increases with increasing Li content .

Fig(3.6) shows ρ(T) of the $Nd_{0.66}(Sr_{1-y}(Li_{Z2})_y)_{0.34}MnO_3$ samples series 2 : y = 0 , 0.05 , 0.1 , 0.14 , 0.18 and Fig(3.7) for y = 0 , 0.26 , 0.33 , 0.40 , 0.46 ( series2) . The resistivity of the sample at the metal –insulator (M-I) transition temperature ($\rho_m$) increases with increasing Li content for $0.18 \leq y \leq 0.46$ . $T_m$ decreases with the Li content y = 0.18 to 0.46 , as shown in Table 4. A similar change of $T_m$ with doping was observed in A-site-doped perovskite manganites [32-33] . However, between at y = 0.1 and 0.14 , $T_m$ of series (2) increases [34] . The figures show also that ρ(T) of the samples with y = 0.05 and 0.14 exhibits a double peak . In particular , for y = 0.05 ( series2) the temperature of the high- temperature peak is $T_{p1} \approx T_c$ =240 K ,and the temperature of the low-temperature peak is $T_{p2}$ = 204 K .The sample with y = 0.14 has $T_{p1}$ = 245 K and $T_{p2}$ = 205 K. For the other samples the second peak is reduced to a shoulder or the two peaks merge .

Two mechanisms have been proposed for the charge transport in systems where the carriers are localized. The first proposed by Mott and Davis [35] , involves a hopping of the carriers between states of nearly equal energy. Such states are placed at random distances in the lattice due to the randomness in the potential.

Mott's three dimensional variable range hopping (VRH) expression reads :

$$\rho(T) = \rho_0 \exp\left[\left(\frac{T_0}{T}\right)^{1/4}\right] \qquad (3\text{-}5)$$

In the second proposal , the conduction takes place by hopping of small polarons, but they hop only to the nearest neighbors and are assisted by the thermal energy. The resistivity, ρ, in this model is expected to follow the equation :

$$\rho = \rho_0 \exp(E_0/k_B T) \qquad (3\text{-}6)$$

where $E_0$ is the activation energy of the polarons and $\rho_0$ is a constant. In manganites the resistivity in the paramagnetic state shows the carriers to be localized.

Both these models can be fitted to temperature dependence of ρ equally satisfactorily. It is difficult to choose between the two models based on the resistivity data alone.

Both equations can be condensed into one by writing : $\ell n\ \rho/\rho_0 = \left[\frac{k T_0}{kT}\right]^{1/n}$ . Then , $kT_0 = E_0$ and n = 1 gives back the Arrhenius law (polaron hopping) . A $T^{-1/2}$ law ,which is characteristic of variable –range hopping with a soft gap due to electron correlation [36], leads to acceptable

fits. In order to find out which power is empirically best suited , we have plotted $\ell n\, \rho/\rho_0$ against $\left[\frac{1}{T}\right]^{\frac{1}{n}}$ with n = 1 , 2 , 3 ,4 , 5 . This is shown for the high temperature region above $T_C$ for the sample with y = 0.1 of series(2) in Fig(3.8). Nevertheless Table 3, Table 4 also show the values of $T_m$ , $\rho_r$ , $E_0$ , $\ell n\, \rho_0$ , $\rho_m$ , and the characteristic temperature $T_0$ for n = 4 and for various Li contents.

Table 3. The values of $T_m$ , $\rho_m$ , , $\ell n\, \rho_0$ , $E_0$ , and $T_0$ for various Li contents of series (1) .

| y | $\rho_r$ (Ω cm ) (105 K) | $\rho_m$ (Ω cm ) | $T_m$ (K) | Ln $\rho_0$ n = 1 | $\rho_0$ (Ω cm ) | $T_0$(K) n = 4 | $E_0$ (eV) |
|---|---|---|---|---|---|---|---|
| 0 | 0.02 | 0.17 | 249 | -2,21 | 0.109 | $3 \times 10^7$ | 0.12 |
| 0.18 | 0.09 | 0.60 | 191 | - 1,75 | 0.170 | $4 \times 10^7$ | 0.13 |
| 0.33 | 0.12 | 1.38 | 150 | -3.09 | 0.100 | $7 \times 10^7$ | 0.14 |

Table 4. The values of $T_m$ , $\rho_m$ , $\ell n\, \rho_0$ , $E_0$ , and $T_0$ for various Li content of series (2)

| y | $\rho_r$ (Ω cm (105 K) | $\rho_m$ (Ω cm) | $T_m$ (K) | Ln $\rho_0$ n = 1 | $\rho_0$ (Ω cm ) | $T_0$(K) n = 4 x $10^7$ | $E_0$ (eV) | $T_{P1}$(K) | $T_{P2}$ (K) |
|---|---|---|---|---|---|---|---|---|---|
| 0 | 0.04 | 0.29 | 243 | -2.26 | 0.1 | 5 | 0.130 | --- | --- |
| 0.05 | 0,12 | 0.42 | 225 | -1.36 | 0.2 | 0.1 | 0.060 | 225 | 189 |
| 0.10 | 0.03 | 0.17 | 230 | -3.05 | 0.15 | 7 | 0.140 | --- | --- |
| 0.14 | 0.08 | 0.14 | 242 | -2.32 | 0.09 | 0.02 | 0.040 | 242 | 205 |
| 0.18 | 0.17 | 0.87 | 212 | -4.20 | 0.015 | 9 | 0.146 | --- | --- |
| 0.26 | 0.22 | 1.24 | 190 | -4.50 | 0.01 | 14 | 0.155 | --- | --- |
| 0.33 | 0.39 | 2.32 | 178 | -4 | 0.018 | 16 | 0.156 | --- | --- |
| 0.40 | --- | 298 | 84 | -2.6 | 0.07 | 19 | 0.157 | --- | --- |
| 0.46 | --- | 839 | 100 | -3.3 | 0.036 | 26 | 0.169 | --- | --- |

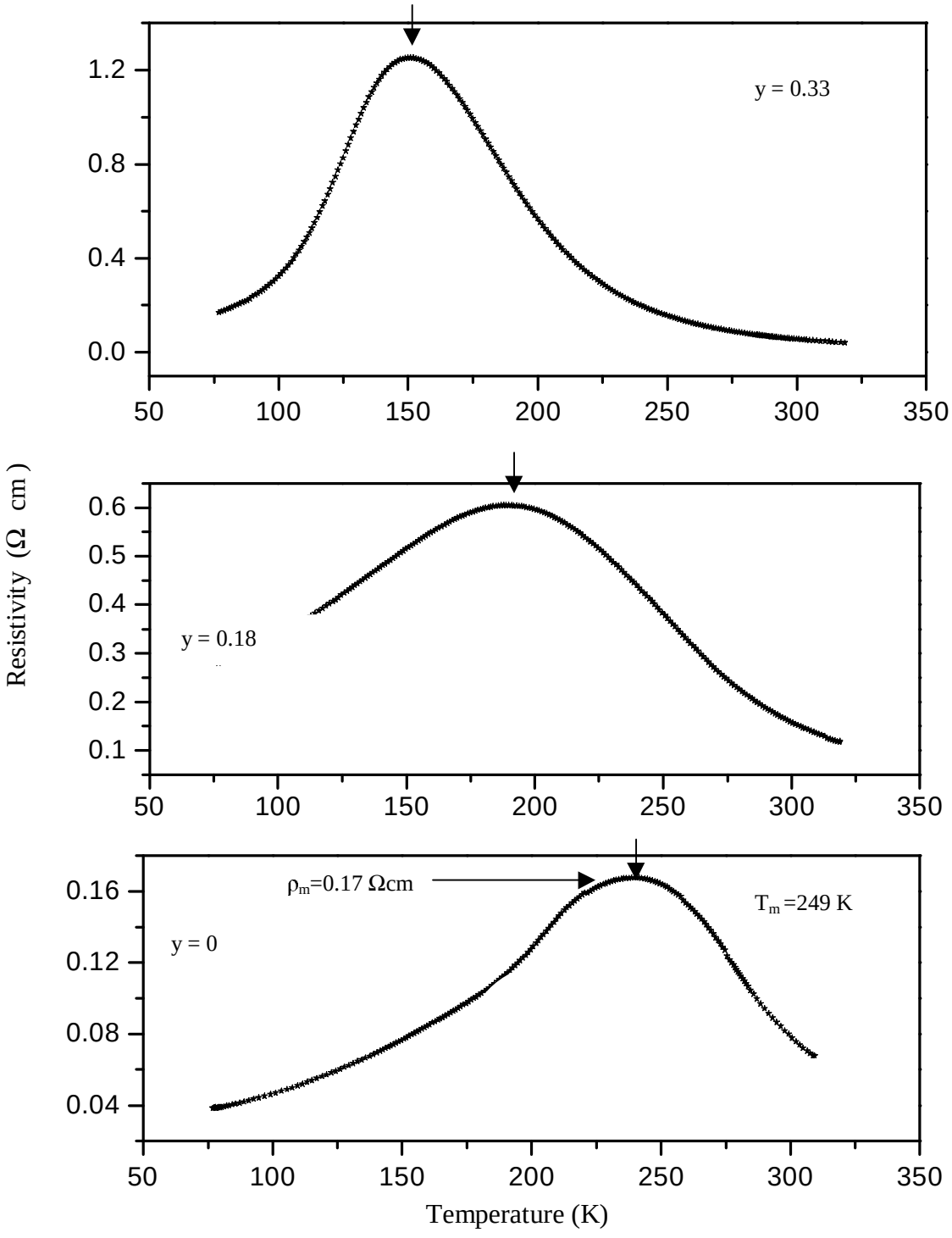


Fig.3.5: The temperature dependence of the resistivity of $Nd_{0.66}(Sr_{1-y}(Li_{z1})_y)_{0.34}MnO_3$ ( y = 0 , 0.18 , 0.33 ; series1 ) samples in zero field .

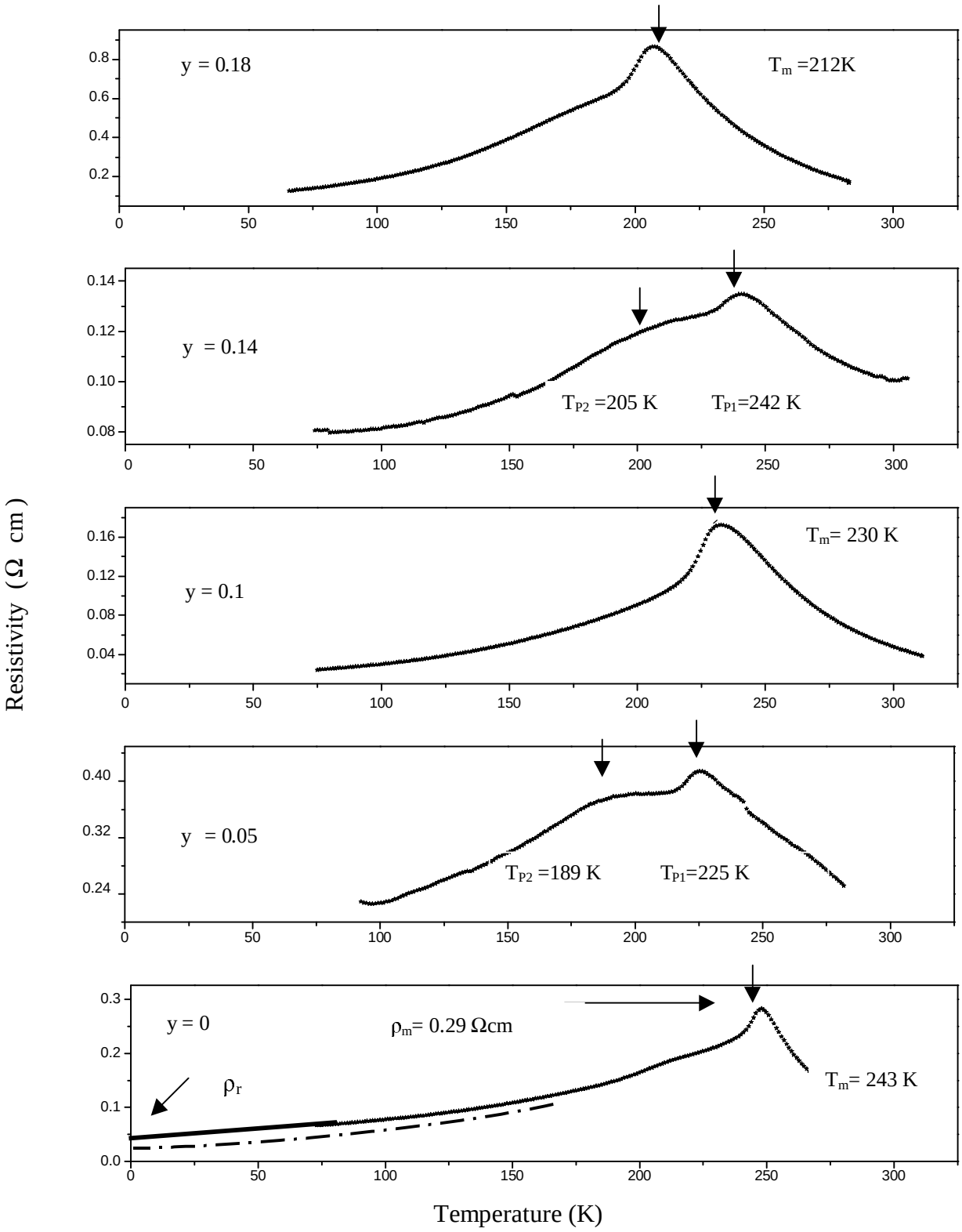


Fig.3.6: The temperature dependence of the resistivity of $Nd_{0.66}(Sr_{1-y}(Li_{Z2})_y)_{0.34}MnO_3$ ( y = 0 , 0.05 , 0.1 , 0.14 , 0.18 : series 2 ) samples in zero field .dashed line ρ(T) acc.to [23] , where $\rho_r$= 0.012 mΩ cm , and $\rho_r$ = 90 μΩ cm [37] .

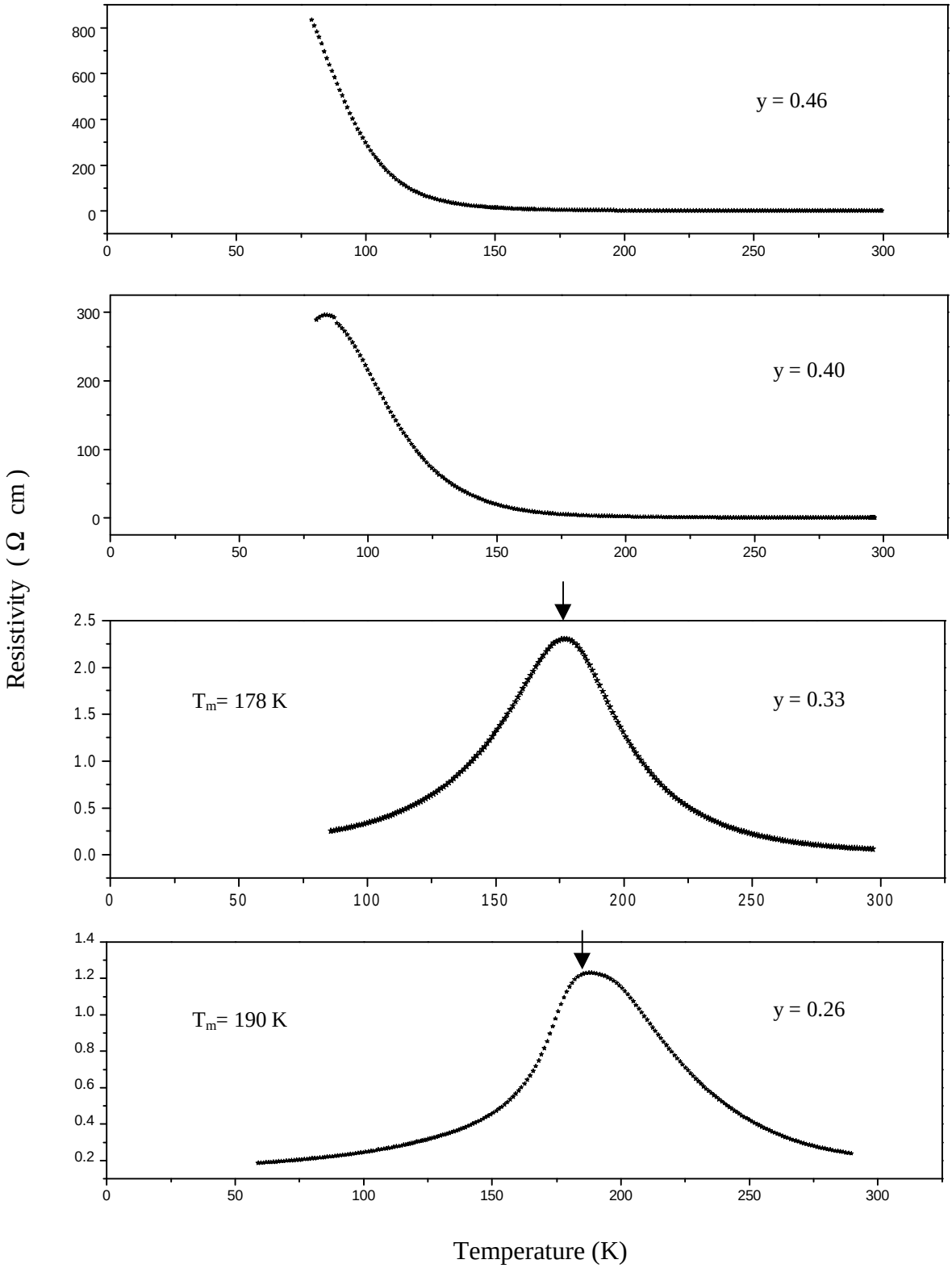


Fig.3.7: The temperature dependence of the resistivity of $Nd_{0.66}(Sr_{1-y}(Li_{Z2})_y)_{0.34}MnO_3$ ( y = 0.26 , 0.33 , 0.40 , 0.46 ; series2) samples in zero field

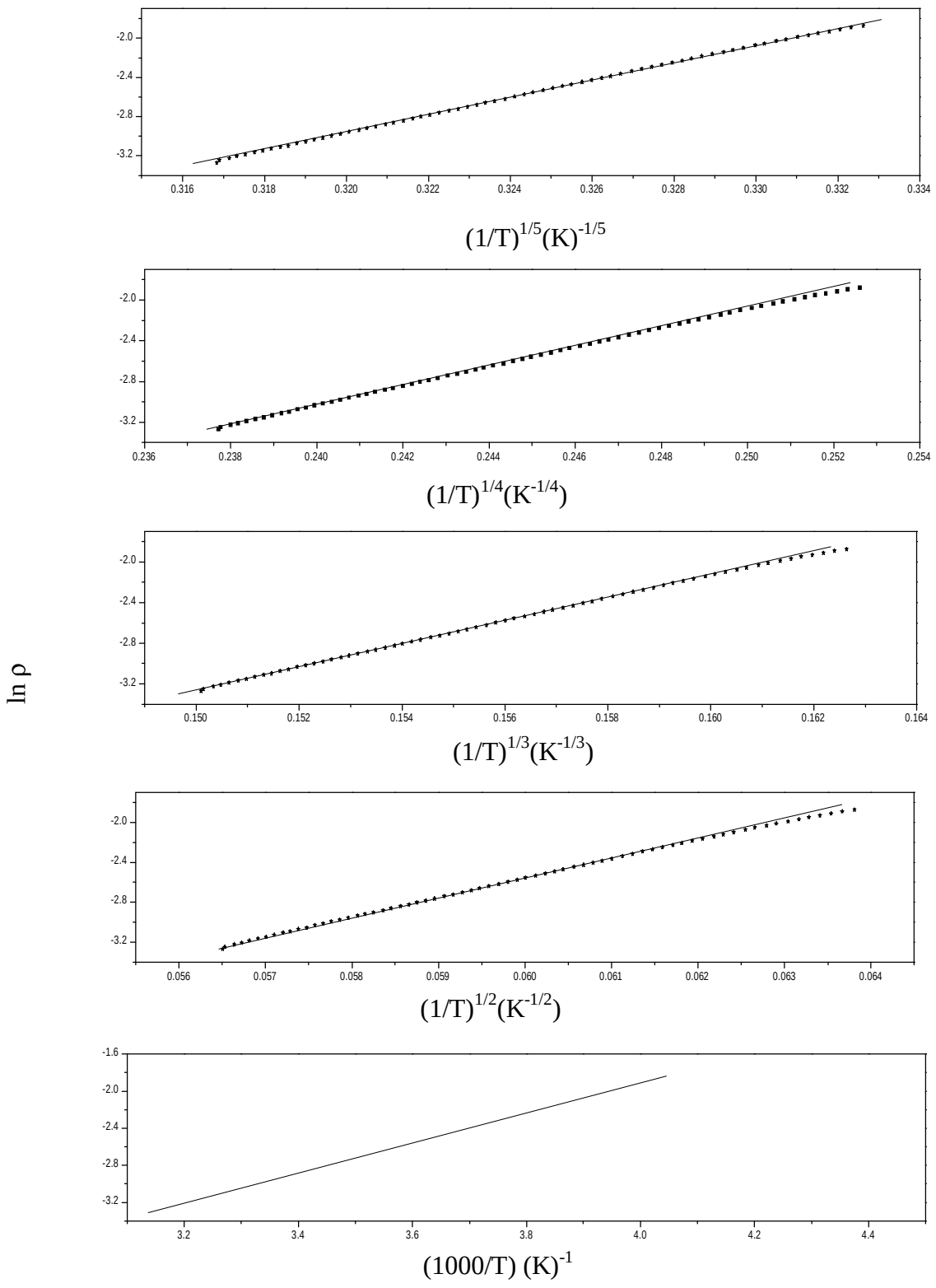


Fig.3.8: plot of ln(ρ) against 1/T ,$1/T^{1/2}$, $1/T^{1/3}$ , $1/T^{1/4}$ and $1/T^{1/5}$ for sample with y = 0.1 series 2

### 3.2.1 Magnetoresistance

Fig (3.9) and Fig(3.11) show the temperature dependence of the magnetoresistance for the samples $Nd_{0.66}(Sr_{1-y}(Li_{Z1})_y)_{0.34}MnO_3$ of series (1) with y = 0 , 0.18 , 0.33 .
When a magnetic field is applied, the resistivity of our compounds $Nd_{0.66}(Sr_{1-y}(Li_Z)_y)_{0.34}MnO_3$ decreases and the resistivity peak shifts a little to higher temperatures as shown in Fig(3.9) for series (1) and Table 4 .The results of Series (2) are shown in Fig(3.10) and Table 4 [34,38] .
$\Delta R/R$ of series (2) is shown in Fig( 3.12) . Both samples series(1) and series (2) have a negative MR which is maximal around $T_m$ .

Table 4. $T_m$ at zero field and at field (H = 0.5T)

| y | $T_m$(K) H = 0 (series1) | $T_m$(K) H = 0.5T (series1) | $T_m$(K) H = 0 (series2) | $T_m$(K) H = 0.5T (series2) |
|---|---|---|---|---|
| 0 | 249 | 251 | 243 | 246 |
| 0.05 | --- | --- | 225 | 227 |
| 0.10 | --- | --- | 230 | 232 |
| 0.14 | --- | --- | 242 | 244 |
| 0.18 | 191 | 195 | 212 | 214 |
| 0.26 | --- | --- | --- | --- |
| 0.33 | 150 | 156 | --- | --- |
| 0.40 | --- | --- | --- | --- |
| 0.46 | --- | --- | --- | --- |

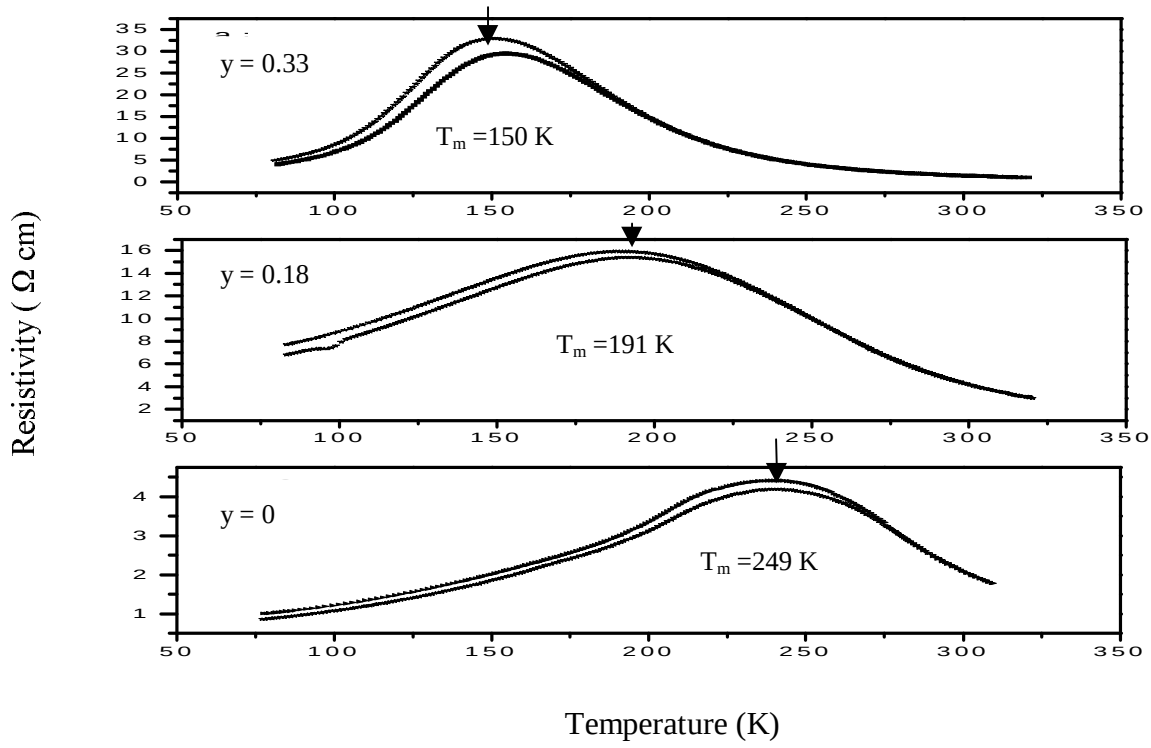


Fig.3.9. The temperature dependence of the resistivity of $Nd_{0.66}(Sr_{1-y}(Li_{Z1})_y)_{0.34}MnO_3$ ( y = 0 , 0.18 , 0.33 : series1) . Upper / lower curve , B = 0 and 0.5T .

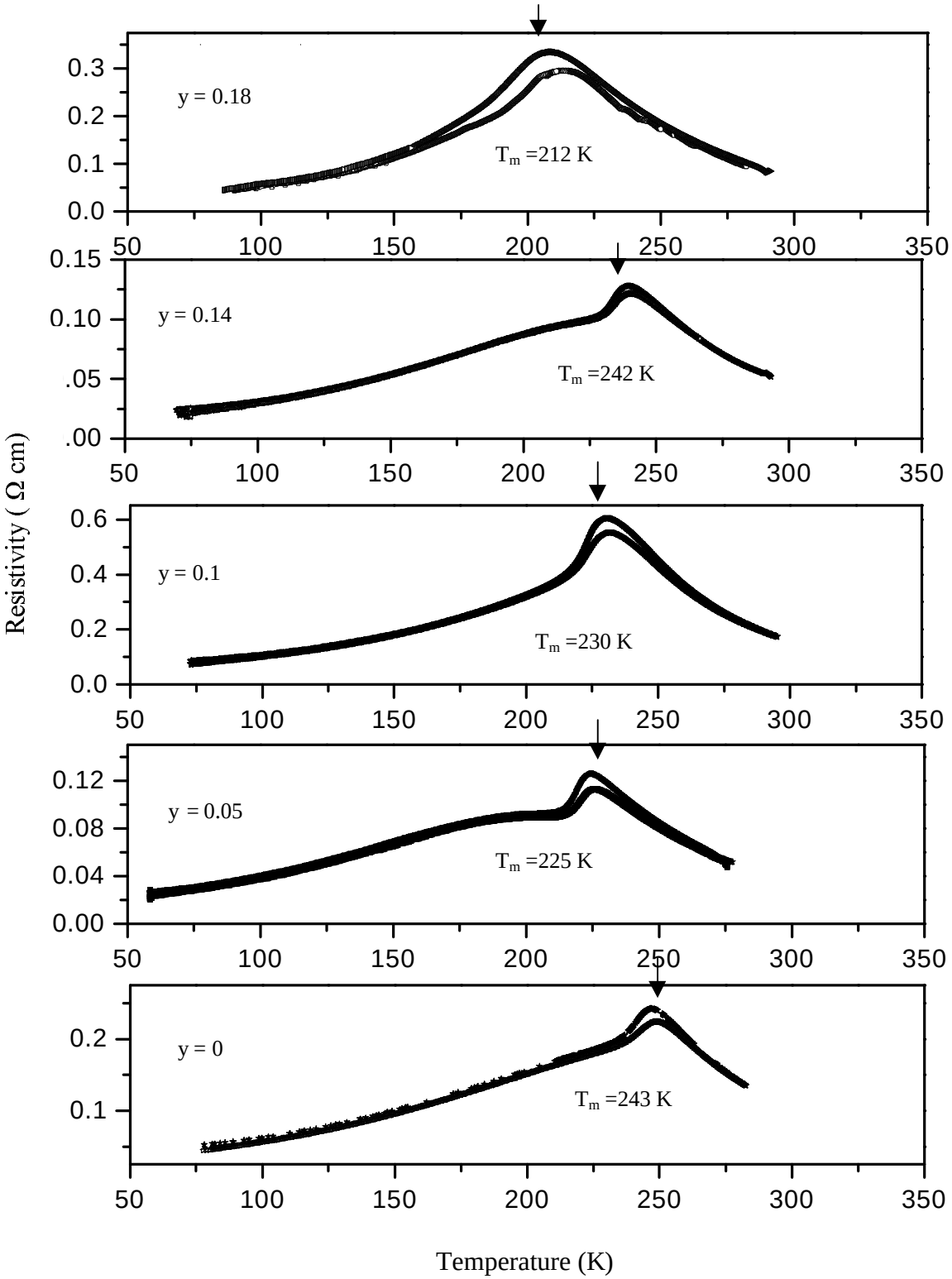


Fig.3.10 : The temperature dependence of the resistivity of $Nd_{0.66}(Sr_{1-y}(Li_{Z2})_y)_{0.34}MnO_3$
( y = 0 , 0.05 , 0.1 , 0.14 , 0.18: series2)
Upper / lower curve , B =0 and 0.5T

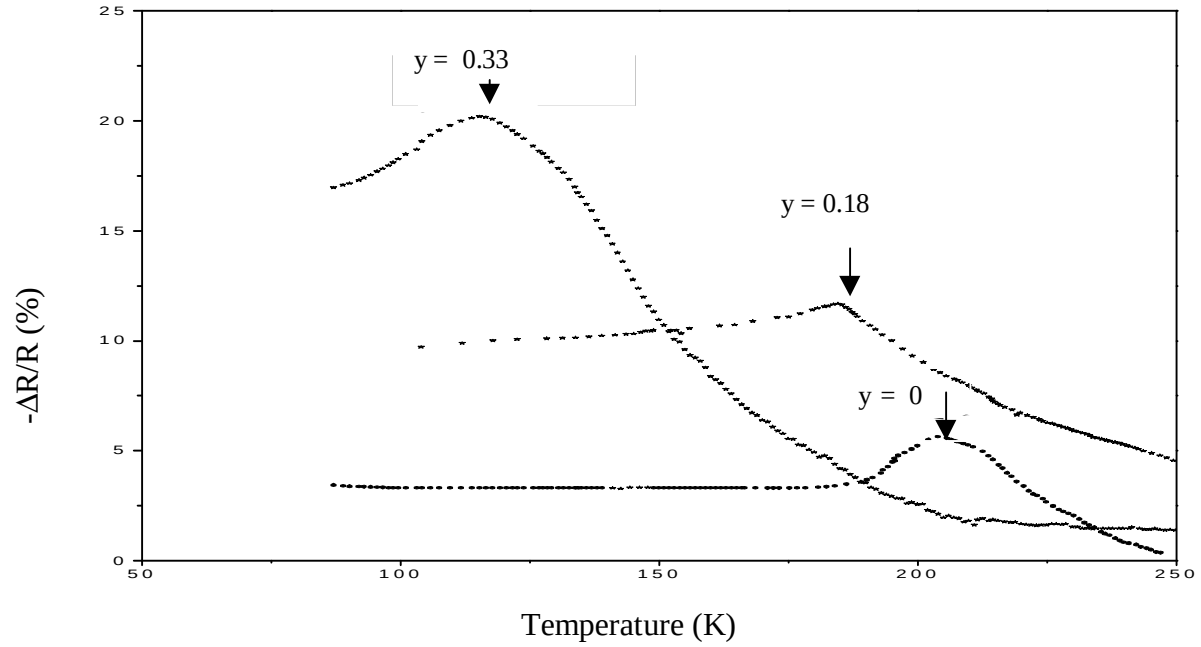


Fig.3.11: The temperature dependence of the magnetoresistance of $Nd_{0.66}(Sr_{1-y}(Li_{Z1})_y)_{0.34}MnO_3$ with y = 0 , 0.18 , 0.33 samples in 0.5T field : series(1), arrows $T_m$ .

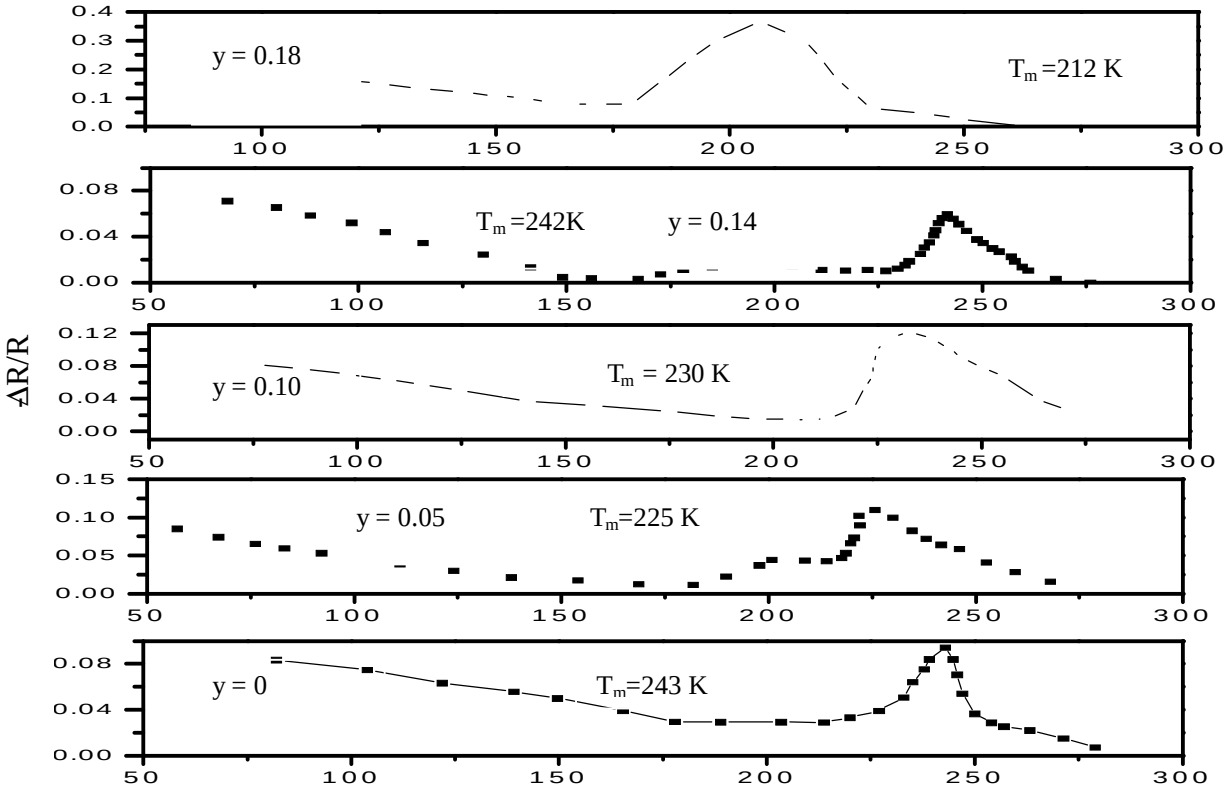


Fig.3.12: The temperature dependence of the magnetoresistance of $Nd_{0.66}(Sr_{1-y}(Li_{Z2})_y)_{0.34}MnO_3$ with ( y = 0 , 0.05, 0.1 , 0.14 , 0.18: series2 ) samples in 0.5T field .

## 3.3. Specific Heat Capacity $C_P(T)$

Fig(2.2) shows that the $C_P$ (T) curve of y = 0 series (2) exhibits a sharp endothermal peak $\Delta C_P$ (T). As the Li content increases see Fig(3.13) and Fig(3.14) , the endothermal peak broadens and shifts toward lower temperatures. For $y \geq 0.33$ the $\Delta C_P$ (T) tends to disappear , probably because of the increasing chemical randomisation . Note, that the peak position ($T_C$) for series 2 drops very fast on going from y = 0 to y = 0.05, as expected from eq.1, but then goes back to almost the y = 0 position for y = 0.1 and y = 0.14. Then , for y = 0.18, $T_C(y)$ drops again. The same behaviour is found for the maximum of the resistivity curve ($T_{max}$ ; see Table 4). For series (1) the broading of the $C_P(T)$ – peak set in even earlier probably because of stronger randomisation . The peak temperature , $T_P$ , of $C_P(T)$ curve agrees with the $T_C$ as derived from magnetization curves *M* (T) within ≤ 8K . That implies that the endothermal peak is associated with the magnetic transition [39].

The calculated entropy changes $\Delta S$ at different $T_P$ are shown in Table 1.

$$T_P . \Delta S = \int_1^2 C_P^m dT \qquad \left[ \frac{J}{g} \right] \tag{3-6}$$

Where the integral is the area under the peak , limited by the lattice contribution (Debye function)

Table 6.Transition temperature $T_P$ ,$T_C$ and entropy change ΔS for series 2 ; $\theta_D$ Debye temperature.

| mol % $Li_2CO_3$ y | $T_P$ (K) | $T_C$ (K) | $\theta_D$ (K) | $\Delta S$ (J/gK) |
|---|---|---|---|---|
| 0 | 245 | 248 | 600 ± 10 | $0.72 \times 10^{-2}$ |
| 0.05 | 226 | 223 | 510 ± 10 | $0.69 \times 10^{-2}$ |
| 0.10 | 235 | 230 | 500 ± 10 | $0.54 \times 10^{-2}$ |
| 0.14 | 237 | 240 | 500 ± 10 | $0.30 \times 10^{-2}$ |
| 0.18 | 198 | 204 | 500 ± 10 | $0.25 \times 10^{-2}$ |
| 0.26 | 170 | 184 | 482 ± 10 | $0.23 \times 10^{-2}$ |
| 0.33 | --- | 178 | 480 ± 10 | --- |
| 0.40 | --- | 101 | 470 ± 10 | --- |
| 0.46 | --- | 140 | 445 ± 10 | --- |

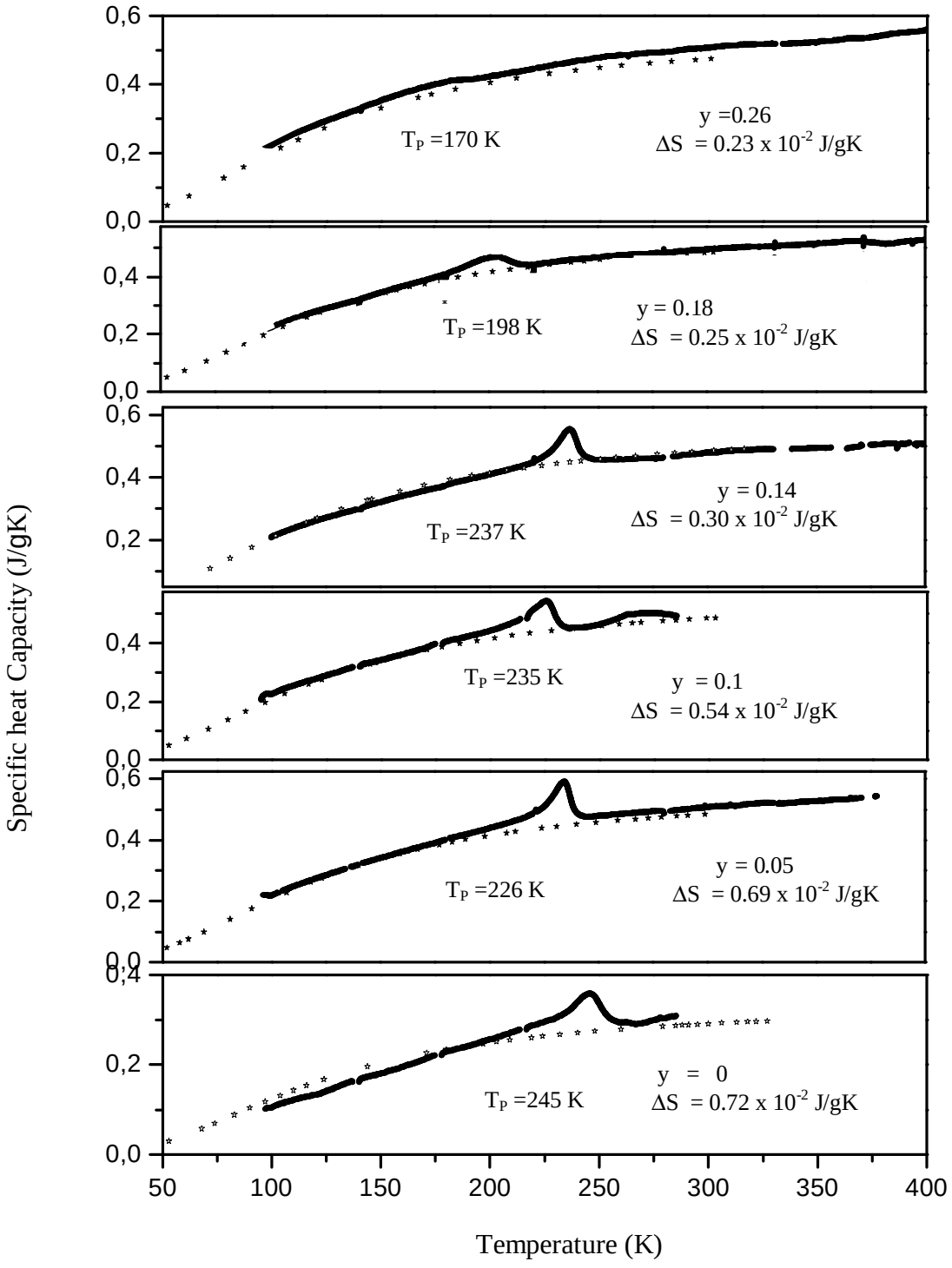


Fig.3.13: Temperature dependence of the specific heat capacity of $Nd_{0.66}(Sr_{1-y}(Li_{Z2})_y)_{0.34}MnO_3$ with y =0 , 0.05 , 0.1 , 0.14 , 0.18 , 0.26 : series(2). Points : calculated lattice specific heat contribution after Debye . Solid line : measurements

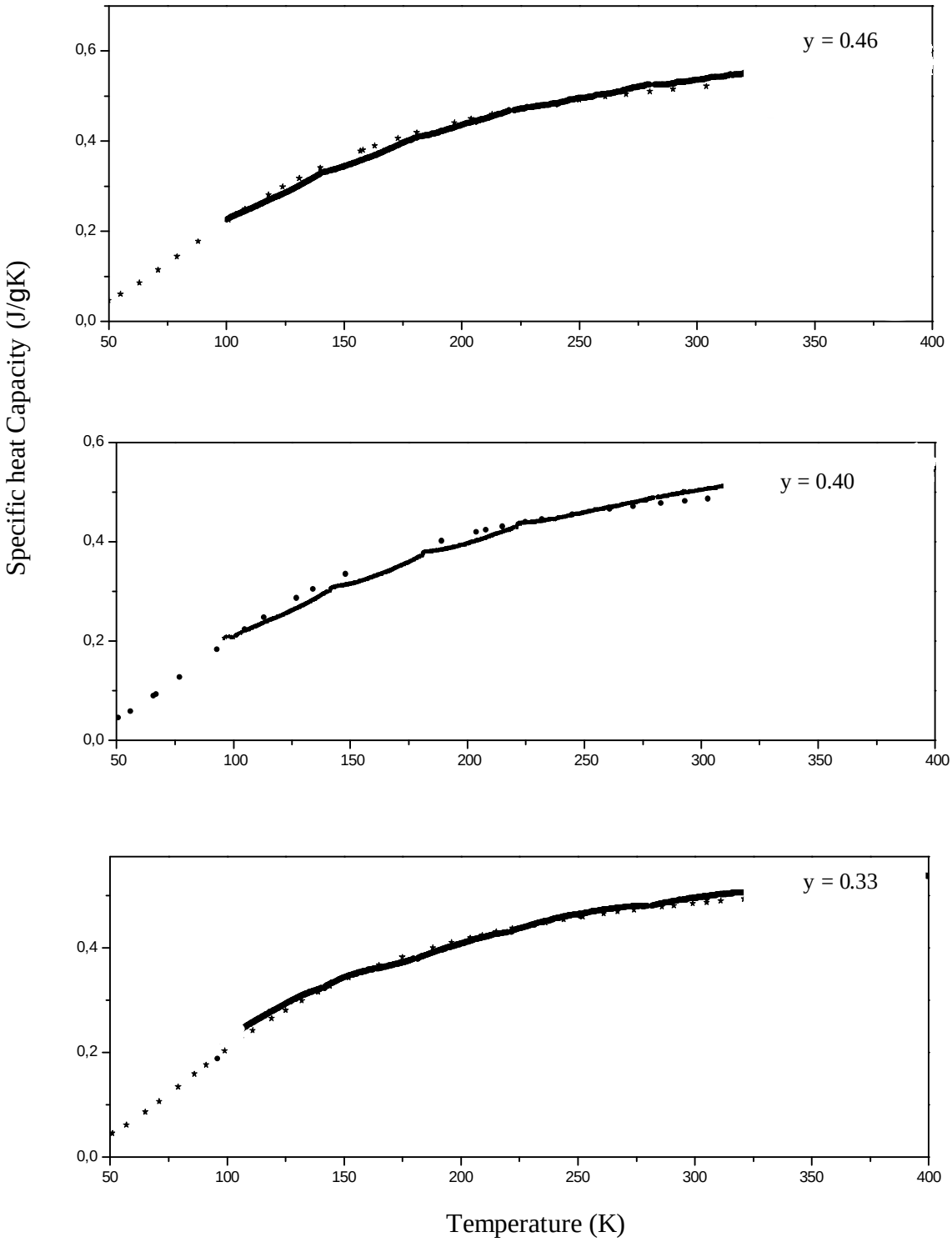


Fig.3.14: Temperature dependence of the specific heat capacity of $Nd_{0.66}(Sr_{1-y}(Li_{Z2})_y)_{0.34}MnO_3$ with y = 0.33 , 0.40 , 0.46: series (2) .
Points : calculated lattice specific heat contribution after Debye .
Solid line : measurements

## 3.4. Thermoelectric Power (TEP)

Measurement of the electric field induced by a temperature gradient across a sample provides complementary information to the resistivity. The Seebeck coefficient S is defined as $\Delta V/\Delta T$ ,the thermoelectric voltage per degree of temperature difference. Because no current flows when the voltage is measured potentiometric , the thermopower does not depend on the connectivity of the conducting regions, and the thermopowers of individual grains are additive. There have been many measurements of the thermopower of samples with $x \approx 0.3$ which exhibit a metal –insulator transition [40-41] .Our thermoelectric power of bulk samples $Nd_{0.66}(Sr_{1-y}(Li_{Z2})_y)_{0.34}MnO_3$ with y =0 , 0.1 , 0.14 , 0.18 ( series 2) in the temperature range (77-320K) is shown in Fig(3.15) , and for y = 0.26 ,0.33 0.40 ,0.46 , S(T) is shown in Fig(3.16).The samples with y = 0 ,0.1, 0.14 , 0.18 ,0.26 ,0.33 exhibit both negative and positive thermopower values while y = 0.40 , 0.46 exhibits positive thermopowers only . In general , the thermopower increases with increasing Li content, and thus also with increasing resistivity. The Thermopower S(T) is also measured using the TTE – method as described in Chap.II.

In general , we find a greement with $V^*_3$ and S as measured conventionally see Fig(3.17) and Fig(3.18). There are small differences which probably arise from the fact that $V^*_3$ is measured close to the surface where there could be a small oxygen deficit , while the conventional S is measured in the bulk. Note also; that $T_m$ is either close to the inflection point of S(T) suggesting an influence of the metal – insulator transition (for $y \leq 0.4$) or $T_C$ is close to the (positive) maximum of S(T) ($y > 0.4$) .

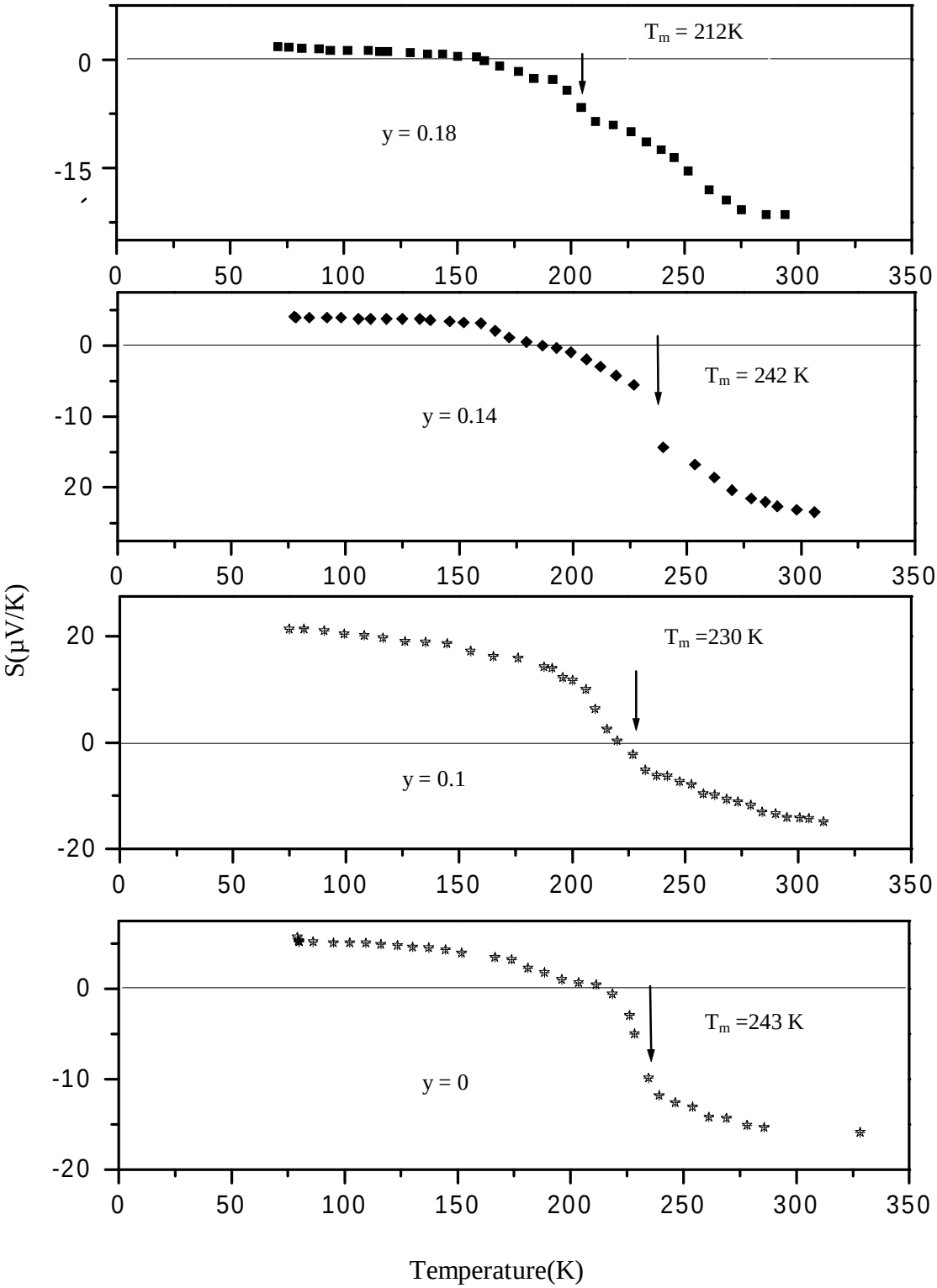


Fig.3.15: The temperature dependence of the thermopower of $Nd_{0.66}(Sr_{1-y}(Li_{Z2})_y)_{0.34}MnO_3$ with y = 0 , 0.1 , 0.14 , 0.18 samples: series(2).

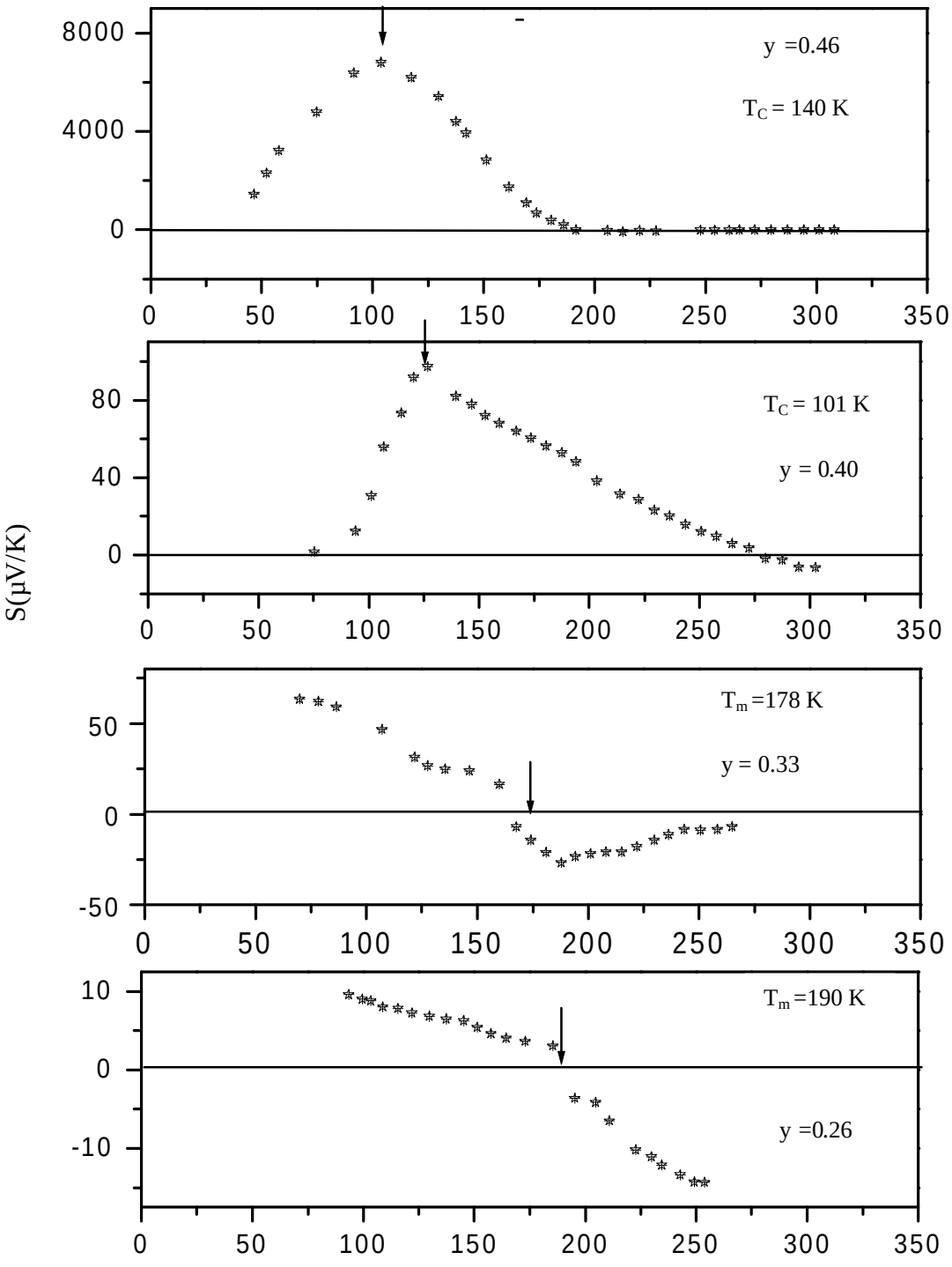


Fig .3.16: The temperature dependence of the thermopower of $Nd_{0.66}(Sr_{1-y}(Li_{Z2})_y)_{0.34}MnO_3$ with y = 0.26 , 0.33 ,0.40, 0.46 samples: series (2)

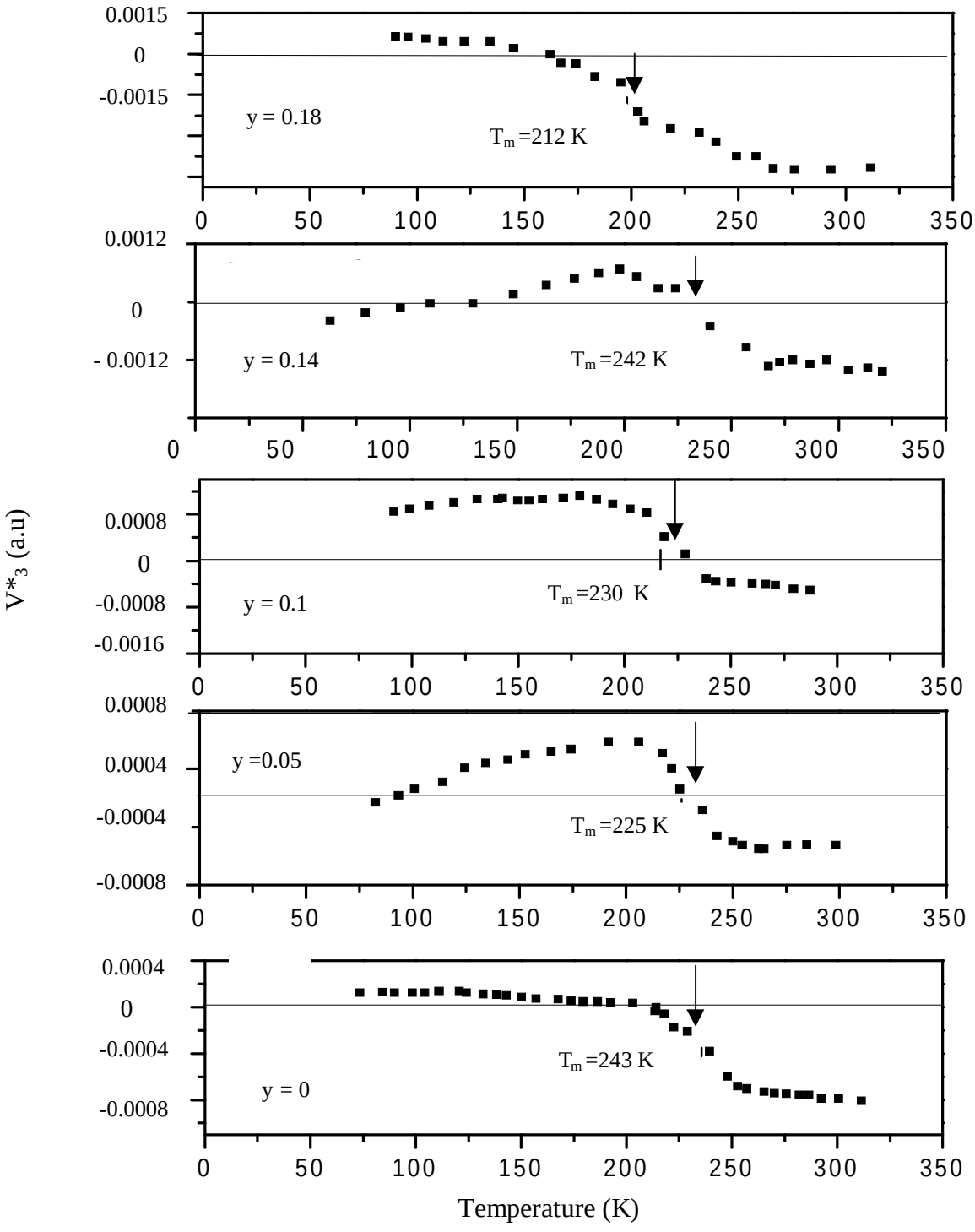


Fig.3.17: The temperature dependence of $V^*_3 \sim S$ as measured by the TTE – method of $Nd_{0.66}(Sr_{1-y}(Li_{Z2})_y)_{0.34}MnO_3$
with y = 0 , 0.05 , 0.1 , 0.14 , 0.18: series (2).

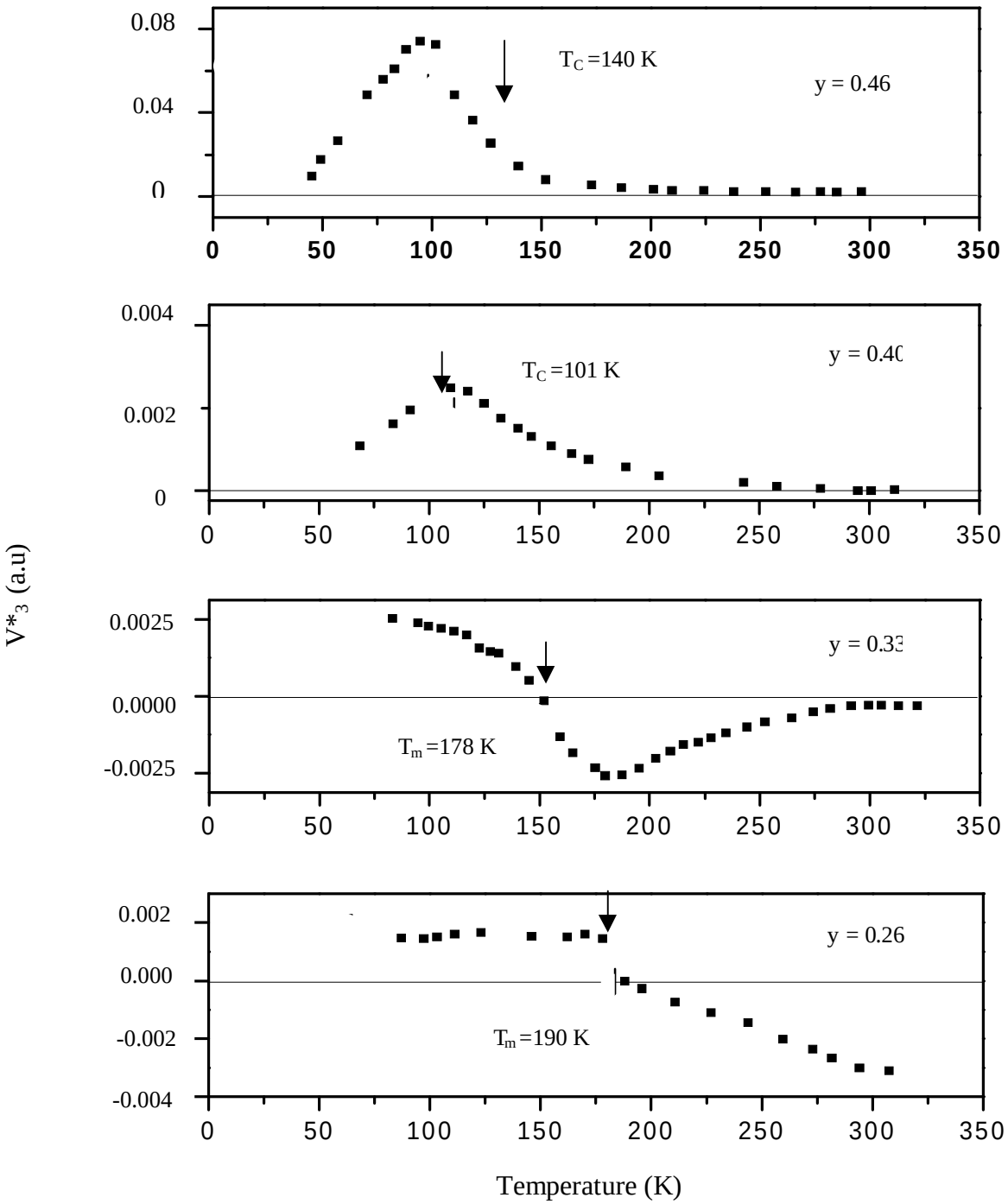


Fig.3.18: The temperature dependence of $V^*_3$ or $Nd_{0.66}(Sr_{1-y}(Li_{Z2})_y)_{0.34}MnO_3$ with y = 0 .26 , 0.33 , 0.40 , 0.46 : series (2).

## 3.5.Heat diffusivity and heat conductivity

The heat diffusivity of sample $Nd_{0.66}(Sr_{1-y}(Li_{Z2})_y)_{0.34}MnO_3$ with y = 0 , 0.05 , 0.1 , 0.14 ,0.18 (series 2) and in the temperature range (77-320K) are shown in Fig(3.19) , Fig(3.20) .The heat diffusivity of all samples decreases with increasing temperature . Fig(3.21) and Fig(3.22) show the heat conductivity in the temperature range (77-320K). Note that sometimes ( y = 0.14

,0.33 ,0.46 ) a step is observed both in k and D at the combined Curie – and metal-insulator transition temperature , while in the other cases there is a smooth transition or no change at all.

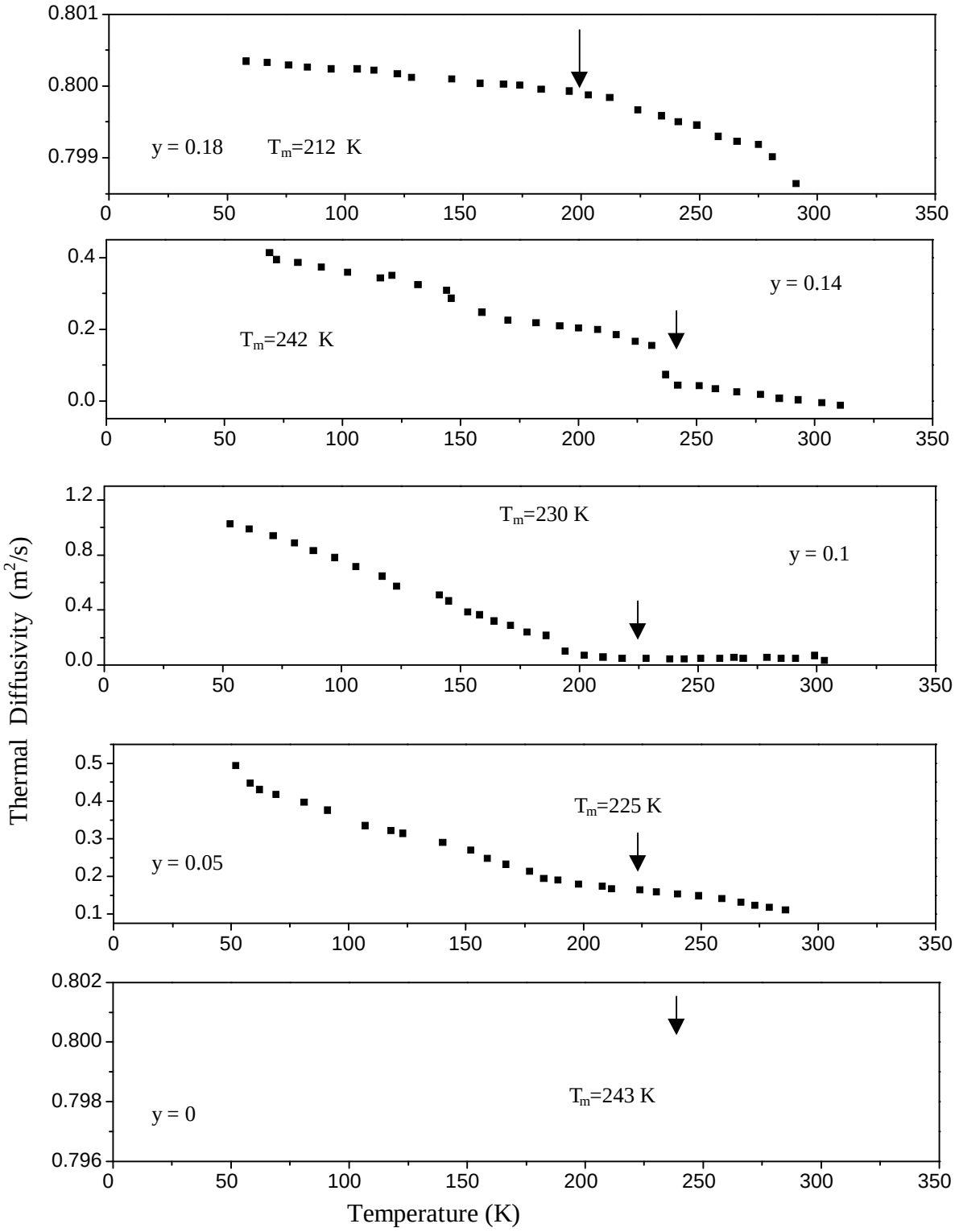


Fig .3.19: The temperature dependence of the thermal diffusivity D of $Nd_{0.66}(Sr_{1-y}(Li_{Z2})_y)_{0.34}MnO_3$ with y = 0 , 0.05 , 0.1 , 0.14 , 0.18samples: series (2).

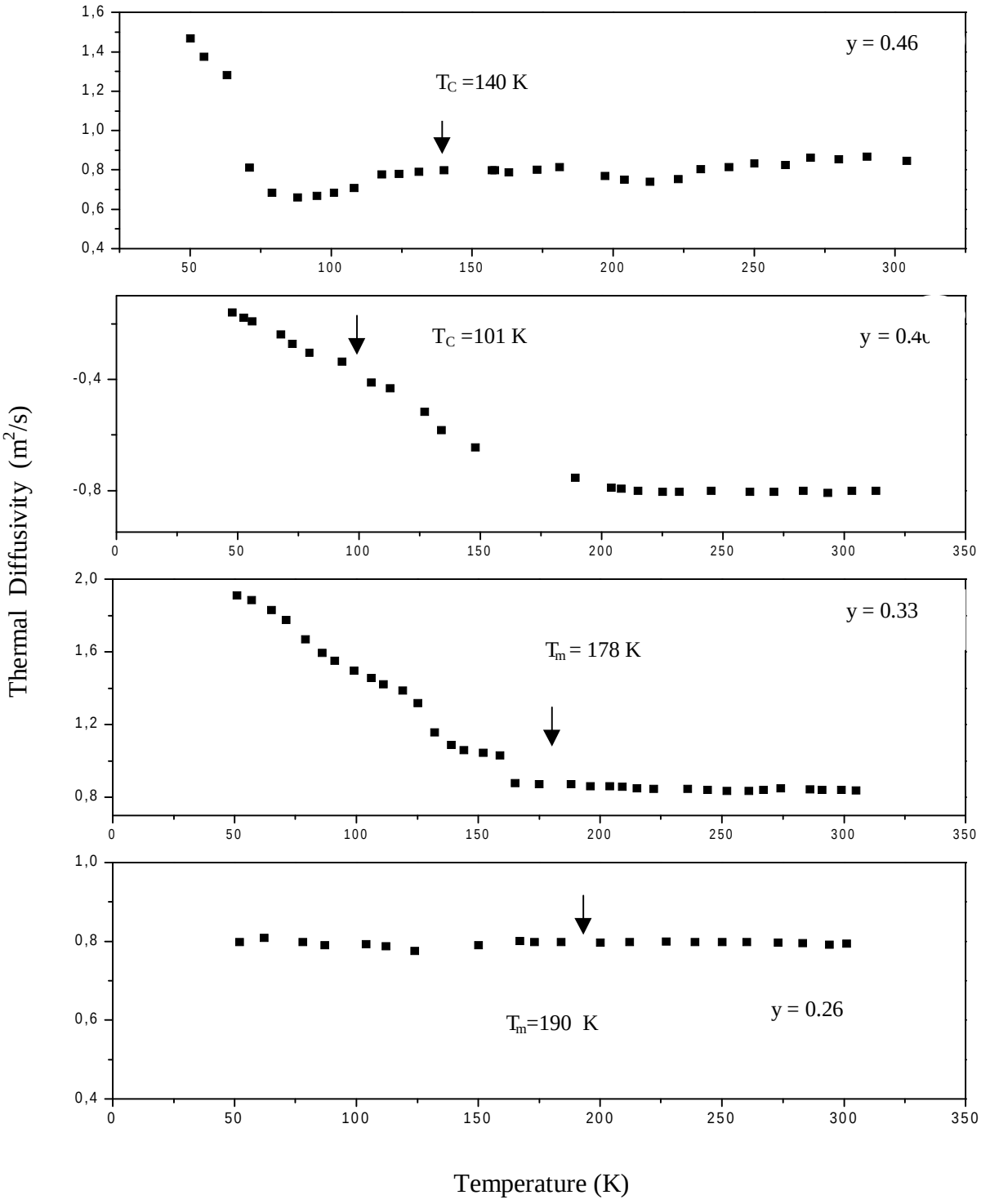


Fig .3.20: The temperature dependence of the thermal diffusivity D of $Nd_{0.66}(Sr_{1-y}(Li_{Z2})_y)_{0.34}MnO_3$ with y = 0.26 , 0.33 , 0.40 , 0.46 samples: series (2).

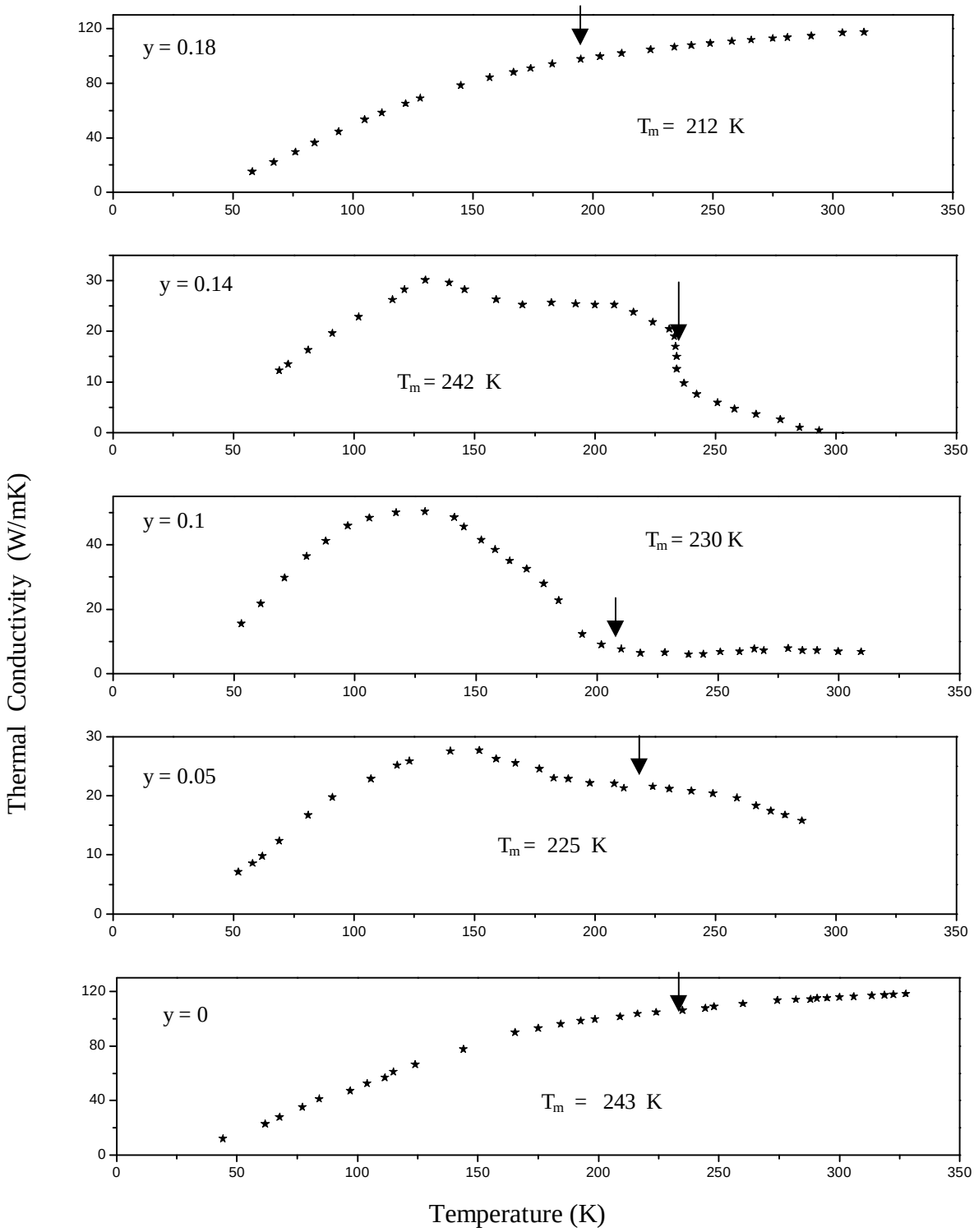


Fig .3.21: The temperature dependence of the thermal conductivity *k* of $Nd_{0.66}(Sr_{1-y}(Li_{Z2})_y)_{0.34}MnO_3$ with y = 0 , 0.05 ,0.1 , 0.14 , 0.18 samples: series (2).

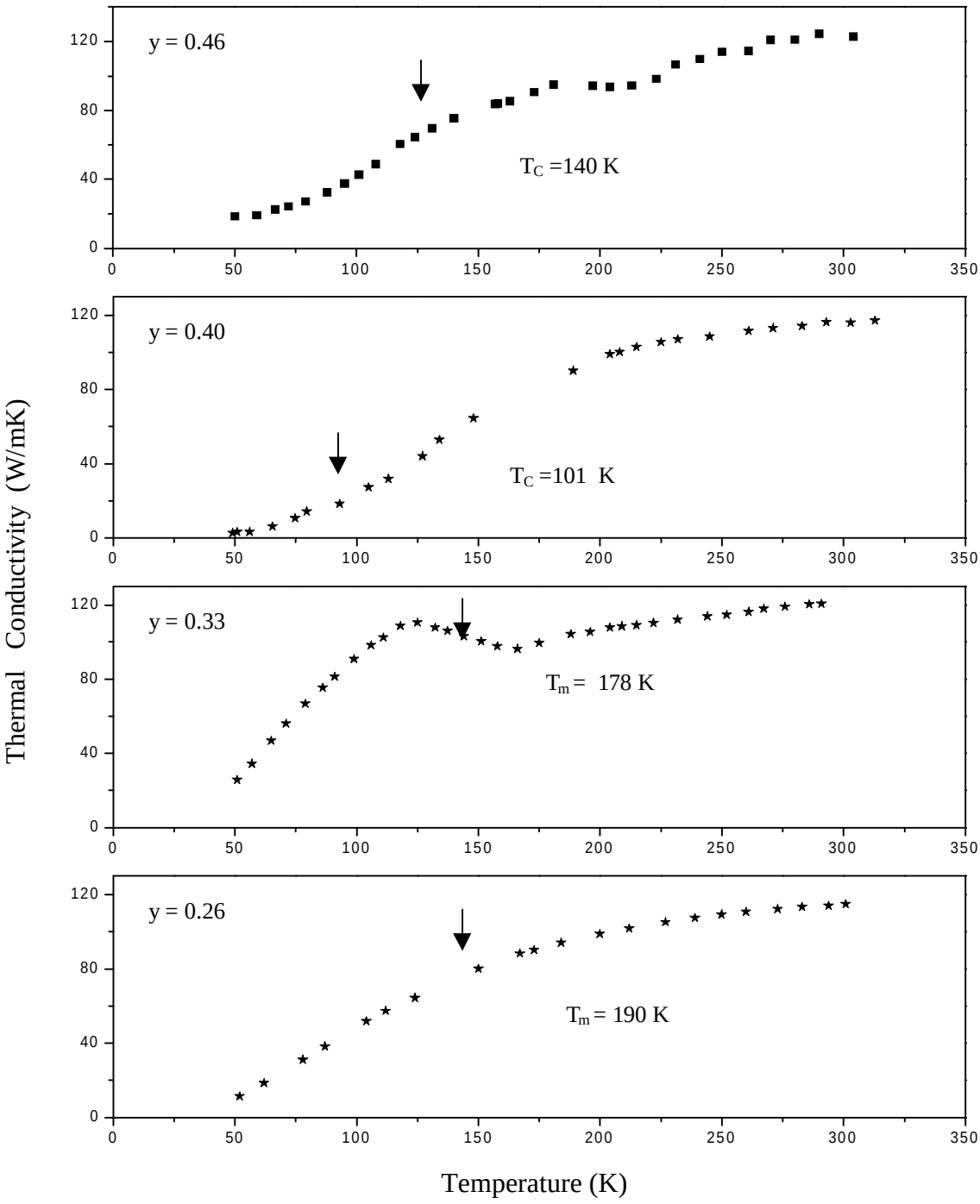


Fig .3.22: The temperature dependence of the thermal conductivity *k* of $Nd_{0.66}(Sr_{1-y}(Li_{Z2})_y)_{0.34}MnO_3$ with y = 0.26 , 0.33 , 0.40 ,0.46 samples: series(2).

## CHAPTER IV
## Discussion

We start the discussion by looking at the dependence of the Curie temperature $T_C$ on the Li – content y . According to de Gennes [4] ,we have

$$kT_C = b\, x'' z \qquad (4\text{-}1)$$

Where $x''$ is the number of Zener carriers per $cm^3$, b the width of the Zener band , z is the number of nearest neighbours .Without Li - substitution $x''$ is equal to the hole doping x . Thus the drop of $T_C$ with increasing y comes either from a change of $x''$ with y or a change of b with y , or both . The transfer integral b can change with y as the Li – doping changes the tolerance factor $\langle t \rangle$ . The tolerance factor itself is supposed to change the transfer integral or Zener bandwidth b. Alternatively , the drop in $T_C$ could result from a reduction of the Zener carrier concentration $x''$ . $x''$ could be reduced by localising a former free electron at a $Sr^{2+} \rightarrow Li^{+}$ substitutional site (Zener bond blocking ) . Then for each blocking site , one free Zener carrier is trapped , reducing both the metallicity and the ferromagnetic coupling.

### 4.1. Calculation of the tolerance factor

The variation of the tolerance factor $\langle t \rangle$ with Li – content y is shown in Table 1. X- ray diffraction at room temperature shows that the prepared samples are polycrystalline and have an orthorhombic structure**.** Going from y = 0 to y = 0.05 the lattic constant a and the unit cell volume decrease , while c increases , probably because the substitution of $Sr^{2+}$ by $Li^{+1}$ converts $Mn^{3+}$ to $Mn^{4+}$which has a smaller ionic radius as $Mn^{3+}$ . This is consistent with the increasing reflection intensity of (011) , (221) for y > 0.33 and with the variation of the tolerance factor $t = (r_A+r_O) / \sqrt{2}\,(r_B+r_O)$ of $R_{1-x}A_xMnO_3$ where $r_A$ , $r_B$ and $r_O$ represent the average ionic size of $(Sr/Li)_{0.34}$ , Mn and oxygen .

The partial substitution of the smaller $Li^{+}$ ions (of ionic radius ~ 0.76 Å) for the larger $Sr^{2+}$ions (ionic radius of ~ 1.12 Å) , produces an average ionic radius of the A site $\langle r_A \rangle$ which systematically decreases [42] in series 1, see Fig(4.1). Possibly, this kind of distortion is directly related to the concentration of $Mn^{3+}$ ions .The tolerance factor $\langle t \rangle$ of series 1 , series 2 and $\langle r_A \rangle$ [43] are shown in Table 1 . Fig(4.1) show the relation between $\langle t \rangle$ , $\langle r_A \rangle$ and Li content , $\langle t \rangle$ and $\langle r_A \rangle$ decrease with increasing Li content and always we have $0.5 < \langle r_A \rangle < 0.96$ .

Table1. The variation of tolerance factor $\langle t \rangle$ and $\langle r_A \rangle$ with Li content y for series1 and series2.

| y | Series 1 $\langle r_A \rangle$ Å | Series 1 $\langle t \rangle$ | Series 2 $\langle r_A \rangle$ Å | Series 2 $\langle t \rangle$ |
|---|---|---|---|---|
| 0 | 0,381 | 0,677 | 0,381 | 0,677 |
| 0.05 | --- | --- | 0,384 | 0,678 |
| 0.01 | --- | --- | 0,388 | 0,679 |
| 0.14 | --- | --- | 0,391 | 0,681 |
| 0.18 | 0,369 | 0,671 | 0,394 | 0,682 |
| 0.26 | --- | --- | 0,401 | 0,685 |
| 0.33 | 0,356 | 0,667 | 0,408 | 0,687 |
| 0.40 | --- | --- | 0,415 | 0,690 |
| 0.46 | --- | --- | 0,422 | 0,693 |

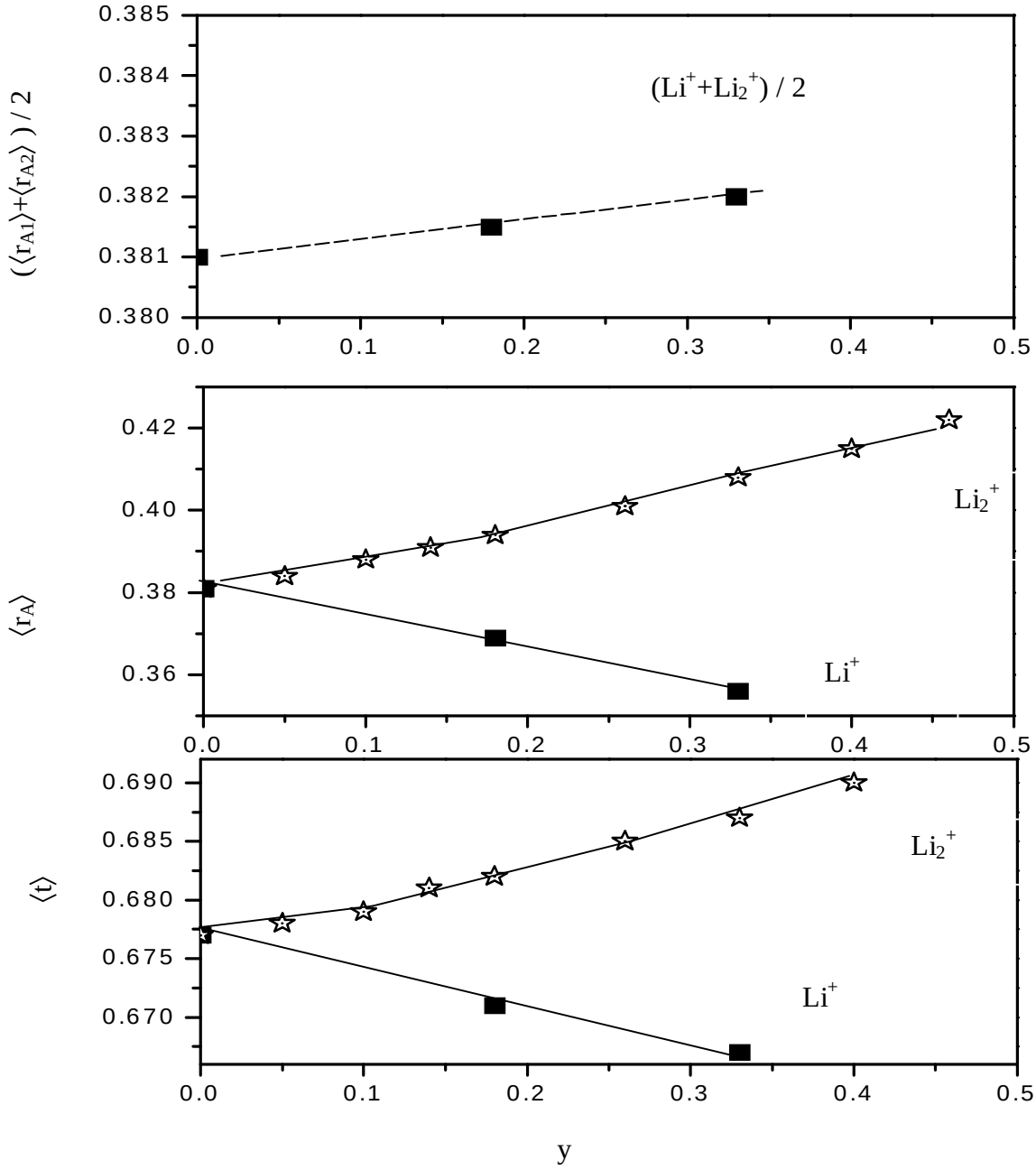


Fig .4.1: The dependence of $\langle r_A \rangle$ and the tolerance Factor $\langle t \rangle$ on the Li content y for $Nd_{0.66}(Sr_{1-y}(Li_Z)_y)_{0.34}MnO_3$ ; for z = 1 and z = 2

The tolerance factor decreases with y for series 1 and increases with y for series2. Since the Zener band width b is supposed to vary with $\langle t \rangle$ and since the Curie temperature $T_C$ is proportional to b, if the Zener carrier concentration is constant,we would expect $T_C$ (y) to drop for series 1 and to increase for series 2. $T_C$ drops indeed for series 1 but $T_C$(y) for series 2 is more complex. In particular $\langle t \rangle$ of triplets $Li^+$-$Li_2^+$ would increase and not decrease as found experimentalls. Also , the relative change of $\Delta\langle t \rangle$ / $\langle t \rangle$ is only 1.5 % while $\Delta T_C$ / $T_C$ is about 67% (Fig.2.1) thus the Li – doping induced changes of b alone cannot explain the decrease of $T_C$(y) for series (2).

## 4.2.Zener bond blocking

### 1. Series 1

Assuming that the substitution of the $Li^{1+}$ ions shifts the disproportion towards $Mn^{4+}$ , if one $Mn^{3+}$ is changed to $Mn^{4+}$ because of the local charge conservation (one $Sr^{2+}$is substituted by one $Li^{1+}$), the Zener chain is blocked , which increases the resistivity and decreases the ferromagnetic coupling by about two blocked Zener bonds per one $Li^{1+}$ ion [44].
.
Suggesting that each $Li^{1+}$ ion on the average reduces the formal carrier cocentration x by taking one Zener carrier out , the true free carrier concentration is $x''$ and $T_C \sim x''$ . If we calculate the probability of a Zener bond to be qualified,acc.to Goodenough/ Rao theory[13,33] ,we obtain :

$$T_C \sim x'' (1- x'') 2 x'' (1-2 x'') \qquad (4\text{-}2)$$

Where $x'' = x + y$ is the number of $Mn^{4+}$ and x = 0.34 . Thus we arrive at ;

$$T_C / T_0 = 1- (3/2) y + \ldots \qquad (4\text{-}3)$$

$T_0$ is the Curie temperature of the base compound .
According to Eq. (4-3) , $T_C$ vanishes at $y = 2/3$ and no Zener bond remains. Thus we expect that ultimately $y = 0.67$ limits the region of existence of the Sr/Li mixed phase .
Experimentally the limit appears to be lower, i.e. at $y \geq 0.46$ .

### 2 . Series 2

With the Li – doping , we may either assume an increase in the hole doping or an increase of blocking bonds, i.e. $Nd_{0.66}(Sr_{1-y}(Li_{Z1})_y)_{0.34}MnO_3$ might become more conducting with increasing y or less conducting , similar to $La_{1-x}Ca_xMn_{1-y}Ge_yO_3$ with $Ge^{+4}$[45] . As the resistivity increases with y , we have to reject the first possibility . With the second approach , if one $Li^{1+}$ ion has the equivalent blocking effect as one $Ge^{4+}$ion , then $T_C$ is proportional to the number of still intact valence mixed (Zener) $Mn^{3+}$- $Mn^{4+}$ bonds .
$Nd_{0.66}(Sr_{1-y}(Li_{Z2})_y)_{0.34}MnO_3$ has $T_C = 245K$ at $y = 0$ . At low y , $T_C$ (y) drops like with series 1 . The increase of $T_C$ which follows for $0.05 < y < 0.15$ ( see Fig.4.2) , could be related to the increased appearance of isolated pairs $Li_2^{1+}$ . This means that $Sr^{2+}$ is substituted by $Li_2^{1+}$ and this rehabilitates a blocked Zener bond. More Li-doping , $y > 0.15$ , finally blocks the rehabilitated sites again through the advent of a third $Li^+$ etc , and $T_C$(y) of series 2 drops again .

## 4.3. Magnetic Coupling

In comparison to $Nd_{0.66}Sr_{0.34}MnO_3$, x-ray structure refinement reveals that there is a larger lattice distortion in $Nd_{0.66}Sr_{1-y}(Li_Z)_y)MnO_3$, accompanied by a significant deformation and rotation of the $MnO_6$ octahedra. According to double exchange theory, the metallic conduction and ferromagnetism of the perovskite manganites are established simultaneously via the hopping of $e_g$ electrons between manganese ions, mediated by the oxygen anions [3]. The distortions of the compound may influence the electron hopping and complicate the magnetic structure of the compound. In general, it is believed that both the ordering of the $e_g$- orbitals and the deformations and rotations of the $MnO_6$ octahedra can result in the occurrence of strong superexchange interactions, most of which are antiferromagnetic [46-48]. According to de Gennes[4] , the

competition of antiferromagnetism and double exchange interactions between manganese ions can lead to canted or helical spin structures . Taking into account the low magnetization, the low moment state in NSLM probably comes from a randomised canted spin structure . It is observed that the magnetization of the low moment state strongly depends on the Li content and varies from a negligible value for y = 0.46 to a value corresponding to a fully spin-polarized moment for y = 0. Thus the (parasitic) magnetization might originate from the different local distortions of the lattice around $Sr^{2+}$ and $Li^{1+}$ ions and the trapping of Zener electrons at blocking sites, while $Nd_{0.66}Sr_{0.34}MnO_3$ is ferromagnetic with a fully spin-polarized moment hole doping and without blocking sites. For the canted (or parasitic) spin structure, the resistivity appears to be much higher and its temperature dependence becomes metallic only below 100 K .

As Li substitution for Sr increases, the magnetic transitions become increasingly broader. Specifically , with the increase of $Mn^{3+}$ - $Mn^{4+}$ blocking sites due to $Sr^{2+}$ hole subsitution by $Li^{1+}$, we observe a reduction of *M* .This we ascribe to an increase of the spin frustration associated with the increase of the competing negative $Mn^{4+}$- O – $Mn^{4+}$ superexchange pair interactions , together with an increasing randomization. It seems that the Li doping tends to weaken both the double exchange and the negative superexchange interaction and this results in the fast decrease of the net magnetization , which represents the averaged ordered moment of sum of the $t_{2g}$ spins and the forcibly aligned $e_g$ spins .

The large difference between $T_C$ and $\theta_C$ ($\theta_C > T_C$) also suggests the existence of different exchange paths ,one of which is the double exchange interaction . For $Mn^{4+}$– $O^{2-}$– $Mn^{4+}$ bonds, only a weak antiferromagnetic interaction is predicted . Antiferromagnetic transitions are really not observed in this study. On the other hand, the $Mn^{3+}$ – $O^{2-}$ –$Mn^{3+}$ superexchange interaction is relatively strong as compared to the $Mn^{4+}$ – $O^{2-}$ – $Mn^{4+}$ interaction ,and it becomes ferromagnetic for a < 3.87 Å and antiferromagnetic for a > 3.87 Å [49] . We have always the second (afm) case ; see Table 3 .

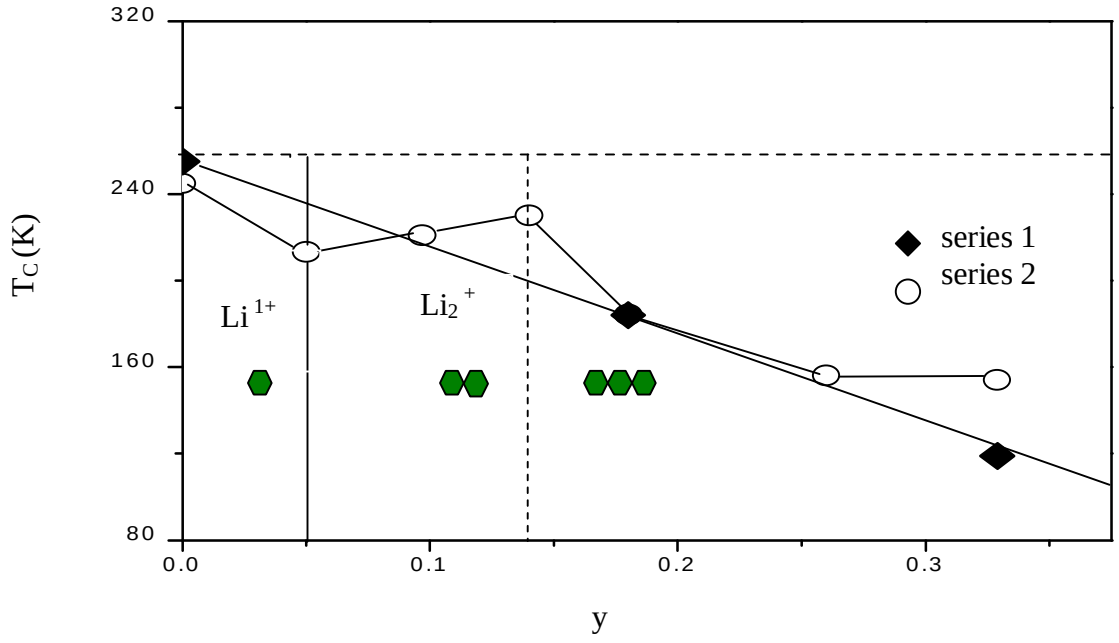


Fig.4.2: The relation between $T_C$ and Li content y for $Nd_{0.66}(Sr_{1-y}(Li_Z)_y)_{0.34}MnO_3$
For series 2 and $T_m$ for series 1

## 4.4. Resistivity

At low temperatures the magnetic moment is large and the spin system is characterized by strong ferromagnetic coupling between the magnetic ions which prevents the formation of magnetic polarons and any significant spin disorder. Consequently, the scattering potentials are weak and metallic conduction occurs . The magnetic field has virtually no effect in this low-temperature regime. As the temperature increases above 200 K, the magnetization rapidly decreases and, concurrently, we observe a rapid rise in the resistivity. Also, the transport behavior becomes field sensitive. At the metal –insulator transition temperature $T_m$ , the resistivity displays a sharp peak and the magnetoresistance shows a deep minimum.

At low temperatures the residual resistivity $\rho_r$ , i.e. the scattering on impurities or defects,is increased from 0.02 Ω cm to 0.12 Ω cm with increasing of Li content y for series 1 . Gupta et al [50] have demonstrated that the residual resistivity increases rapidly with decreasing crystallite size .Either the Li – doping produces an increasing number of scattering sites ( Zener bond blocking sites ) , or the grain size increases with increasing Li – content . As we did not change the preparation conditions, Zener bond blocking is more probable . Also, the measured grain size (Ch.I) does not vary much.

The resistivity of series 2 has a more sharp metal insulator transition than ρof series 1 , this means that series 2 probably has less inhomogeneities and larger crystallites. The residual resistivity $\rho_r$ for the samples at y = 0.1 and y = 0.14 in series 2 is very small 0.08Ω cm and 0.03Ω cm respectively , this means that these two samples have low impurity levels or a smaller number of blocking sites see Fig.(4.3) . As $Li_2^{2+}$ avoids the formation of bond blocking sites , this is consistent with the increase in the Curie temperature $T_C$ ,observed between y = 0.05 and 0.15 . The presence of the weak shoulder for $T < T_C$ , for y = 0 and y = 0.18 has been attributed to spin polarons [51] in connection with grain (or phase) boundaries [44]. This shoulder converts to a secondary peak at $T < T_C$ in the samples with y = 0.05 and y = 0.14.

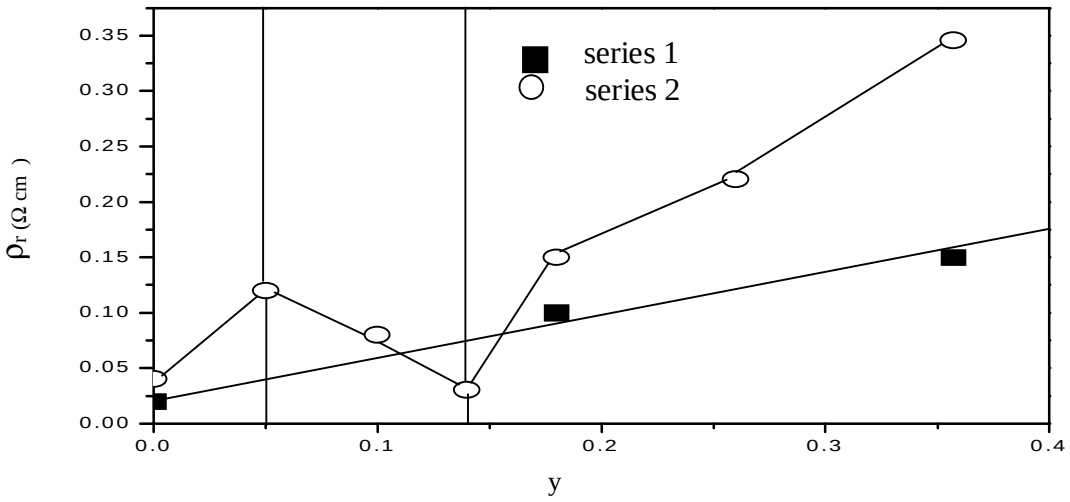


Fig. 4.3: The relation between The residual resistivity $\rho_r$ and Li content y for $Nd_{0.66}(Sr_{1-y}(Li_Z)_y)_{0.34}MnO_3$ for series 1 and series 2.

### 4.4.1. Resistivity for $y \geq 0.4$ and $T > T_C$

In the paramagnetic phase, $T > T_C$ the conduction is thermally activated, indicating a conduction by polarons, with activation energy increasing from 0.1 eV to 0.2 eV with increasing Li content y , while the activation energy is 0.147 eV for $Nd_{0.67}Sr_{0.33}MnO_3$ [52].
The resistivity data fit to a small polaron hopping law $\rho = \rho_0 \exp(E_0 / k_B T)$,but almost equally well to a variable range hopping model $\rho = \rho_0 \exp (T_0 /T)^{1/4}$ respectively, where $T_0$ would be a characteristic temperature which is related to the density of states in the vicinity of the Fermi energy $N(E_F)$ and the localization length $\xi$ , i.e., $kT_0 \approx 21 / [\xi^3 N(E_F)]$. $T_0$ would be $5 . 10^7$ K for $Nd_{0.7}Sr_{0.3}MnO_3$ at T = 200 K [53].

The characteristic temperature $T_0$ would increase with increasing Li y , from $3 . 10^7$ to $7 . 10^7$ for series1 ,and from $0.02 . 10^7$ to $26 . 10^7$ for series 2 see Table 4 (chp.III) , $T_0$ also increases monotonously as $T_m$ decreases [53] .This would mean that the density of states in the vicinity of the Fermi level decreases with increasing Li content y and increasing activation energy assuming the localisation length to be constant [52].. The motion of the polarons is very much hindered [53] . Between y = 0 and y = 0.05 the activation energy and $T_0 \sim 1 / N(E_F)$ indeed decreases . However this approach would not explain the increasing residual resistance with y .

The temperature dependence of the resistivity exhibits a semiconducting behavior without an M–I transition above 80 K for the samples with y = 0.40 and y = 0.46 . That is to say, these two compounds are semiconductors in the high-temperature paramagnetic phase as well as in the low-temperature ferromagnetic phase . With double exchange, both FM and metallic nature must coexist. Therefore, the FM order at low temperatures for samples with y = 0.40 and 0.46 does not originate from the DE interaction. It is well known that the $Mn^{+3} – O – Mn^{+4}$ bond angle is a crucial factor in determining the nature of the magnetic interactions in manganites. A $Mn^{+3} – O – Mn^{+4}$ 180° superexchange interaction generally leads to antiferromagnetic ordering while a 90° superexchange interaction of $Mn^{+3} – O – Mn^{+4}$ will result in ferromagnetic ordering [49]. Thus, the observed transition to weak ferromagnetism at large y may arise from positive superexchange contributions between Mn ions.

### 4.4.2. Resistivity for $y < 0.4$

For Li –contents $y < 0.4$ we observe a metal to insulator transition at $T_{mi}$ , As the resistivity of metals is much smaller as that semiconductors and also as the scattering mechanisms are different ,one better discusses both phases separatly . In principle , in the fm metallic regime one expects spin disorder scattering and see eq.(4-4) [54-55] , while in the semiconducting region we find activated behaviour (see 4.4.1) .When we have Zener blocking sites one expects a residual resistance , $\rho_r$ too. This is shown schematically in Fig 4.4.

$$\rho \quad \alpha \quad \frac{1 - \{M(T) / M(0)\}^2}{1 + \{M(T) / M(0)\}^2} \qquad (4\text{-}4)$$

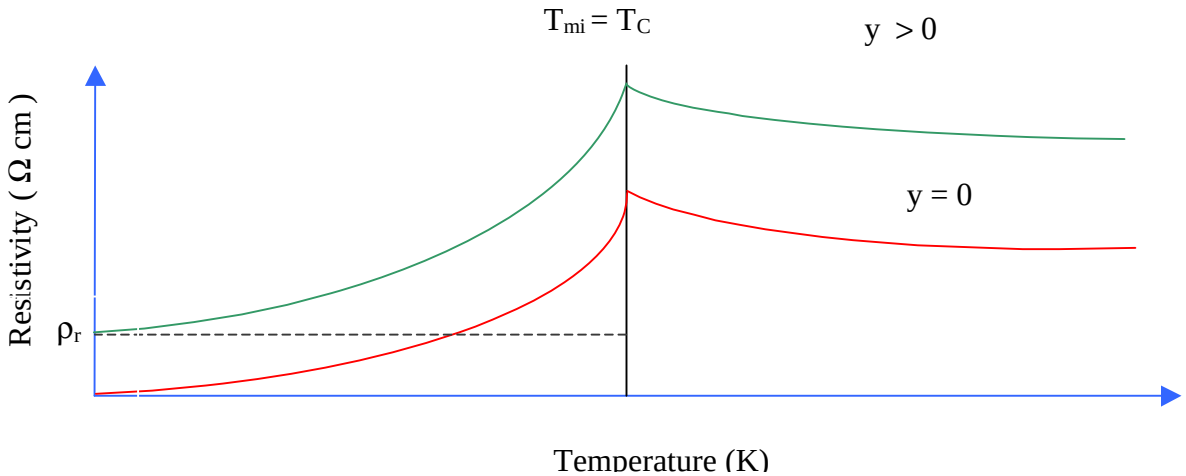


Fig.4.4: The temperature dependence of the resistivity for $y < 0.4$.

The scattering of charge carriers on the spin disorder can be described as magnon scattering , but in our case the magnetic excitations are more complicated i.e. magnetic polarons which might even contain a structural (magnetostrictive) component. The resistivity data for $T < T_{mi}$ are consistent with this picture.
However , sometimes a secondary maximum is observed in $\rho(T)$ , which has been connected with spin scattering on grain boundaries [56].

### 4.4.3. Magnetoresistance

Due to the instability of magnetic polarons in an external magnetic field, the magnitude of the resistivity is drastically diminished as one applies a magnetic field. The polarons form as the ferro-to paramagnetic transition is traversed on cooling , self – trapping the carriers.The polarons then melt when a magnetic field is applied and the result is a small negative magnetoresistance near the ordering temperature [57]. An intrinsic MR is found inside the grain, and gives the maximum values at $T_m$ .A similar approach which includes the field – induced variation of the electronic gap is given in [58] . An extrinsic MR is found at low temperatures. Realization of this effect requires that polarised conduction electrons tunnel in a single step from the conduction band of one grain to that of the other across the grain boundary. If the electrons are trapped for a time long as compared to the spin relaxation time （either at surface states or at intermediate trapping centers） during tranversal of a grain boundary, they lose their spin information and cannot contribute to the MR effect. At lowest temperatures, the spin relaxation might be slow and the carriers that tunnel from conduction band to conduction band across a grain boundary in one step might dominte the MR . Also , these electrons must exist at higher temperatures if a grain-boundary MR mechanism is to be realized at room temperature.

## 4.5. Thermoelectric Power (TEP)

The TEP results using the TTE method (1) are practically the same as the TEP results obtained conventionally (2) . The small differences might result from :

(1) measurement in a surface layer (TTE)
(2) measurement in the bulk (conventional )

### 4.5.1. TEP of the compounds with $y \geq 0.4$ .

Therefore , we only discuss the data – set (2) . For samples with $y \geq 0.4$ . S(T) changes sign, becoming negative as T increases . This behavior suggests the coexistence of two different types of carrier. In fact, in hole-doped semiconductors, at low temperature S(T) is positive as expected from the hole-doping and its extrinsic conductivity, but S(T) becomes negative in the intrinsic regime at higher temperatures, when the electrons are excited from the valence band (VB) into the conduction band (CB) [59]. Due to the higher mobility of the electrons within the CB the thermopower becomes negative. Thus a change of sign of S is commonly observed for hole doped semiconductors. The sudden drop of the thermopower at $T_C$ may arise from condensation of trapped carriers into (zener) extended states or into states according to mechanisms proposed recently [60] , leading to a corresponding decrease in resistivity. The hole – traps are probably identical with the Zener carrier blocking sites.

### 4.5.2. TEP of the compounds with $y \leq 0.4$ .

Metals generally have lower TEP's as semiconductors i.e. $\leq 50$ µV/ K versus 1-10 mV/ K . Thus ,if one has a MI – transition one expects a step in S at $T_{mi}$ . If one has a two carrier situation , the step can either go up or down . This is shown schematically in Fig 4.3 .

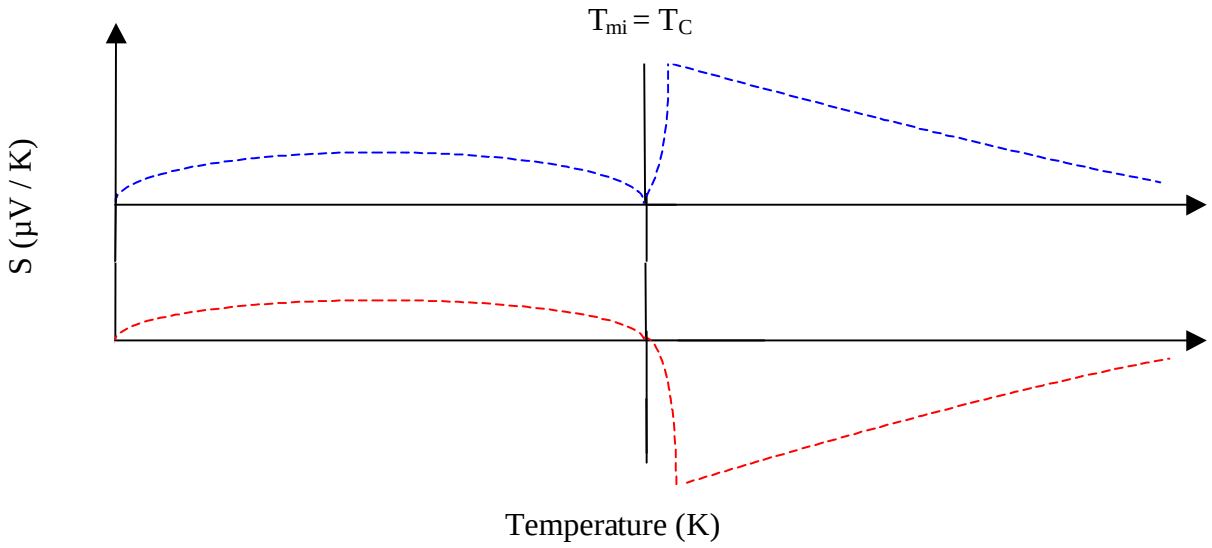


Fig.4.5: The temperature dependence of the thermopower for $y < 0.4$ ; schematically .

In Fig 4.5 ,we have specifically used a hump – shaped magnon TEP , blow $T < T_{mi}$ and eq.(4 -4) for $T > T_{mi} = T_C$ , which describes a polaron TEP in a semiconducting situration . As seen from Fig 3.18 , the step at $T_{mi}$ is more or less continuous , depending on whether the metal – insulator transition is more or less continuous and may or may not coincide with the zero crossing. Fig 4.6 show the temperature dependence of the thermopower in the case of magnon thermopower.

As the molecular field a approximation is valid near $T_C$ and the spin – wave approximation near T = 0 the TEP finally adopts a hump shape see Fig.(4.6). The hump shaped thermopower increases with increasing Li content, and thus also with increasing resistivity for the samples y = 0.40 and y = 0.46 , the thermopower is positive and has its biggest values. It should be expected that

when the effective band gap becomes larger, the negative electron-like contribution to S should become smaller [58] .

Bearing in mind that we can have a fm- metal to pm- insulator transition, for the ferromagnetic metallic range we expect diffusion thermopower $S_d \sim T$ [61], superimposed to a magnon thermopower contribution $S_m$, as shown in Fig.4.6 while for the activated regime the TEP of polaron hopping in a gap –like situation has been described as [62]:

$$S(T) = \frac{k_B}{e}\left[\frac{E_s}{k_B T} - \ell n\left[\frac{5}{4}\right] - \ell n\left[\frac{c(1-c)}{(1-2c)^2}\right]\right] \qquad (4\text{-}4)$$

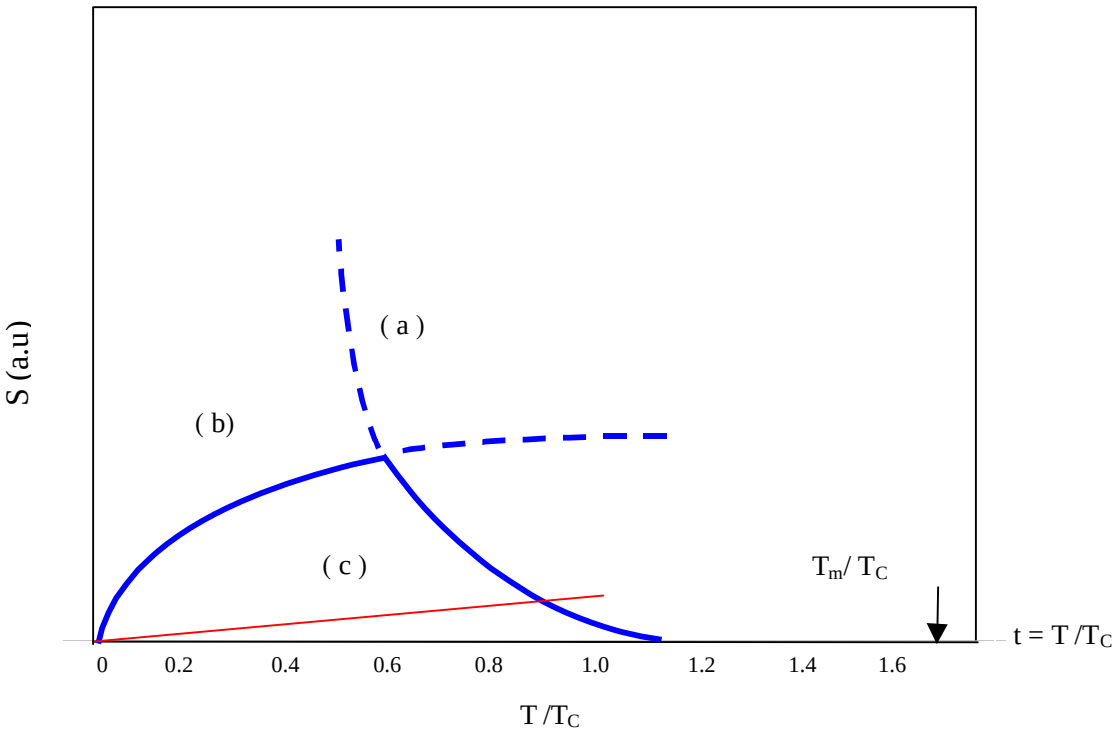


Fig. 4.6: One example of the temperature dependence of the thermopower .
( a ) the anomalous part of S is calculated by a simple molecular field approximation .
( b ) the anomalous part of S is calculated by a spin wave approximation.
( c ) the normal part of S and is given by 0,011 t , where t = T /$T_C$

where $E_S$ is the activation energy and c the polaron concentration. The first term is typical of thermally activated transport. The second term represents the spin entropy of a spin-3/2 hole moving in a spin-2 background and the third term represents the mixing entropy in the case of correlated hopping with nearest neighbour repulsion. $E_S$ is slightly larger as the 10 meV, reported by Jaime et al for y = 0 [62]. Other values are $E_S$ = 12.2 meV and c = 0.28 ; for $Nd_{0.67}Sr_{0.33}MnO_3$ [49].The large difference between $E_0$ (146.5 meV) and $E_S$ values is typical for polaronic transport.The term which contains c is always much less than the polaron thermopower [41,63- 67].

## 4.6. Heat conductivity

In the case of magnetic materials, the heat conductivity can be written as a sum of heat conductivities arising from the lattice, the electronic system and the spin system :

$$k = k_l + k_e + k_m \quad [68] \qquad (4\text{-}5)$$

The temperature dependence of the lattice contribution $k_l$ usually goes over a broad maximum, since $k_l \rightarrow 0$ for $T \rightarrow 0$ and $k_l \sim T^{-n}$ at high temperatures where phonon-phonon (umklapp-) processes dominate the lattice heat conduction. In the case of amorphous materials or polycrystals, the broad maximum usually degenerates to a shallow maximum or k(T) might be simply saturating at high temperatures, i.e $dk/dT \geq 0$ for all T [69]. Evidence for a significant electronic contribution can be derived from the effective Lorenz number $L = k_e / \sigma T$ and in the case of metal insulator–transitions (at $T_{mi}$), eventually from a step at $T_{mi}$ .

As the increase in k with y might have to do with the increased doping, we have calculated the effective Lorenz numbers $L = k \rho / T$ at 300K (Table 2) and find the sample with $y = 0.14$ to come closest to $Lo = 2.45\ 10^{-8}\ W\Omega/K^2$; as expected; however, even at best conductions (at y = 0.14) L is only $1.7\ .10^{-7} W\Omega/K^2$, suggesting that $k_e$ plays a minor role even in the fm metallic state of the manganites. Since we also do not find systematic structures in k(T) at $T_m$ for all y , the electronic contribution appears to be small always . The magnon part is usually considered to be small too.

Table 2 . Values of ρ ; k and L at 300K

| y | ρ(300K) (Ω cm ) | K (300K) | L(300K)(WΩ/K$^2$) Lo =2.45.10$^{-8}$ | S(T) μV/K |
|---|---|---|---|---|
| 0 | 0.12 | 115 | $4.6 \times 10^{-4}$ | -14.2 [64] |
| 0.05 | 0.23 | 17 | $1.3 \times 10^{-4}$ | --- |
| 0.10 | 0.05 | 10 | $1.7 \times 10^{-5}$ | -9.3 |
| 0.14 | 0.10 | 0.05 | $1.7 \times 10^{-7}$ | -20 |
| 0.18 | 0.20 | 117 | $7.8 \times 10^{-4}$ | -19 |
| 0.26 | 0.26 | 120 | $1.0 \times 10^{-3}$ | -13 |
| 0.33 | 0.05 | 120 | $2.0 \times 10^{-4}$ | -3.2 |
| 0.40 | 5.89 | 120 | $2.4 \times 10^{-2}$ | 7.0 |
| 0.46 | 24 | 120 | $9.6 \times 10^{-2}$ | 283 |

However, broader structures in k(T) are observed occasionally. Similar structures have been found in the TTE-measured heat conductivity of $La_{1-x}Sr_xMn\ O_3$ [21] and there they have been attributed to particular oxygen-deficit related (cluster) oscillatory modes in the TTE - measured surface layer . That would explain their unsystematic appearance with y. The randomisation in the oxygen deficient surface layer would indeed be stronger as in the bulk which would also explain the mostly positive slope of k (T) , $dk/dT > 0$ .

## CONCLUSION

We can conclude from the structural, transport and magnetic properties of $Nd_{0.66}Sr_{0.34}MnO_3$ doped with Li the following:

i- Li-doped manganates $Nd_{0.66}Sr_{0.34}MnO_3$ show Zener bond bloking at smaller Li-concentration y = 0.05 due to single site $Li^+$ substitution of $Sr^{+2}$.

ii- At medium Li- contents $0.05 < y < 0.2$ , we observe a rehabilitation of blocked Zener bonds due to the formation of Li- pairs $Li_2^+$ which charge substitute for $Sr^{+2}$.

iii- At high Li- contents $y > 0.2$ again blocking occurs probably due to clusters of three or more Li- ions.

The blocking (rehabilitation) is expressed through a reduction (enhancement) of the curie and metal insulator temperature $T_C = T_{mi}$ and also in the absolute values of the resistivity, magnetization and thermopower.

## References


1 - W. Schnelle, A. Poddar, P. Muruguraj, E. Gmelin, R.K. Kremer, K. Sasaki, J. Maier, J.Phys

2 - P. Mandal, A. Poddar, A.G.M. Jansen, K. Barner, L. Haupt, R.v. Helmolt, Phys.C 12 (2000) 4401

3 - C. Zener,Phys. Rev. 82 (1951) 403

4 - P.G. de Gennes , Phys. Rev. 118 (1960)141.

5 - Goldschmidt, V. M. Skifter Norske Videnskaps - Akad. Mat. Naturvid. Kl. 2 (1926).

6 - du Boulay, D. J., Thesis, Structure, Vibration and Electron Density in Neodynium- Iron-Boride and some Rare-Earth Perovskite Oxides, Department of Physics , The University of Western Australia, 1996

7 - Munoz, A., Alonso, J. A., Martinez-Lope, M. J., Garcia-Munoz, J. L. & Fernandez -Diaz, M.T. Journal of Physics-Condensed Matter 12, (2000) 1361.

8 - M.S.Islam,"Academic Background and Selected Recent Publications a ccessed on:30th May 2001."http://www.surrey.ac.uk/Chemistry/staff/ri_msislam.htm

9 - Rado, G. T., and H. Suhl, , Eds., Magnetism (Academic,New York) Vol. I, (1963) p. 25.

10 - Herring, C., in Magnetism, edited by G. T. Rado and H.Suhl (Academic, New York), Vol. II.B, (1963) p. 2.

11 - Anderson, P. W., in Magnetism, edited by G. T. Radoand H. Suhl (Academic, New York), Vol. I, (1963a), p. 25.

12 - Anderson, P. W., in Solid State Physics, edited by H. Ehrenreich, F. Seitz, and D. Turnbull (Academic, NewYork), Vol. 14, (1963b) p. 99.

13 - J.B. Goodenough, Phys. Rev. 100 (1955) 564.

14- G.H. Rao, J.R. Sun, A. Kattwinkel, L. Haupt, K. Baerner , E. Schmitt, E. Gmelin, Physica B 269 (1999) 379.

15 - H. Kuwahara, T. Okuda, Y. Tomioka, A. Asamitsu, and Y. Tokura, in Science and Technology of Magnetic Oxides, edited by M. Hundley, J. Nickel, R. Ramesh, and Y .Tokura , MRS Symposia Proceedings No. 494 (Materials Research Society), Pittsburgh , (1998), p. 83

16 - Z. Jira´k, S. Krupic¡ka, Z. S¡ims¡a, M. Dlouha´, and S. Vratislav, Magn. Magn . Mater. 53,(1985) 153.

17 - H. Kawano, R. Kajimoto, H. Yoshizawa, Y. Tomioka, H. Kuwahara,and Y. Tokura, Physical Review letters, 78(22), (1997) 4253

18 -Voorhoeve R J H, Remeika J P, Trimble L E, Cooper A S, Disalvo F J and Gallagher P K J. Solid State Chem. (1975) 14 395

19 - Itoh M, Shimura T, Yu J D, Hayashi T and Inaguma Y, Phys. Rev. B 52 (1995)12 522

20- Shimura T, Hayashi T, Inaguma Y and Itoh M, J. Solid State Chem. (1996)124 250

21 - Diehl T, Chaudouet P, Joubert J C and Pierre J, J. Appl. Phys. 81 (1997)4970

22 - S.L. Ye ,W.H. Song, J.M. Dal, S.G. Wang, K.Y. Wang, C.L. Yuan, Y.P. Sun, J.Appl.Phys. 88 (2000) 5915.

23 - A. Poddar ,P.Muruguraj, R.Fischer , E. Gmelin, K. Bärner, L. Haupt,P.Mandal, G.H.Rao , Physica B 254 (1998) 21.

24 - W. Prellier, A. Biswas, M. Rajeswari, T. Venkatesan, and R. L. Green, Appl. Phys. Lett. **75** (1999) 397
25 - H. Kawano, R. Kajimoto, H. Yoshizawa ,Y. Tomioka, H. Kuwahara, and Y. Tokura,Physic . Rev. Lett .78 ( 1997) 22
26 - K .Shah, D. K. Aswal, A. Singh, L .C. Gupta, S. K. Gupta and V. C. Sahni . Pramana C – J . Phys.58 ( 2002) 1085.
27 - S.M. Sarge, w.Hemminger, E. Gmelin, G.W.Höhne, H.K. Cammenga, W.Eysel, J. Thermal Anal. 49 (1997) 1125
28 - M.Sasaki, H.Negeshi, M. Inoue, J. Appl. Phys.59 (1986) 796
29 - J. Liebe,K. Heinemann. K. Baerner,I.V. Modevedeva. Yi.Tang .S.Dong, R. Braunstein . Mater.Sci.Eng.B 47 (1997) 244.
30 - A. Kattwinkel, E. Kraus, Ch. Kleeberg, T.Gron, K. Bärner, E.Schmitt, E. Gmelin, Aca Physica Polonica A 93 (1998) 745
31 - E. Kraus, diploma thesis, Göttingen 1995; Status Solidi (a) 165 (1998) 219.
32- L .M. Rodriguez-Matinez, J. Paul Attfield, Phy.Rev. B54 (1996) R 15622.
33 - G.H. Rao, J.S. Sun, J.K. Liang, W.Y. Zhou, Phys. Rev. B 55 (1997) 3742.
34 - G.H. Rao, J.S. Sun , K. Bärner, N. Hamad, J.Phys:Condens .Matter 11 (1999) 1523.
35 - N. F. Mott and E. A. Davis, Electronic Processes in Non-CrystallineMaterials, 2nd ed.
36 - A.L Efros and B.L. Shklovskii, J.Phys C 8 (1975 ) L 49
37 - J.G.Park, M.S. Kim, H.C.Ri, K. H. ´Kim, T. W. Noh, S. W.Cheong , Phys. Rev.B 60, 21 (1999) 14804.
38 - S. Das, P. Mandal , Z. Phys. B 104 (1997) 7.
39 - G.H. Rao, J.R. Sun , A. Kattwinkel, L. Haupt , K. Bärner, E.Schmitt, E. Gmelin, Physica B 269 (1999) 379.
40 - J.Volger , Physica 20 (1954) 49.
41 - M. Jaime,M.B. Salamon, K. Pettit , M. Rubinstein, R.E. Treece,J.S. Horwitz ,D.B.Chrisey, Appl. Phys.Lett .,68 (1996) 1576.
42 - K.Cherif, J. Dhahri, E. Dhahri,- M. Oumezzine, and H. Vincent, J. Solid .State. Chemistry 163 , (2002) 466.
43 - R. D. Shannon and C. T. Prewitt, Acta Crystallogr. B 25, (1969) 725; 26, (1970) 1046.
44 - N. Hamad , I. El-Kassab , L. Haupt , N. Kasper , K. Barner , G.H. Rao , U. Sondermann , E. Gmelin , Journal of Alloys and Compounds 317–318 (2001) 145.
45 - A.M. Ahmed,1, A. Kattwinkel, N. Hamad, K. Baerner, J.R. Sunb, G.H. Rao, H. Schicketanz, P .Terzieff, I.V. Medvedevad, J. Mag. = 7 - C. Zener, Phys. Rev. 82, (1951) 403.
46 - Z. Jira, S. Krupic, Z. Sims, M. Dlouh, and S. Vratisla, J. Magn. MagnMater.53,(1985)153.
47 - V. A. Bokov, N. A. Grigoryan, M. F. Bryzhina, and V. V. Tikhonov, Phys. Status Solidi 28 , (1968)835.
48 - E. Pollert, S. Krupicka, and E. Kuzmicova, J. Phys. Chem. Solids 43, (1982)1137.
49 - J.B. Goodenough , Magnetism and the Chemical Bond, Wiley ,New York – London (1963) 233
50 - A.Gupta, G.Q.Gong,Gang Xiao,P.R Duncombe,P.Lecoeur,P.Trouilloud,Y.Y.Wang, V.P. Dravid and J.Z.Sun, physical Review B 54(1996) R15629
51 - L. Haupt, R.V. Helmolt , U. sondermann, K. Baerner, Y.Tang, E.R .Giessinger, E. Ladiszinsky , R. Braunstein, Phys. Lett. A 165(1992) 693.
52 - M. Pattabiraman, P. Murugaraj, G. Rangarajana, V. Prasad, S. V. Subramanyam, V. S. Sastry , Sang-Mo koo and K. V. Rao , Pramana- journal of physics Vol. 55, 3 ( 2000). 455.
53 - K. M. Satyalakshmi, B. Fisher, L. Patlagan, and G. Koren, App. Physc. Lett. 73, (1998) 320
54 - T. Kasuya , Progr. Theor. Phys. 16 (1956)58.
55 - C.W. Searle and S.T. Wang, Can.J. Phys.48 (1970)2023
56 - I. El-Kassab, A.M. Ahmed, P. Mandal, K. Baerner, A. Kattwinkel, U. Sondermann , Physica B 305 (2001) 233.

57 - C.P. Adams , J.W. Lynn, Y.M. Mukovskii,A.A. Arsenov,and D.A.Shulyatev(Polaron Formation and Colossal Magnetoresistance in Manganites).
58 - K.Baerner , P.Mandal , R.V Helmolt , Phys. Stat. Sol. (b) 223 (2001) 811
59 - J. Fontcuberta, A. Seffar, X. Granados, J. L. Garcya-Munoz, X. Obradors, and S. Pinol Appl. Phys. Lett. 68 (1996) 16
60 - J. S. Zhou, W. Archibald, and J. B. Goodenough, Nature (London) 381, (1996)770.
61 - E. Kraus, K. Heinemann, K. Baerner, F.A. Khan, I.V.Medvedeva, H. Schicketanz, P. Terzie , Phys. Stat. Sol. (A) 177 (2000) 547.
62 - M Jaime, M B Salamon, M Rubinstein, R E Treece, J S Horwitz and D B Chrisey, Phys. Rev .B54, (1996) 11914.
63 - J.S. Zhou, J.B. Goodenough, A. Asamitsu, Y. Tokura, Phys. Rev. Lett. 79 (1997) 3234.
64- H. Kang, P. Mandal, I.V. Medvedeva, K. Baerner, A. Poddar, E. Gmelin, Phys. Stat. Sol. (A) 163 (1997) 465.
65 -.Xianming Liu, Hong Zhu and Yuheng Zhang , Phys. Rev. B 65 (2001)024412-1
66 - M.F. Hundley, J.J. Neumeier,.
67 - R.R. Heikes, Thermoelectricity, Wiley Interscience, 1961.
68 - J. Liebe, E. Kraus, L. Haupt, P. Mandal, K. Baerner, R.v. Helmolt, Appl. Phys. Lett. 68 (1996) 2343.
69 - Y.S. Touloukian, Thermal Conductivity, Metals and Alloys, Plenum, New York, 1970.

## CURRICULUM VITAE


**Family name** : Hamad

**Name** : Nagat El-Sabaey Farag

**Sex** : Female

**Marital Status** : Married and have four children

**Nationality** : Egyptain

**Date of Birth** : July., 22,1964

**Place of Birth** : El – Menoufia - Egypt

**Occupation** : Associate Lecture at Faulty of electronic Engineering, Menoufia university

**Now** : Ph.D. graduate studies at the University of Goettingen; Germany

**Address Res**. : IV. Physikalisches Institut ; University of Goettingen Bunsenstr.; 13-15; 37073 Goettingen

**Home Address** : Department of Physics, Faculty of electronic Engineering, Menoufia Univ., Menouf, Menoufia state, Egypt

**E-mail** : nagat2@freenet.de,


**Univ. Degrees:**

: B.Sc. Faculty of Science; Menoufia Univ. grade “Excellent” (1986)

:M.Sc. Faculty of Science; Menoufia Univ.,(1995)

**Title of Thesis**. Study of the electrical and magnetic properties of some solid

**Society Memberships** : Egyptian Scientific Syndicate.

## Lebenslauf

**Persönliche Daten**

**Familienname** : Hamad

**vorname** : Nagat El-Sabaey Farag

**Nationalität** : Ägypterin

**Geburtsdatum** : 22. Juli 1964

**Geburtsort** : El -Menoufia -Ägypten

**Familienstand** : Verheirtet (4 Kinder)

**Adresse** : Albrecht Thaer Weg 24G/11
37075 Göttingen

**Ausbildung**

**Grundschule** : von 1970 bis 1976
**Primary school** : von 1976 bis 1979

**Secondary schcool** : von 1979 bis 1982

**Studium**

Aufnahme des Physikstudiums an der Universität Menoufia Von 1982 bis 1986

Diplomprüfung Physik an der Universität Menoufia 1994

**Die Thema** : (Study of the electrical and magnetic properties of some solid)

**April 1998 (beginen)**
: Promotion am IV. Physikalisches Institut, Institut für halbleiterphysik, der Georg-August- universität Göttingen unter der wissenschaftlichen Leitung von Herrn Prof. Dr. K. Bärner, Finanzierung der Doktorarbeit durch ein fünfjähriges stipendium des Landes Ägypten.